universität wien

MASTERARBEIT

Titel der Masterarbeit

„Validation of biomarkers of resistance to BRAF inhibitors in melanoma“

verfasst von

Judith Wenzina BSc

angestrebter akademischer Grad

Master of Science (MSc)

Wien, 2014

Studienkennzahl lt. Studienblatt:	A 066 834
Studienrichtung lt. Studienblatt:	Masterstudium Molekulare Biologie
Betreut von:	Univ.-Prof. Dr. Manuela Baccarini

Acknowledgments

First of all, I thank Prof. Reinhard Dummer and Prof. Mitchell Levesque who gave me the opportunity to work on this project. Above all, I am extraordinarily grateful to Prof. Levesque for his permanent, benevolent supervision in scientific and supportive issues throughout my whole stay in Zurich and afterwards. Moreover, I also thank Prof. Baccarini who agreed to be my supervisor at the University of Vienna and therefore made it possible for me to accomplish the lab work for my Master`s Thesis in Switzerland.

Additionally, I highly appreciated the assistance of the whole research group during my stay in Switzerland and especially thank D. Widmer and M. Raaijmakers who were there for me whenever I needed support.

Furthermore, I thank my parents who encouraged me in executing my Swiss plans together with all my relatives and friends, who came to Zurich in order to visit me. M. Ivankovic, J. Wachter and M. M. Wohlgenannt deserve my thanks for the inspiring time we spent together at the University of Vienna during the recent five years.

Table of Contents

1 Abstract

The incidence of malignant melanoma is constantly increasing worldwide; approximately 50-60% of all malignant metastatic melanoma carry a mutation (V600E) in the serine/threonine protein kinase B-RAF (BRAF) activating the MAP-Kinase signal transduction pathway (Davies et al.). Due to pharmaceutical interventions, targeted therapies specifically affect these cancer cells. However, patients become resistant within 6 to 8 months after the beginning of the treatment with a Braf inhibitor (Flaherty et al.). In order to reveal resistance mechanisms to the Braf inhibitor, I made use of the melanoma biobank of the University Hospital of Zurich and investigated tissue samples of a patient who had suffered from progressive disease. To find new resistance mechanisms, I ruled out the known ones and used digital PCR for mutation detection. Moreover, whole exome sequencing revealed 13 mutated genes, which all of the resistant metastases had in common; therefore I investigated one of these further, namely *TACC1*. I found out that *TACC1* is expressed in 88% of melanoma and that it is a possible tumor-suppressor as the overexpression of Tacc1 decreased viability in melanoma cells.

2 Zusammenfassung

Das Vorkommen von bösartigen Melanomen nimmt weltweit konstant zu; etwa 50 bis 60% aller bösartigen metastasierenden Melanomen weisen eine V600E Mutation in der Serin-Threonin Protein Kinase B-RAF (BRAF) auf, wodurch der MAP Kinase Signaltransduktionsweg aktiviert wird (Davies et al.). Mit Hilfe der Pharmazie ist es gelungen, diese spezifischen Krebszellen mittels gezielt darauf ausgerichteter Therapie zu töten. Jedoch werden Patienten binnen 6 bis 8 Monaten nach dem Beginn der Therapie mit dem Braf Inhibitor resistent (Flaherty et al.). Um Resistenzmechanismen gegen den Braf Inhibitor aufzudecken, machte ich von der Melanom Biobank des Universitätspitals Zürich Gebrauch und untersuchte Gewebeproben eines Patienten, der an progressiver Erkrankung litt. Um neue Resistenzmechanismen zu finden, habe ich schon bekannte ausgeschlossen und verwendete digital PCR zum Nachweis von Mutationen. Überdies hat Whole Exome Sequencing 13 mutierte Gene aufgezeigt, die in allen resistenten Metastasen zu finden waren; eines davon – *TACC1* – untersuchte ich weiter. Ich zeigte, dass

TACC1 in 88% von Melanomen exprimiert ist und dass es einen möglichen Tumor-Suppressor darstellt, da die Überexpression von *TACC1* die Lebensfähigkeit von Melanomzellen herabsetzt.

3 Introduction

3.1 The MAP-Kinase Pathway

The MAP-Kinase pathway is one of the most affected pathways in cancer as alterations in the involved proteins can lead to uncontrolled cell growth and prevention of apoptosis. However, the most important proteins in this signal transduction cascade are Erk1/2 as these proteins are responsible for the phosphorylation and therefore activation of a broad range of regulative factors in the cell (Steelman et al.).

In healthy cells, an extracellular signal is necessary for the activation of this pathway: Growth factors, cytokines, interleukins and mitogens bind to the corresponding receptor on the cell surface. Thereby the receptor becomes activated and as a consequence transmits the signal to Shc which recruits Grb2 and Sos; the latter functions as GEF which is essential for the activation of Ras (Ras belongs to a group of small GTPases) as the GEF proteins are responsible for the displacement of GDP from the membrane-bound Ras and subsequent loading of GTP (Chappell et al.). Due to the anchoring of GTP, Ras becomes activated and can further activate either Raf/Mek/Erk signaling or Pten/Akt/mTOR signaling. Both pathways are able to alter the gene expression of the cell (Shull et al.). However, Ras activity can be suppressed by GAP, which stimulates the GTPase activity of Ras and therefore the inactivation of this protein. One of the GAP proteins is Nf1 which has been discovered as a tumor-suppressor (Simmons et al.). However, it has been shown that Ras can also become active though insulin receptors (IR) or insulin receptor substrate (IRS) proteins which bind Grb2 (Hayashi et al.); *IRS4* was shown to be mutated in melanoma cells (Shull et al.).

Furthermore, Ras activates its downstream target Raf (Steelman et al.). As B-Raf is the most commonly protein mutated in melanoma, the following two sections outline the differences between the three Raf proteins and the precise structure and enzymatic activity of B-Raf.

3.1.1 The Family of Raf Proteins

The three Raf Proteins belong to a group of serine/threonine protein kinases and play an important role in the MAP-Kinase signal transduction pathway. The activation of

these kinases is normally accomplished by Ras, which needs to be present in the GTP-bound form (Avruch et al.).

A-Raf, B-Raf and C-Raf are all different isoforms of *RAF* that possess the same structure and the same regulation but vary in their lengths of the non-conserved N- and C-terminal ends. However, all of these proteins share the three conserved regions CR1-3. Whereas CR1 and CR2 together are responsible for the regulation of the catalytic activity, the CR3 possesses the kinase activity (Pearson et al.).

3.1.2 Structure and Activity of B-Raf

Braf is one of the specific Ser/Thr kinases and is composed of three domains: CR1 is the Ras-GTP binding domain (Daum et al.), CR2 is a hinge region which is Serine rich and is needed as a flexible linker between CR1 and CR3. CR3 represents the catalytic protein kinase which is responsible for the phosphorylation of the target (Cutler et al.). The activation of Braf is accomplished through Ras – like Craf and Araf. However, Braf has the capability of becoming activated by Rap1 which is the major difference to Craf and this activation is also the dominant mechanism for Braf activation (Pearson et al.). Additionally, the activation of C-Raf via Ras is dependent on calcium/calmodulin-dependent protein kinase II (CaMK-II) which phosphorylates and therefore activates it – B-Raf does not show this dependency (Salzano et al.). Once Braf is activated, hydrogen bonds and electrostatic interactions lead to dimerization of the kinase domain CR3 (Bollag et al.). Another difference to Craf is that activated Braf exists as a homodimer whereas Craf is only active as a heterodimer in composition with Braf (Garnett et al.). Additionally, CR3 consists – amongst others - of an N-lobe which is important for ATP binding (the adenine nucleotide is attached to a non-polar binding pocket) and of a C-lobe which is needed for the anchoring of the substrate protein. Subsequently after binding the target protein, the phosphate group of ATP is transferred to the target and consequently ADP and the phosphorylated protein are released (Hanks and Hunter).

The downstream targets of the Raf proteins are Mek1/2. However, Mek1 can also be activated by KSR which can form dimers with Raf proteins which might affect the binding of the Braf inhibitor (McKay, Freeman and Morrison).

Consequently, Mek phosphorylates Erk1 and 2 which have a variety of substrates: Kinases, phosphatases, growth factor receptors, cytokines, cell cycle regulator

proteins, transcription factors and proteins involved in mRNA translation and apoptosis (McCubrey et al.). In the following section, I will discuss some essential substrates of Erk.

Concerning mRNA translation, Erk phosphoylates Mnk1/2 which subsequently activates eIF4E; eIF4E plays a key role in the translation of mRNAs which are difficult to translate (Steelman et al.). Moreover, Erk also initiates the phosphorylation of C-Raf and Mek1, which leads to a change in their activity – depending on the phosphorylation site of C-Raf, the phosphorylation can either have an enhancing (Balan et al.) or an inhbiting (Dougherty et al.) effect on the activity of the protein. Furthermore, Erk is capable of phosphorylating Sos at multiple sites which leads to separation of Sos from Grb2 preventing the activation of Ras and therefore a downstream signal transduction (Buday, Warne and Downward). However, Erk can directly phosphorylate EGFR and thus reduce/inhibit its activity (Li et al.). Besides that, the phosphorylation of transcription factors by Erk generally prevents these proteins from ubiquitination and ensures their stability (McCubrey et al.). Erk indirectly also has the ability to remodel chromatin structures through the phosphorylation of mitogen and stress-activated protein kinases (MSKs) which in turn activate histone H3 (Kyriakis and Avruch).

Slight alterations in this pathway are often linked to abnormal and uncontrolled cell growth which is an early event in the development of cancer. Thus, proteins in this pathway have recently become specific drug targets in order to inhibit an overactivation of the MAPK pathway.

3.2 An Overview on Melanoma

Melanoma is a malignant tumor of melanocytes (Bandarchi et al.) that is responsible for 75% of skin cancer deaths (Jerant et al.). The development of melanoma is caused by excess UV exposure (Kanavy and Gerstenblith). Once, the tumor has developed, surgical removal is the first step to control further growth and spreading to other organs. Additional immunotherapy, chemotherapy and radiation therapy can contribute to the patient`s recovery. In 2011, the FDA approved a targeted therapy for the treatment of melanoma patients, namely the Braf inhibitor. This drug specifically inhibits constitutively active Braf and therefore stops the signal transduction cascade which would lead to the activation of Erk1/2 and thus further growth of the tumor

cells. Notably, the drug only targets Braf if it carries a mutation at the position V600 (Bollag et al.). Figure 1 shows the comparison of the common MAP-Kinase pathway, the overactive and the inhibited MAP-Kinase pathway.

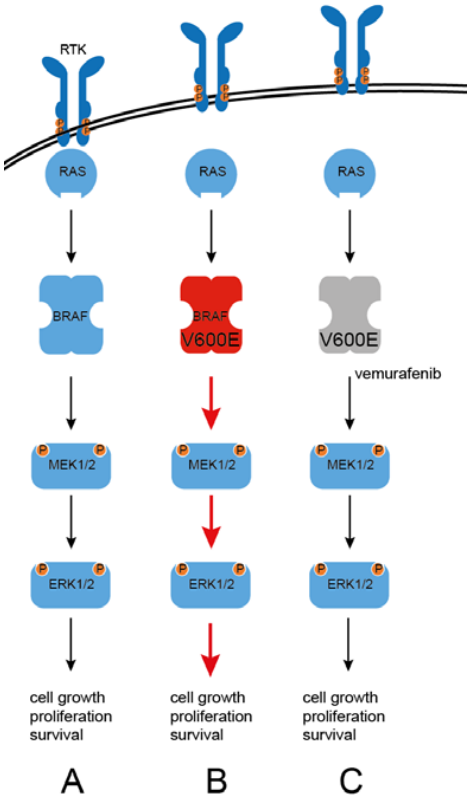

Figure 1. (**A**) Usual MAPK signaling leading to cell growth, proliferation and survival. (**B**) *BRAF* carries the V600E mutation and therefore becomes overactivated; this overactivation finally leads to high levels of pErk1/2 and subsequently to increased cellular growth and proliferation and continuing survival. (**C**) Inhibition of the mutated Braf by a Braf inhibitor (e.g. Vemurafenib) and therefore no overactive MAPK signaling. Adapted from: Nazarian et al.

3.3 DNA damage due to UV exposure

Melanoma is likely caused by unprotected sunlight exposure. The UV light from the sun damages the DNA by creating mutations in the cells which allow the cells to become highly proliferative. The sunlight contains UVB light and UVA light, both of these UV types can lead to mutations in the genome. UVB light can lead to malignant melanoma due to the formation of cyclobutane pyrimidine dimers in the DNA which means that neighbouring pyrimidine dimers stick together (cytosine-cytosine, thymine-thymine and cyotsine-thymine). The absorbance of UVA light, as compared to the uptake of UVB light, is less efficient (Rünger et al.). Moreover, it only causes thymine-thymine dimers in the DNA. In addition, UVA light leads to the production of

reactive oxygen species (Sage, Girard and Francesconi) which can cause oxidative damage to the cellular DNA and therefore can cause cancer (Waris and Ahsan).

Once these cyclobutane pyrimidine dimers have been formed, these structures can be repaired by nucleotide excision repair (Goodsell). However, if these structural alterations stay unrepaired, DNA replication is accomplished inaccurately, and in consequence causes mutations. The most common mutation caused by pyrimidine dimers is the point mutation from C to T (Hodis et al.). Mutations in tumor-suppressors or in proto-oncogenes can lead to uncontrolled and increased growth of the cell and therefore to malignant tumor formation.

3.4 Oncogenic drivers in the MAP-Kinase Pathway

3.4.1 Overactivation through BRAF

About 60% of melanomas carry a mutation in *BRAF* coding for the proto-oncogene Braf which is an important protein in the MAPK pathway (Davies et al.). More than 80% of all the mutations in Braf appear in the kinase domain at position V600 (Hocker and Tsao). Mostly, the original amino acid valine (V) is exchanged by glutamic acid (E), but an exchange by lysine (K), aspartic acid (D) or arginine (R) is also possible (Ascierto et al.). However, mutations in *BRAF* can also occur in other positions of exon 15 and in exon 11 as well, but they are also located in the kinase domain (Hocker and Tsao). These mutations in *BRAF* lead to increased activation of the MAPK signaling and consequently to the uninterrupted activity of Erk activating transcription factors for cellular development, growth and differentiation.

3.4.2 Activating mutations in NRAS

Another protein – upstream of Braf – in the MAPK pathway that possesses the role of a proto-oncogene is the GTPase Nras. Nras enables the activation of the MAPK pathway as well as the PI3K pathway which makes it an important regulator for the cells (Ellerhorst et al.). Besides Braf, Nras harbors the second most common mutations in malignant melanoma (Curtin et al.). Nras is the most important member of the Ras family besides Kras and Hras in melanomas. The most frequent mutation in *NRAS* is the exchange of alanine to guanine at position 182 resulting in the amino acid change at position Q61 to arigine (R).

3.4.3 Activation through Receptor Tyrosine Kinase

The receptor tyrosine kinase (RTK) encoded by *KIT* is embedded in the cell membrane and becomes activated by binding of c-kit ligand (Edling and Hallberg). As a consequence, the receptor dimerizes and triggers the phosphorylation and therefore activates the downstream proteins in the signal transduction pathway (Mehnert and Kluger). Mutations in *KIT* result in a constantly active receptor and therefore in an uninterrupted MAPK pathway leading to cellular proliferation.

3.4.4 Mutations in Mek1/2 lead to constant Erk signaling

The acquirement of mutations in Mek followed by constant signaling and activation of Erk are a common mechanism in melanoma. It was shown that a patient treated with a Braf inhibitor and a Mek inhibitor suffered from progressive disease due to mutations which occurred in Mek1 (P124L and Q56P). Both mutations disrupt the drug binding pocket and lead to uncontrolled signaling (Emery et al.).

An alternative is the Q60P mutation in Mek2 which is also reported as an oncogenic driver during treatment with Braf and Mek inhibitors. Moreover, this mutation corresponds to the Q56P mutation in Mek1. However, this effect leads to progressive disease due to constant activation of Erk (Villanueva et al.).

3.5 Targeted Therapies in Melanoma

The aim of targeted therapies is to specifically inhibit the function of a certain protein that is part of a signal transduction pathway. Concerning melanoma, the two most affected pathways are the MAPK pathway and the PI3K pathway. For both pathways, drugs exist that target one of the proteins in the signal cascade resulting in the inhibition of the transduction to the downstream protein (Raaijmakers et al.). Figure 2 shows possible targeted therapies for the MAPK and for the PI3K pathway in melanoma.

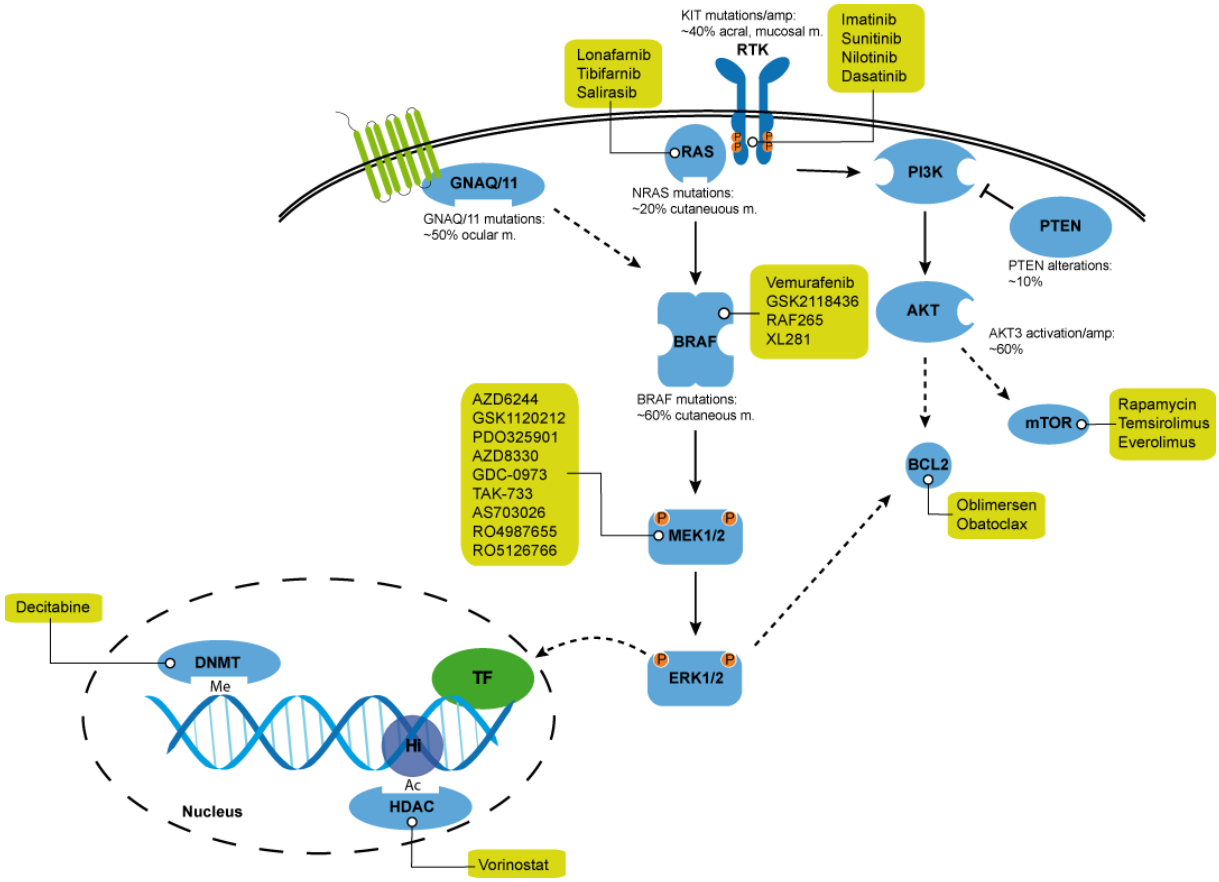

Figure 2. Key pathways and therapeutic targets in melanoma. Activation of receptor tyrosine kinases (RTK) and their downstream MAPK pathway is very important in most melanomas. Currently tested molecules (green boxes) for the treatment of melanoma affect the activity of proteins involved in MAPK or PI3K/AKT signaling. The phosphatidylinositide 3-kinase (PI3K) pathway can be over-activated by either loss of PTEN or activation of AKT. DNA methylation (Me) and/or histone (Hi) acetylation (Ac) suppress transcription of tumor suppressor genes. DNA methyltransferase (DNMT), transcription factor (TF), histone deacetylase (HDAC).Adapted from: Nikolaou et al.

Focusing on the MAPK pathway, the most common mutation is the V600E mutation in Braf. The mutation in this gene leads to an overactivation of the protein and consequently to the activation of the downstream target resulting in an uninterrupted signaling of the MAPK pathway constantly phosphorylating Erk1/2 which activates the transcription factors for cellular proliferation. In order to inhibit constantly active Braf, the Braf inhibitor specifically binds to the ATP-binding site of the mutated protein and therefore prevents ATP from binding which would be essential for further activation. Hence, the treatment with the Braf inhibitor leads to an inhibition of the MAPK pathway and furthermore it causes apoptosis in melanoma cell lines (Sala et al.).

3.6 Resistance to the Braf Inhibitor – Genetic Mechanisms

Even though targeted approaches belong to the most promising therapies in cancer and considerably prolong the patient`s life, melanoma patients become resistant to the Braf inhibitor within approximately 6 months - many of them through additional activating mutations in key players of MAPK and PI3K signaling (Chapman).

3.6.1 Activating Mutations in the MAP Kinase Pathway

There are different mechanisms causing resistance through activating mutations in either the MAP-Kinase pathway or the PI3K pathway. One of the proteins which can be mutated and which affects both pathways is Nras. Normally, Nras - on the one hand - phosphorylates Braf in order to activate it and therefore the whole signal transduction cascade (MAPK), on the other hand it is responsible for membrane translocation and activation of the PI3K pathway. Therefore, one way to acquire resistance is by activating Nras (most commonly Q61R) overcoming the inhibition of Braf and reactivating the MAPK pathway which again leads to proliferation and differentiation (Nazarian et al.). Moreover, it was shown that mutations in Nras lead to a switch from Braf to Craf in further signal transduction overcoming the inhibited Braf and activating downstream proteins (Dumaz et al.).

Additionally it was shown that downstream targets of Braf, namely Mek1/2, develop mutations in order to reactivate MAPK signaling. Because of these mutations, an activation of Mek1/2 through Braf is not necessary anymore. This leads to the affect that Braf is constitutively inhibited, but the MAP Kinase pathway is reactivated through independent activation of MEK (Trunzer et al.).

3.6.2 Alterations in PI3K/Akt Signaling

Another resistance mechanism is the activation of the PI3K pathway, which also leads to a proliferative effect. After the activation of PI3K by Nras, PI3K phosphorylates and therefore activates the oncogene Akt. If Akt is mutated, it does not necessarily need the phosphorylation through PI3K, therefore the activation of Akt cannot be controlled anymore, leading to uncontrolled downstream signaling, increased survival and proliferation (Carpten et al.).

However, PI3K itself is a common proto-oncogene, but is rarely altered in melanoma (Omholt et al.). In melanoma cells, the PI3K/Akt – signaling is preferentially activated

through the inactivation of PTEN. PTEN is a major tumor suppressor deleted in 30-50% of melanoma and results in permanent signaling of PI3K/Akt leading to overactivation (Stahl et al.).

3.7 Resistance to the Braf Inhibitor – Transcriptional Alterations

3.7.1 Mek Activation through Cot1

Mek activation can be achieved through Cot1 overexpression by activating Erk through Mek without the need of activated Braf. Hence, if Cot1 is overexpressed, it directly activates Mek through a mechanism independent of Braf signaling and thereby activates Erk (Johannessen et al.).

3.7.2 Mis-splicing of Braf

Another mechanism of resistance is the aberrant splicing of *BRAF.* Melanoma cells that are resistant to the Braf inhibitor express a 61kD variant of Braf (V600E). This new form of Braf lacks the exons 4 to 8 and therefore the Ras binding domain (Poulikakos et al.).

Other possibilities of gaining resistance to the Braf inhibitor are by splicing out the whole ATP-binding pocket or mis-splicing so that the V600E mutation is not part of the ATP-binding pocket anymore. Both events prevent the binding of the Braf inhibitor to the protein and so Braf is constitutively active in the cells – if the protein has still been functional after mis-splicing.

3.7.3 Dysregulation of RTK

One class of Receptor Tyrosine Kinases was shown to be upregulated in melanoma cells resistant to the Braf inhibitor. The PDGFRβ family is present in high levels in melanoma cells that already carry an activating Nras mutation. However, *PDGFRβ* overexpression in combination with overactive Nras leads to a proliferative effect of melanoma cells and therefore contributes to melanoma progression. Notably, the overexpression of PDGFRβ does not appear to originate from genetic mutations but from transcriptional regulation.

3.7.4 Stroma-Mediated Resistance

Stromal cell secretion of HGF leads to activation of the HGF-specific RTKs – METs. METs are capable of reactivating the MAPK and the PI3K signaling when activated

and thus lead to immediate resistance to the Braf inhibitor. The inhibition of Braf combined with inhibition of HGF or MET results in sensitivity to the Braf inhibitor in melanoma cells. Due to these facts, it is important that studies on resistance also include the tumor-microenvironment (Straussman et al.).

3.8 Unmodified *BRAF*^{V600E} in Resistance

Due to the activating V600E mutation and the subsequent development of resistance to the Braf inhibitor, it was expected that *BRAF*^{V600E} accumulated more mutations that altered the protein in a way the inhibitor would not have been able to bind anymore. However, it was shown that no secondary mutations occurred in *BRAF* - although the melanoma cells had become resistant to the inhibitor (Nazarian et al.).

Paradoxically, the Braf inhibitor, which specifically binds Braf^{V600E}, was shown to stimulate wild-type Braf isoforms that might promote tumor growth as they then serve as an activator of the MAP-Kinase pathway (Hatzivassiliou et al.).

3.9 *TACC* and Its Role in Cellular Proliferation

The members of the *TACC* family (in human: *TACC1-3*) are highly conserved amongst species and contribute to the regulation of microtubules, which is an important event during mitosis as it allows proper chromosomal segregation and distribution (van der Vaart, Akhmanova and Straube). Abnormalities in mitosis and/or spindle formation lead to chromosomal instability and aneuploidy which are characteristics of cancer (Pihan et al.). Therefore, proteins encoded by *TACC* are important for the cells in order to grant the correct formation of the spindle (Gergely). Even though these proteins are highly investigated, their function is still unknown. Additionally, it has not yet been revealed if Tacc1-3 function as tumor-suppressors or an oncogenes (Guyot et al.). However, the deregulation of *TACC1-3* is linked to cancer formation (Ha, Kim and Breuer).

3.9.1 TACC1-3 in Mammals

TACC1 has been identified as the transcript of the breast cancer amplicon 8p11 and is located next to *FGFR* which is overexpressed in breast cancer (Still et al.). It has been shown that Tacc1 is located at the spindle during anaphase and cytokinesis and is responsible for the relocalization of the nucleus in interphase. Additionally, Tacc1 interacts with Aurora Kinase A-C during cytokinesis (Delaval et al., Gabillard et

al.). These facts suggest that Tacc1 plays an important role during cell division, but is not exclusively responsible for proper cytokinesis because the knock down of Aurora Kinase B leads to abnormal cell division (Conte et al.). However, Tacc1 is phosphorylated by Aurora Kinase C, but the significance of this modification is not known yet (Gabillard et al.). Furthermore, the oncogenic transcription factor Gas41 interacts with Tacc1 and is upregulated in human cancer cell lines. This additional fact suggests that Tacc1 may also be involved in tumor formation (Lauffart et al.).

TACC2 is located at the centrosome during the whole cell cycle (Peset and Vernos) and has been shown to be down-regulated in breast cancer (Chen et al.). If knocked down, the cell cycle is arrested at G2/M-phase whereas overexpression of *TACC2* increases S-phase suggesting that it is important for the progression of G2/M-phase (Takayama et al.).

Many different interaction-partners of *TACC3* have already been revealed but the functions of these interactions are not yet known in detail – for example, the interaction of Tacc3 with Stat5 (Piekorz et al.). Moreover, Tacc3 is recruited to promoters, which are methylated and therefore inaccessible to the transcription machinery. The recruitment is accomplished by Mbd2 and Tacc3 can reactivate the transcription without previous demethylation (Gangisetty et al.). Furthermore, Tacc3 is capable of initiating cellular proliferation by activating the MAPK- and/or PI3K-pathways (Ha, Park and Breuer).

3.10 Hypothesis

A collaborator in Zurich performed whole-exome sequencing (WES) of samples from a melanoma patient who became resistant to the Braf inhibitor. WES data revealed 13 genes which were mutated in all of the resistant metastases but did not show this mutation in the samples excised from before the treatment. One of these altered genes was *TACC1*, which was already known to play a role in different types of cancers but its function was still unknown. Therefore, I performed experiments in order to reveal the function of this gene – as we supposed that it plays a role in resistance as it was only mutated after the treatment with the Braf inhibitor. Moreover, the Kaplan-Meier survival curve revealed that the higher *TACC1* is expressed, the longer is the patients' survival and therefore we expected Tacc1 to act as a tumor-suppressor and the L452V mutation to be a loss-of-function mutation.

Additionally, WES showed that one metastasis carried $BRAF^{V600E}$ and $NRAS^{Q61K}$ mutations. Therefore, I performed digital PCR experiments as this approach had a mutation detection level of 5%. Hence, firstly we expected to find some more metastases which are positive for this *NRAS* mutation and secondly we wanted to exclude that the $TACC1^{L452V}$ mutation is not present in a tissue sample excised from before the treatment. Additionally, we expected the presence of melanoma cells in the blood – hence, we also screened a blood sample from this patient for circulating melanoma cells.

4 Materials and Methods

4.1 Quantitative Real-Time PCR

4.1.1 Taqman Mutation Detection Assay

Quantitative real-time PCR was carried out using the Bio-Rad CFX96 real-time PCR detection systems (Hercules, CA, U.S.), which was capable of detecting the fluorescence emitted by a fluorochrome. The amplification cycles consisted of different temperature changes: Starting with 95°C for 10 minutes followed by 50 cycles of 95°C for 15 minutes and 60°C for 1 minute. After 50 cycles, the reaction was terminated by cooling the plate to 4°C. The obtained C_q values corresponded to the number of cycles which were needed to exceed a determined threshold. During the exponential amplification phase, the sequence of DNA target doubled with every cycle. If the C_q values are low, the sample skips the threshold after several cycles which is a consequence of the fact that the expression is high. In our experiments, we made use of Taqman probes which - in contrast to those used for usual qPCR - significantly increased the specificity of the detection. The probe consists of one fluorophore (5‘ reporter dye 6-FAM for mutation detection, VIC for wild type detection) and 1 quencher (MGB). Figure 3 illustrates a complete cycle of extension.

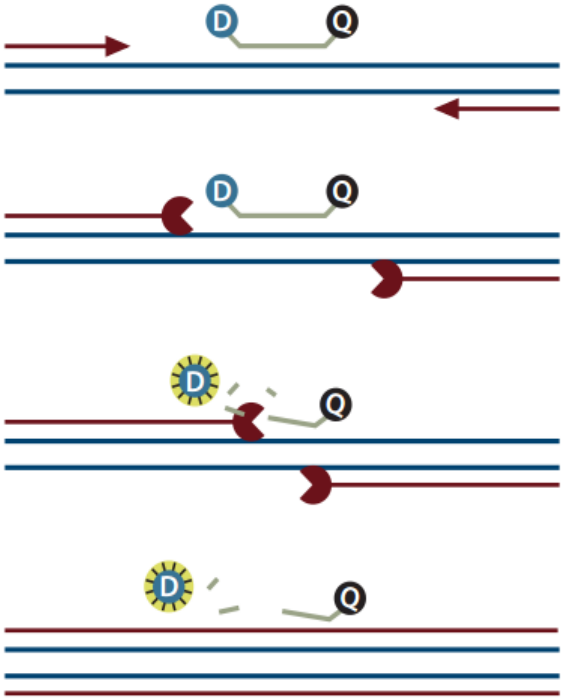

Primers and Taqman Probe hybridize to the target sequence and extension starts.

The polymerase possesses exonuclease activity and thereby hydrolyses the Taqman Probe.

Due to the hydrolysis, the connection between fluorophore and quencher breaks down; this allows the dye to fluoresce. Fluorescence can be measured after every extension cycle.

Figure 3. Illustration of reaction process; D Dye, Q Quencher; Source: Life Technologies

For amplification of the mutated/wild type gene, DNA, forward and reverse primers (end concentration: 2µM), the Taqman probe (end concentration: 1µM) and the Taqman Fast Advanced Master Mix were added to a total amount of 20µL. Taqman probes and the corresponding primers are shown in table 1.

Table 1. Primers and Taqman probes used for quantitative PCR from 5`end to 3`end.

Gene	Wt Probe	Mut Probe	Primer Forward	Primer Reverse
BRAF V600E	VIC-CTAGCTACAGTGAAATC-MGB	6-FAM-TAGCTACAGAGAAATC-MGB	CTACTGTTTTCCTTTACTTACTACACCTCAGA	ATCCAGACAACTGTTCAAACTGAT
NRAS Q61K	VIC-AGCTGGACAAGAAGA-MGB	6-FAM-CAGCTGGAAAAGAA-MGB	GGTGAAACCTGTTTGTTGGACAT	TGTATTGGTCTCTCATGGCACTGT
TACC1 L452V		6-FAM-TGAAATCGTAGAATCA-MGB	CCATGGATCCCTTTAAACCA	TAAACGCGACTTTGCCTTCT

Taqman probes and primers were designed by oneself; primers were ordered from Microsynth (Balgach, Switzerland), Taqman probes and Taqman Fast Advanced Master Mix from Life Technologies (Carlsbad, CA, USA).

4.1.2 Expression Assay

For quantitative gene detection, SYBR Green (Roche, Basel, Switzerland) was used as a fluorometric dye. Reactions were accomplished on the same device as Taqman mutation detection assays, but cycling conditions were adapted: After the initial step at 95°C for 10 minutes, 40 cycles of 95°C for 10 seconds and 58°C for 30 seconds followed; for melting curve analysis, samples were heated up to 95°C again for 15 seconds, afterwards samples were cooled to 60°C for one minute and re-heated again up to 95°C for 15 seconds.

Concerning the reaction mix, 5µL SYBR Green, 3.5µL RNAse-free water, 0.5µL forward and reverse 10µM Primers (Microsynth) and 1µL cDNA (the concentration of genomic DNA was 5ng/µL) were added to a total amount of 10µL.

Sequences of the primers used for expression assays using quantitative real-time PCR are shown in table 2.

Table 2. Sequences of primers used for quantitative detection of expression levels from 5`to 3`.

Gene	Forward Primer	Reverse Primer
BRAF	CGCCAAGTCAATCATCCACA	TCTGATGACTTCTGGTGCCA
C11ORF3	ATCTCAGCAGGGATGAATGC	ACTGCTCTCCGAACTTCAGC
TACC1	CCATGGATCCCTTTAAACCA	GCATGGCCATCCCTATTAGA
MAP3K8	TGTCCATCTCTTTATGGAAGC	TGCACAGGATGACCTCTGG
P27KIP1	CGAAGAGTTAACCCGGGACT	CCTCTAGGGGTTTGTGATTCTG
DUSP6	GAAATGGCGATCAGCAAGACG	CGACGACTCGTATAGCTCCTG
SPRY-2	ATCAGATCAGAGCCATCCGAA	TGGAGTCTCTCGTGTTTGTGC
BCL-6	AGCCCATAAAACGGTCCTCA	CGCAAATTGAGCCGAGATGT
GADD45A	AACGACATCAACATCCTGCG	TCCATGTAGCGACTTTCCCG

96-well plates (Life Technologies) served as a surface for DNA amplification - all samples were applied in triplicates. Afterwards, data obtained was analysed by Vii Software. Furthermore, data was processed using Microsoft Excel 2010 in order to normalize data to the house-keeping gene expression and expressed as fold change over control (ΔΔCT was normalized to control).

4.2 Digital PCR

Figure 4 gives on overall overview from sample preparation to final readout.

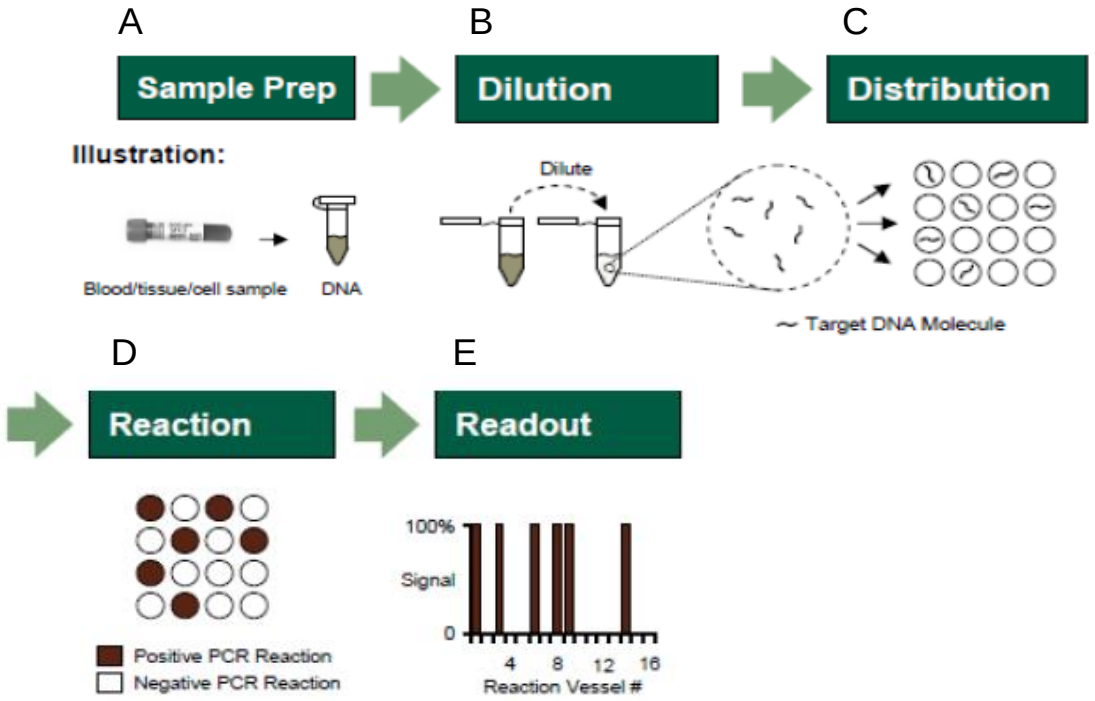

Figure 4. (**A**) DNA Isolation from PBMCs, Cryo samples, Paraffin blocks and cell pellets; genomic DNA as well as cDNA samples can be used for digital PCR. (**B**) Dilution of DNA in order to achieve a single copy of template per reaction once distributed. (**C**) Distribution of reaction mix in 20.000 reaction wells. (**D**) Common PCR reaction for single template amplification. (**E**) Determination of template molecules (copies/µL). Source: Life Technologies

Digital PCR was carried out using the AB Gene Amp PCR System 9700 (Applied Biosystems (Carlsbad, CA, USA)), the 15µL reaction mix consisted of the provided ready-to-use mastermix (AB Quant Studio 3D), equal amounts of primers and probes diluted to a final concentration of 4µM; Sequences of primers and probes are shown in table 1 in 4.1.1. Taqman Mutation Detection Assay. DNA concentration varied from 0.3ng/µL to 6.6ng/µL depending on the expected frequency of the target sequence. For chip loading the Quant Studio 3D Chip loader was used, conditions were adopted from Life Technologies instructions.

Thermocycling steps are shown in 3.

Table 3. Thermocycling conditions for template amplification on digital PCR Chips.

Stage	Step	Temp. (°C)	Time (mm:ss)
Hold	DNA polymerase activation	96	10:00
Cycling (39 cycles)	Anneal/Extend	60	02:00
	Denature	98	00:30
Hold	Final extension	60	02:00
Hold	Storage	10	∞

As soon as chips were heated to room temperature, fluorescence measurement was performed using the Quant Studio 3D and output was processed by Quant Studio 3D Analysis Suite Software. Fluorescence values were Poisson corrected and copies per µL were calculated by

$$Copies\ per\ \mu L = \ln\left(\frac{\#negatives}{\#total}\right) * \frac{1000}{0.865}$$

in due consideration of dilution factor. Every sample showing a precision higher than 15% and a copy number lower than the negative control was classified as negative for the specific mutation. Generally, we made use of the overall dPCR guidelines (Huggett et al.).

4.3 RNA Isolation

For RNA extraction from cell cultures, the cells were washed with 1x PBS (prepared by Kantonsapotheke Zurich) and thereafter resolved from the bottom by Trizol (Life Technologies); for 75mL flasks, 1mL of Trizol was used to break down the cellular components.

For Cryo-samples, Trizol was added until the tissue was completely covered. Samples were incubated for 5 minutes and then homogenized by mashing. The subsequent steps were equal for both samples types: 200µL chloroform (Sigma-Aldrich, St. Louis, MO, U.S.) were added to the samples, incubated for 5 minutes at room temperature and spun for 15 minutes at 4°C. After this, 3 different phases were visible whereof the upper phase was carefully transferred to a new sterile tube – as this phase contains the RNA; the interphase contained DNA and the chloroform phase contained the proteins. Afterwards, RNA was precipitated using 500µL isopropyl alcohol (Sigma-Aldrich). The precipitation mix was incubated for 10 minutes at room temperature and then spun for 10 minutes at maximum speed at 4°C; thereby RNA was pelleted. In the next step, RNA was washed 3 times with ethanol (Sigma-Aldrich) to improve the purity. Afterwards, the RNA pellet was air-dried upside down until all the residual ethanol had evaporated. RNA was resolved in 12µL RNAse free water and stored at -80°C. The concentration was measured using the spectrophotometer Nanodrop ND-1000 (Thermo Fisher Scientific (Waltham, Massachusetts, U.S.)).

Depending on further procedure, RNA samples were purified using the RNeasy Clean-up Kit from Qiagen (Venlo, Netherlands) including a DNAse step – if primers used for qPCR or dPCR were not exon spanning.

4.4 cDNA Generation

1µg of RNA were converted into cDNA. For cDNA generation, the kit Reverse Transcription System from Promega (Fitchburg, Wisconsin, U.S.) was used according to the manufacturer`s manual. Afterwards, samples were diluted 1:20 with RNAse free water.

4.5 DNA Isolation

4.5.1 DNA Isolation from Cells

Cells were pelleted for 5 minutes at 1500rpm in 1xPBS, PBS was aspirated and the pellet was resuspended in 200µL sterile 1xPBS. Further steps were accomplished according to the manufacturer`s protocol of the QIAamp DNA Blood Kit (Qiagen).

4.5.2 DNA Isolation from Cryo-Samples

Tissue samples were covered with extraction buffer: 1M Tris pH 8.0 (Ambion (Carlsbad, CA, USA)), 0.5M EDTA (Sigma-Aldrich), 0.5% Tween 20 (Sigma-Aldrich). Per 100µL extraction buffer, 20mg/mL Proteinase K (Roche) were added and incubated over night at 56°C shaking at 400rpm. After 12 hours, Proteinase K was inactivated at 96°C for 10 minutes. Samples were centrifuged at full speed for 10 minutes in order to spin down undissolved tissue residues. Afterwards, DNA isolation was processed using the QIAamp DNA Blood Kit (Qiagen).

4.5.3 DNA Isolation from Paraffin Blocks

For DNA isolation from paraffin blocks, the embedded tissue was punched in the malignant region of the material. To each punch, 1mL Xylene (Sigma-Aldrich) was added, vortexed vigorously for 10 seconds and centrifuged for 2 minutes at full speed. The supernatant was removed and 750µL Xylene were added, vortexed and centrifuged as before in the first step. The supernatant was used and processed with the instructions of the QIAamp DNA FFPE Tissue Kit (Qiagen).

4.6 Cytospin

$1x10^4$ cells were typsinized and centrifuged at 1500rpm for 5 minutes in RPMI medium in order to pellet the cells. The supernatant was discarded and the pellet was resuspended in 200µL 1xPBS/1%BSA (Sigma-Aldrich), cell suspension was applied onto the Cytospin applications and centrifuged for 5 minutes at 800rpm using Cytospin 3 (Shandon, Astmoor, England). After centrifugation, slides were dried and fixation was performed using pre-cooled aceton (Sigma-Aldrich). Slides were blocked with 250µL of 20% normal goat serum in Tris Buffered Saline with 1%BSA pH 8.0 (Sigma-Aldrich) and incubated for 30 minutes. Afterwards, blocking solution was removed and the primary antibody (Anti-TACC1 produced in rabbit; Sigma-Aldrich HPA024702) was diluted 1:100 in Dako Real Antibody Diluent (Dako (Santa Clara, CA, U.S.)) and incubated for 1 hour. Slides were washed with Washing Buffer (Dako) and the secondary antibody (Biotinylated Anti-Rabbit IgG, BA-1000) from Vectorlabs (Burlingame, CA, U.S.) was applied for 30 minutes in a 1:100 dilution using again the dilution reagent from Dako. Slides were washed using the same washing buffer as before and 150µL of a 1:100 dilution of Streptavidin/HRP (Dako) in TBS was applied

for 30 minutes, one washing step followed and AEC (Dako) as a substrate was added to the sample slides and incubated for 10 minutes. Counterstain was performed with Haematoxylin according to Mayer from Artechemis (Zofingen, Switzerland) for 30 seconds. Slides were washed with warm water and subsequently with deionized water and mounted with Mounting Medium (Dako).

4.7 MTT (Viability Test)

Day 1 – seed cells: $1x10^5$ cells were seeded into 24-well plates (Life Technologies), in whole 400µL medium were added per well. Cells were incubated for 24 hours.

Day 2 – drug treatment: As melanoma cells are adherent, the medium was discarded and new medium containing the appropriate concentration of the drug LGX-818 (Novartis, Basel, Switzerland) were added to the wells. A 1:1000 DMSO (Sigma-Aldrich) solution was added to these wells, which did not contain any drug treatment. The wells with DMSO served as control samples as the drug itself is also dissolved in DMSO. Cells were incubated until further processing.

Day 5 – MTT assay: All medium was removed from the wells and 250µL of fresh medium were added. Moreover, the MTT reagent (Sigma-Aldrich; diluted in 1xPBS) was adjoined to a final concentration of 2.5mg/mL MTT. After one hour of incubation, the medium containing the MTT was removed and 200µL of 95% Isopropanol/ 5% Formic Acid and 200µL of 10%SDS (all from Sigma-Aldrich) in 1xPBS were added and incubated for further 5 minutes. 200µL were transferred into a 96 well plate and absorbance was measured at 595nm (reference 620nm) using the BIO-RAD Model 550 Microplate Reader.

All incubation steps were performed at 37°C with 5% CO_2.

4.8 Sanger Sequencing

After DNA amplification, 12ng of each PCR product, 5x Terminator Sequencing Buffer from Applied Biosystems (Foster City, CA, U.S.), 1.5µM primers (Microsynth)

BRAF forward: 5`CTAAGAGGAAAGATGAAGTACTATG
reverse: 5`CTAGTAACTCAGCAGCATCTCAG
NRAS forward: 5`GATAGGCAGAAATGGGCTTGA
reverse: 5`ATCATCCTTTCAGAGAAAATAATGC

TACC1 forward: 5`CCATGGATCCCTTTAAACCA
reverse: 5`TAAACGCGACTTTGCCTTCT
pCMV-6 T7: 5`TAATACGACTCACTATAGGG

and 2µL of BigDye Ready reaction Mix (Applied Biosystems) were added up to a 10µL reaction mix in a 96-well plate. Cycling conditions were performed as follows: 60s at 96°C were followed by 16 cycles for 10s at 96°C, 5s at 50°C and 240s at 60°C in a usual Lab Cycler (Sensoquest, Göttingen, Germany). For sequencing of vector inserts longer than 200bp, 36 cycles were run with adapted time steps. Samples were purified using the Big Dye XTerminator purification Kit (Applied Biosystems) in order to get rid of any unused residues from the PCR reaction. The 96-well plate containing the samples was shaken for 30 minutes at 2000rpm on the MS 3 shaker (IKA, Wilmington, NC, U.S.). Afterwards, the plate was centrifuged for 5 minutes at 3000rpm in order to spin down the purification beads to the bottom of the wells. Subsequent Sanger Sequencing was carried out using the 3500 Genetic Analyzer (Applied Biosystems). Analysis was performed with the Variant Reporter Software (Life Technologies) where every mutation in the sequence which surpassed the threshold of 25% was classified as positive.

4.9 Isolation of Melanoma Cells from PBMCs

$1x10^7$ cells in total were used for isolating melanoma cells from PBMCs. The isolation was performed using the $CD56^+CD16^+$ NK cell isolation Kit Human from Miltenyi Biotec (Bergisch Gladbach, Germany) according to the manufacturer`s manual. Due to the manual the last step is a positive selection process for NK cells whereas the flow through contained the melanoma cells; other immune non-NK cells were depleted in the first step.
After collecting the flow through containing all non-immune cells, cells were pelleted for 5 minutes at 1500rpm and DNA isolation followed.

4.10 Transfection of Melanoma Cells

For transfection with siRNA or expression vector, cells were cultured in DMEM (Gibco (Carlsbad, CA, USA)) with 10% FCS instead of the usual RPMI medium.
Day 1 – seed cells: melanoma cells were seeded into 6-wells plates to a confluence of about 60%.

Day 2 – transfection:

Knock down: TACC1 siRNA 5`-AGGAGAUAUGAGAACCUGAATT with dTdT`-3 overhangs was ordered from Microsynth. siRNA was added to 400µL DMEM without FCS. 12µL INTERFERin® (Polyplus-transfection, Illkirch, France) were subjoined immediately and vortexed for 20 seconds; the final concentration of siRNA adds up to 200nM. Thereafter, the transfection mix was incubated for 30 minutes at room temperature to allow particle formation.

Medium from 6-well plates was aspirated and 1.6mL of fresh medium was added to the wells. Then, the transfection solution was added drop-wise to the wells.

AllStars negativ control siRNA (Qiagen) was used in the same concentration as applied siRNA.

Overexpression: pCMV-6 vector containing the whole TACC1 cDNA transcript variant 3 (NM_001146216.2) was ordered from Lab Force (Muttenz, Switzerland). For transfection, 1µg of the vector was diluted in 150nM NaCl (Braun (Melsungen, Germany)) to a final volume of 100µL. 12µL JetPEI® (Polyplus-transfection) was diluted in 150nM NaCl as well. The 100µL JetPEI® solution was added to the 100µL DNA solution and vortexed immediately. The transfection mix was incubated for 30 minutes at room temperature and 200µL of this mix were added drop-wise to each well.

Day 5 – analysis: RNA isolation and cDNA generation in order to analyze gene knock-down/overexpression by qPCR or protein isolation for further use for Western Blot.

4.11 Chemically Competent E.Coli, Transformation, MiniPrep

Day 1 – Inoculation of overnight culture: One colony of E.Coli strain DH5α was picked for overnight culture in 5mL liquid LB broth (Scharlau Microbiology, Barcelona, Spain) and shaked at 220rpm at 37°C.

Day 2 – Treatment: Re-inoculation of 500µL cells in 100mL of sterile LB medium in a sterile flask. The flask was incubated under the same conditions as on day 1, until an OD_{600} of 0.4 was reached.

All the following steps were accomplished at 4°C: As soon an OD_{600} of 0.4 was reached, cells were centrifuged at 400rpm for 10 minutes, the supernatant was discarded and the pellet was resuspended and washed with 30mL of buffer 1 containing 80mM $MgCl_2$ and 20mM $CaCl_2$ (both from Fluka, St.Louis, MO, U.S.)

dissolved in dH_2O. After washing three times, the cell pellet was resuspended in 2mL of buffer 2 composed of 100mM $CaCl_2$ and 15% glycerol (Fluka) dissolved in dH_2O. 50µL aliquots of the competent cells were made and stored at -80°C until usage for plasmid amplification.

For plasmid amplification, 50µL of chemically competent cells were thawed at 4°C, 200ng of the template plasmid were added and the whole mixture was incubated on ice for 20 minutes. Thereafter, cells were heat shocked for 45 seconds at 42°C and immediately put on ice for 2 more minutes. 900µL LB Borth was added and the composition was incubated for 90 minutes at 37°C. Afterwards, cells were plated onto LB agar plates (Scharlau Microbiology) containing the antibiotics, for which the cells containing the plasmid are resistant. For the plasmid containing the TACC1 transcript variant 3, the plates contained 50µg/µL Ampicillin (Sigma-Aldrich). After overnight incubation at 37°C, one colony was picked for overnight culture in LB Broth containing the same antibiotics concentration as the agar plates.
After 12 hours, bacteria were pelleted at 4000rpm for 5 minutes, the supernatant was discarded and plasmid isolation was accomplished using the QIAprep Spin Miniprep Kit (Qiagen).

4.12 PCR and Gel Electrophoresis

A 10µL reaction volume containing 1xAmpliTaq® 360 Buffer, 1mM Magnesium Chloride, 200µM of each nucleotide, 1µM of each Primer, 1.25U/reaction Amplitaq Gold® DNA Polymerase and <1ug of DNA were used for gene amplification by PCR. All reagents were purchased from Applied Biosystems except for primers (Microsynth) and Amplitaq Gold® DNA Polymerase (Roche). Amplification parameters are shown in table 4.

Table 4. Parameters for PCR gene amplification.

Stage	Step	Temp. (°C)	Time (mm:ss)
Hold	Initial denaturation	95	03:00
Cycle (36 cycles)	Denature	95	00:30
	Anneal	Primer T_m	00:30
	Extend	72	60 seconds/kb
Hold	Final extension	72	10:00
Hold	Final hold	4	∞

After the PCR, PCR products were loaded onto an agarose gel in order to prove gene amplification and specific binding of the primers. Therefore, 6x loading dye (Thermo Fisher Scientific) were added to the samples in order to have a final dilution of 1x. PCR products were then loaded onto a 1% agarose gel (BioRad). Agarose was dissolved in 1xTAE buffer containing Gel Red (Biotium, Hayward, CA, U.S.) in an overall dilution of 1:10000; 100 Volts were applied for 30 minutes. 3µL of GeneRuler DNA ladder mix (Thermo Fisher Scientific) were loaded; Figure 5 shows specific bands of the ladder mix.

50xTAE was produced by dissolving 242g Triszma (Sigma-Aldrich) in 800mL dH_2O, 100mL of 0.5M EDTA (Fluka) and 57.1mL glacial acetic acid (Merck, Darmstadt, Germany) were added and filled up to 1L.

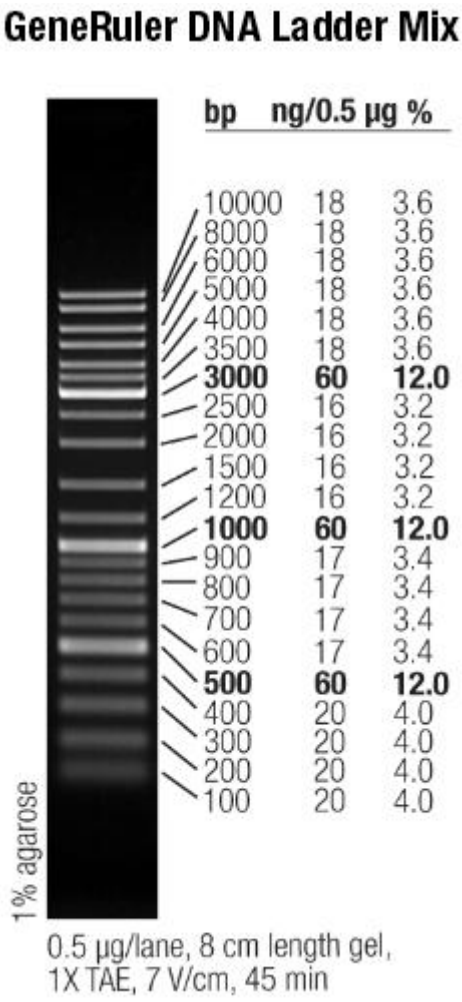

Figure 5. Scheme of DNA ladder mix

4.13 BrdU – Proliferation Assay

Day 1 – seed cells: Cells were seeded in a 24-well plate to the confluence of 60%, the total volume was 400µL per well.

Day 2 – transfection: Knock down or overexpression of a specific gene as described in 4.10. Transfection of melanoma cells.

.Day 5 – add BrdU: BrdU reagent was diluted 1:500 in cell culture medium and 40µL of this solution was added to the wells.

Day 6 – staining: Staining procedure was adopted from the instructor's manual (Merck Millipore, Billerica, MA, U.S.) samples were transferred to a 96-well plate and fluorescence was read at 450nm (reference 550nm) with the BIO-RAD Model 550 Microplate Reader.

4.14 Protein Isolation and Western Blot

For protein isolation, cell culture flasks or dishes were placed onto a metal plate on ice. Cells were washed 2 times with cold 1xPBS and RIPA Buffer was added until the cells were totally covered. RIPA buffer contained 20mM Tris-HCl pH 7.5 (Sigma-Aldrich), 150mM NaCl, 5mM EDTA (both from Fluka), 1% (v/v) Triton-X 100, 1mM Na_3VO_4 (both from Sigma-Aldrich), 1 tablet of protease inhibitor per 50 ml (Roche) and 1mL phosphatase inhibitor (Sigma-Aldrich) per 100 ml total buffer solution. Cells were incubated for at least 5 minutes and scraped until cells were detached from the bottom. The cells and the RIPA Buffer were transferred into a microcentrifuge tube, vortexed and spun at full speed for 20 minutes at 4°C. The supernatant was transferred into a new tube and stored at -80°C until further procedure.

Protein concentration was measured using the DC Protein Assay (Bio-Rad) based on the Bradford method and due to the manufacturer`s protocol. 20ug of protein was loaded onto the gel for subsequent western blot.

All western blot material and reagents were purchased from Life Technologies. For loading the gel, 9µL of loading dye buffer and 3.6µL of sample reducing were added to 23.4µL of protein dilution (in RIPA). The mixture was incubated at 85°C for 10 minutes at 900rpm. The 10% Bis-Tris Gel was unwrapped, tape strip was taken off and the gel was rinsed with dH_2O. The comb was removed and the gel was rinsed again with running buffer. 20x running buffer was diluted to 1x in dH_2O, 200mL of this buffer were added in the middle of the chamber and the remaining solution was distributed in the outside of the cell. The samples and the ladder (1x SeeBlue® Plus 2 Standard) were loaded and the gel was run at 160V for approximately one hour, until the band reached the end of the gel.

After protein separation, the membrane, papers and pads were incubated in transfer buffer. Transfer buffer contained 1x Transfer Buffer and 20% Methanol (Sigma-Aldrich) in dH_2O. For the transfer, the cell was put together as follows from bottom to the top: 3 pads, 1 paper, gel, membrane, 1 pad, 2 pads. The air was removed in order to avoid incomplete transfer of the proteins to the membrane due to air bubble formation. The blot module was placed into the chamber which was filled with transfer buffer inside and with ice water outside; 30V were applied for 90 minutes.

For antibody incubations, the membrane was placed into a plastic box and washed 3 times with 1xTBST (136.9mM NaCl (Fluka), 2.7mM KCl, 24.8mM Tris Base, 1%Tween (all from Sigma-Aldrich) in ddH_20). The membrane was blocked with a

mixture of 5% milk powder (Rapilait, Zurich, Switzerland) and 1% BSA (Sigma-Aldrich) in TBST for 2 hours at room temperature or overnight at 4°C. After blocking, incubation with 10mL of primary antibody diluted in 5% BSA (Sigma-Aldrich) for 2 hours followed at room temperature or overnight at 4°C. Three washing steps with TBST followed. The secondary antibody was diluted as well in 10mL of the 5% milk/1% BSA solution and was incubated for 1 hour at room temperature. The membrane was washed three times with TBST and ECL prime solution was added until the membrane was covered; especially at these regions were the target protein was expected due to the known size. In the dark room, the films were exposed to the membrane for different periods of time and developed using the Fujifilm FPM 800A.
Details concerning antibody dilutions and manufacturers are shown in Table 5.

Table 5. Target proteins for Western Blot analysis.

Target Protein	Size	Dilution	Catalog No.	Company/Head Office
TACC1	125kDa	1:250	HPA024702	Sigma-Aldrich/St. Louis, MO, U.S.
ERK 1/2	44/42kDa	1:1000	4695	Cell Signaling Technology/Danvers, MA, U.S.
pERK 1/2	44/42kDa	1:2000	4370	Cell Signaling Technology/Danvers, MA, U.S.
GAPDH	36kDa	1:5000	9385	Abcam/Cambridge, England

The secondary antibody goat anti-rabbit IgG was purchased from Santa Cruz (Dallas, TX, U.S.) and diluted 1:8000 for all the target proteins mentioned above except for GAPDH; Anti-GAPDH antibody was directly labelled with HRP and served as a loading control.

4.15 Cell Culture

Cells were kept in a Heraeus BBD 6220 incubator under the conditions of 37°C, 5% CO_2 and 85% rH. Working procedure with cells was conducted sterilely in the laminar flow hood. Generally, all tools and materials used in the hood were disinfected with 70% ethanol before usage.
Medium change was performed every 3 days to avoid that cells grew under acidic conditions (acidic conditions are seen by color change of medium from red to yellow would have represented that). Cells in culture were usually grown in RPMI1640 (Invitrogen, Carlsbad, CA, U.S.) supplemented with 5mM L-glutamine (Biochrom, Berlin, Germany), 1mM sodium pyruvate and 10% FCS (both from Gibco).
Cells were split as soon as cells reached a confluence about 80-90%, the medium was aspirated and cells were washed one time with 1x PBS. Trypsin (Biochrom) was

added until cells were totally covered. After 3-5 minutes of incubation time, cells were detached, which was also checked under the microscope. The floating cells were transferred to a 15mL tube; 5mL of medium was added and cells were pelleted at 1500rpm for 5 minutes. The supernatant was discarded and the cell pellet was resuspended in 1mL medium and 4mL were added additionally. 1mL of this solution was transferred into a new flask and filled up with additional medium.

The resulting values are shown as mean of biological and technical triplicates. The statistical significance (p value) was calculated using a two-sided t-test and p values of 0.05 and below were considered as statistically significant and marked (*) in the figures.

5 Results

5.1 Validation of Exome Sequencing

Through Sanger sequencing we validated the presence of *BRAF*^{V600E} in a patient`s tumor samples and in the cell line. Additionally, we detected *NRAS*^{Q61K} in one of the samples and found out that these two mutations occurred in the same cell. Moreover, we confirmed the resistance of this cell line to the BRAF inhibitor LGX818 by MTT viability assay and ruled out possible resistance mechanisms which are already known from literature.

We analyzed the tumor samples for candidate genes that developed mutations during the treatment and were common in all of the resistant metastases. We did so by WES and started to investigate one of these genes (*TACC1*) more closely.

Furthermore, we made use of digital PCR in order to re-confirm *BRAF*^{V600E} in the samples and additionally to rule out the presence of *NRAS*^{Q61K} in all but one metastasis. We also detected mutated *TACC1* in all of the resistant metastases and isolated melanoma cells from the blood.

5.1.1 Detection of BRAF^{V600E}

Tumor samples of a patient suffering from melanoma carrying *BRAF*^{V600E} and treated with the BRAF inhibitor LGX818 were sent to exome sequencing. The samples included tissue material that was excised after the patient had become resistant to the BRAF inhibitor. In order to confirm the presence of *BRAF*^{V600E}, I performed Sanger sequencing of all tumor samples (data not shown). Additionally, I sequenced two late metastases and one cell line that was derived from another late metastasis on the cDNA level. The sequencing results for the cDNA samples are shown in figure 6.

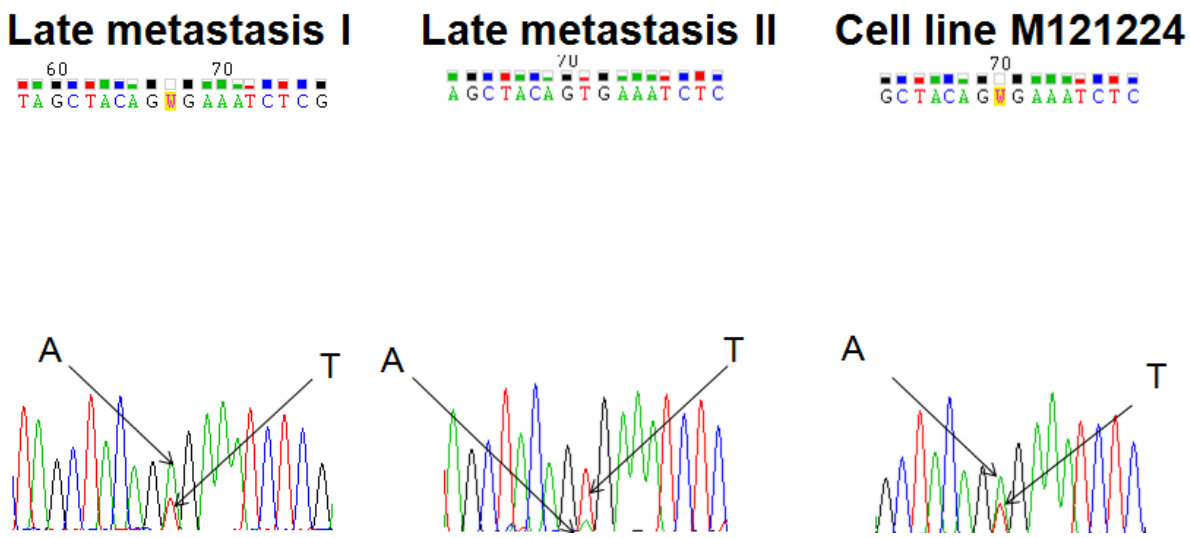

Figure 6. cDNA sequences of the late metastasis (left, middle) and the cell line (right). W in the sequence indicates that the base is either A or T which gives the trinucleotide GTG and therefore the amino acid valine (V) for *BRAF*^{wt} or GAG and consequently the amino acid glutamic acid (E) for *BRAF*^{V600E}.

The *BRAF*^{V600E} was detectable in each of the Sanger sequenced samples. Concerning the late metastasis II, the percentage of analyzed mutated versions of the gene is below the 25% threshold and was therefore not labeled with W in the sequence. However, there is a small heterogeneous peak of alanine visible. Furthermore, the percentage of the mutated gene is also dependent on the tissue material which predominately does not contain pure tumor material.

5.1.2 Confirmation of Resistance

To confirm the resistance of progressive late metastases for the BRAF inhibitor, I performed a viability assay (MTT) with the patient-derived cell line (M121224) and a control cell line (M000921), which also carried the *BRAF*^{V600E} mutation but had been derived from a patient who did not suffer from progressive disease. The data are shown in figure 7.

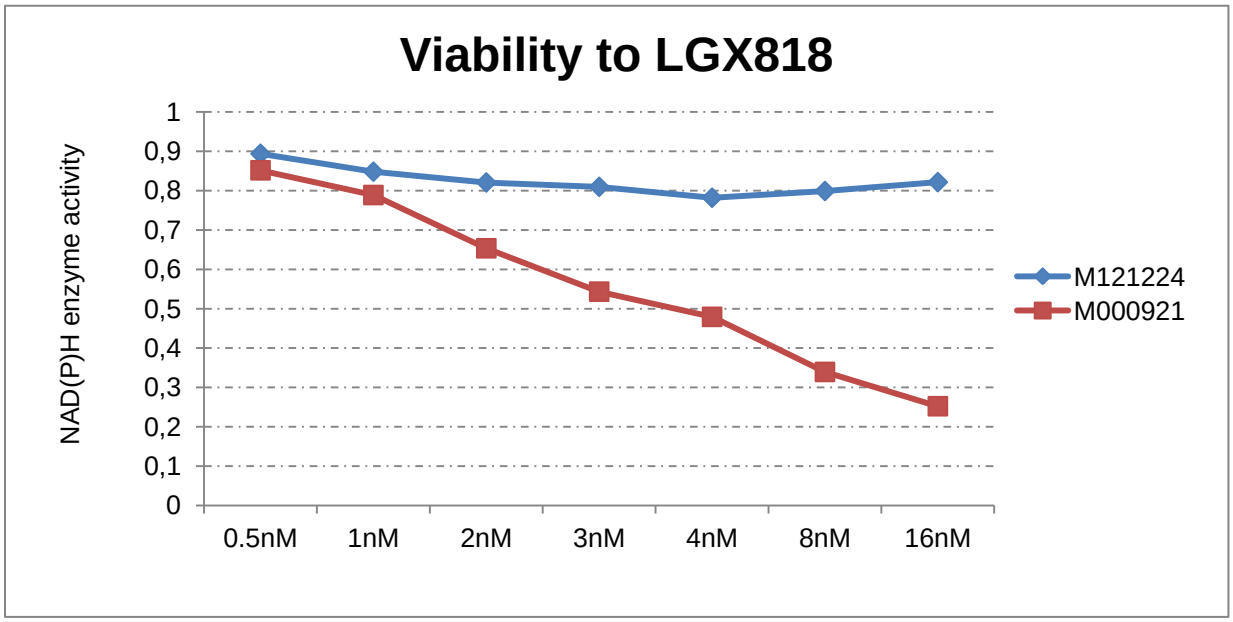

Figure 7. Viability assay for a resistant (M121224) and a non-resistant (M000921) cell line due to treatment with the BRAF inhibitor LGX818.

As expected, the control cell line (M000921) is sensitive to LGX, whereas the cell line derived from a late metastasis (M121224) of the patient treated with LGX is resistant to the drug.

5.1.3 Ruling Out Known Resistance Mechanisms

In order to find new resistance mechanisms, it was important to eliminate known ones such as the expression of *Cot1*. Therefore, I performed RT-qPCR amplification of Cot1 with the result that neither the late metastases (I and II) nor the cell line (M121224) expressed this gene, whereas the house keeping gene was regularly amplified (data not shown).

Moreover, it was possible to replace the function of *BRAF* by another isoform of the *RAF* genes which lack the V600E mutation at all or the mutation is not localized in the ATP-binding pocket. I excluded this by amplifying the 230bp around the predicted point mutation. The results in figure 8 show an agarose gel with the amplified products.

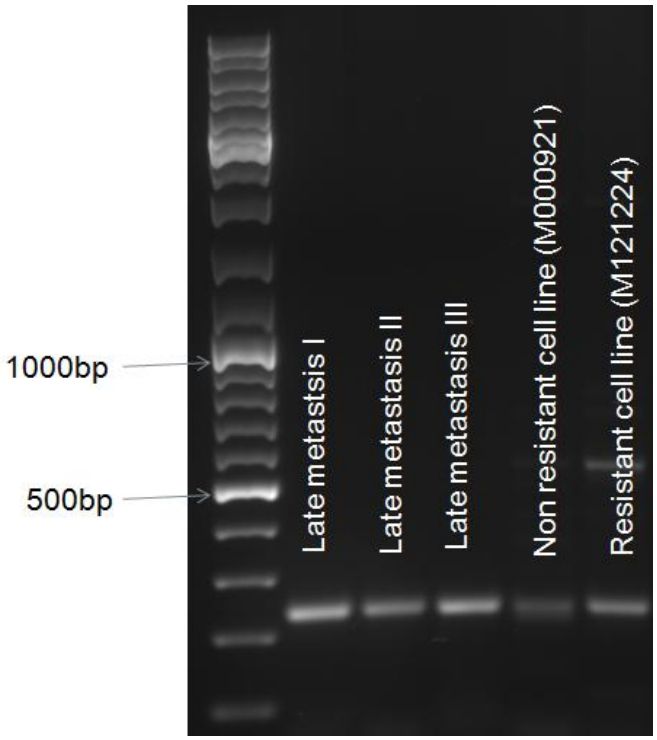

Figure 8. Amplified *BRAF* fragment of 3 late metastases, the cell line derived from the patient`s late metastasis (M121224) and a non-resistant cell line (M000921) at a size of approximately 220bp.

All amplified cDNA samples showed the same size of the product which suggests that there was no difference in splicing between LGX-resistant samples (late metastases I/II/III and cell line M121224) and LGX-sensitive samples. As there was also a band visible that was about 600bp of size, I cut out this piece of gel, extracted the amplified product and did Sanger sequencing, which revealed that the product was an artifact (data not shown). I also performed Sanger sequencing of the patient`s resistant cell line (M121224) and identified an additional $NRAS^{Q61K}$ mutation besides the existing $BRAF^{V600E}$. Hereupon, this cell line was single cell sorted and every culture derived from a single clone (23 clones) was Sanger-sequenced (Figure 9).

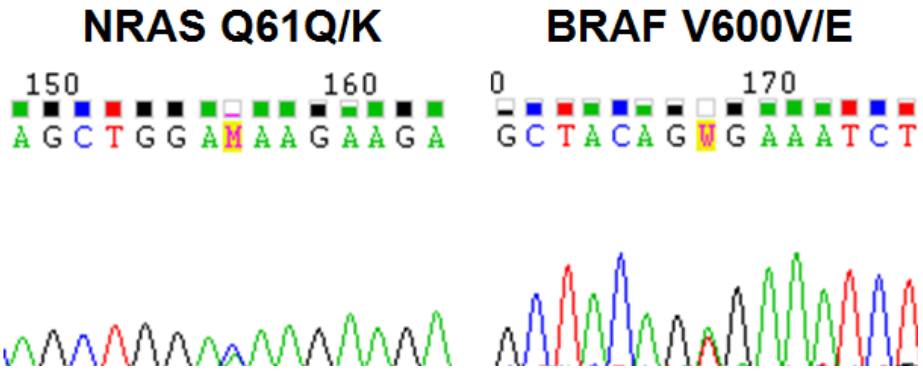

.

Figure 9. Sequences of *NRAS* and *BRAF* from clone No.3; NRAS: M in the sequence stands for base C or A and the trinucleotide CAA for the amino acid glutamine (Q) and therefore for $NRAS^{wt}$ and the trinucleotide AAA codes for lysine (K) which indicates the mutated version of *NRAS*. *BRAF*: See figure 4.

The *NRAS*^{Q61K} and the *BRAF*^{V600E} mutation were identified in each of the 23 sorted clone cultures. Thus, the *NRAS*^{Q61K} mutation is only present in the cell line derived from a late metastasis. As all of the late metastases were progressive, this mutation can be ruled out as a possible resistance mechanism due to the fact that it was absent in all of the other metastases (data shown in 5.1.5. Validation by digital PCR).

5.1.4 Candidate Genes Causing Resistance

Whole exome sequencing data identified 13 gene mutations which all of the late metastases had in common but were neither present in the primary tumor nor in the metastases excised before the treatment. The obtained 13 genes with the localization of the specific mutation are shown in table 6.

Table 6. Data from whole exome sequencing reveal 13 mutations which are exclusively present in the late/resistant metastases.

Gene	Mutation
NFASC	NFASC:NM_001160331:exon13:c.T1667G:p.V556G,NFASC:NM_001160333:exon14:c.T1616G:p.V539G,NFASC:NM_001005389:exon15:c.T1634G:p.V545G,NFASC:NM_015090:exon15:c.T1667G:p.V556G,NFASC:NM_001160332:exon15:c.T1667G:p.V556G,NFASC:NM_001005388:exon15:c.T1634G:p.V545G,
ARMC4	ARMC4:NM_018076:exon18:c.G2630T:p.R877L,
C11orf30	C11orf30:NM_020193:exon2:c.A66T:p.K22N,
ZNF267	ZNF267:NM_003414:exon4:c.G437A:p.S146N,ZNF267:NM_001265588:exon5:c.G341A:p.S114N,
NOD2	NOD2:NM_022162:exon4:c.G1403A:p.R468H,
LYPD5	LYPD5:NM_182573:exon4:c.T322G:p.S108A,LYPD5:NM_001031749:exon4:c.T451G:p.S151A,
SPTBN1	SPTBN1:NM_178313:exon15:c.G3508T:p.A1170S,SPTBN1:NM_003128:exon16:c.G3547T:p.A1183S,
CCDC48	CCDC48:NM_024768:exon5:c.G1284C:p.R428S,
ADAMTS19	ADAMTS19:NM_133638:exon23:c.G3507T:p.W1169C,
SNAP91	SNAP91:NM_001242792:exon26:c.C2503A:p.Q835K,SNAP91:NM_014841:exon26:c.C2503A:p.Q835K,SNAP91:NM_001256717:exon27:c.C2230A:p.Q744K,SNAP91:NM_001242793:exon25:c.C2413A:p.Q805K,SNAP91:NM_001256718:exon25:c.C2131A:p.Q711K,SNAP91:NM_001242794:exon17:c.C1582A:p.
HEATR2	HEATR2:NM_017802:exon1:c.C550A:p.R184S,
ABCA13	ABCA13:NM_152701:exon18:c.C7817A:p.P2606H,
TACC1	TACC1:NM_006283:exon3:c.T1354G:p.L452V,TACC1:NM_001146216:exon3:c.T769G:p.L257V,

All of the resistant metastases had these 13 mutations in common suggesting that one of these genes may be a driver in drug resistance. Due to these data shown in figure 6, we selected two genes (*c11orf30* and *TACC1*) which were already known to have an impact on breast cancer and ovarian cancer. Hence, I Sanger sequenced tumor tissue of the late metastases for these genes. Sequencing results for *TACC1*^{L452V} are shown in figure 10, results for *c11orf30*^{K22N} are not shown. Concerning *TACC1*, exome sequencing revealed two mutations, namely L452V and L257V; both mutations have the same amino acid change, but the different positions in the protein originate from the alternative splicing upstream of exon 3.

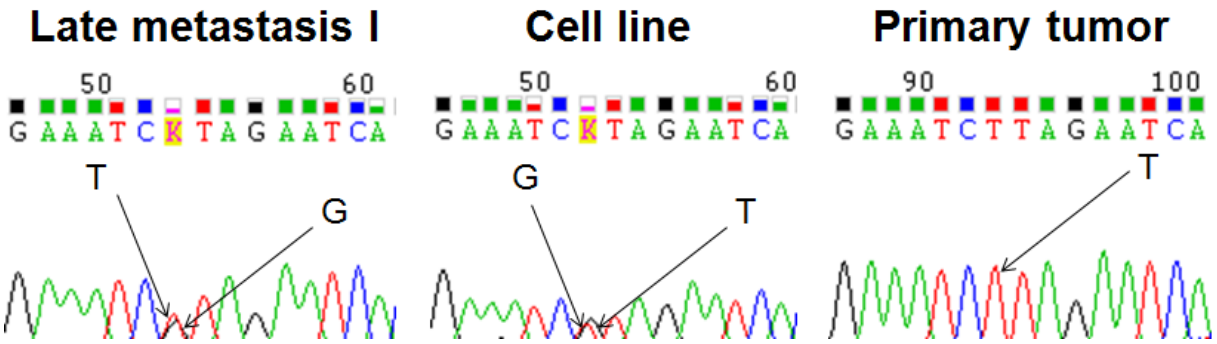

Figure 10. *TACC1* sequencing for L452V; K stand either for G or T, whereas the trinucleotide TTA codes for leucine and thus for the WT gene and the G for GTA, which is translated into valine which indicates *TACC1*^{L452V}.

TACC1^{L452V} was obviously present in the late metastasis I and in the cell line – as it was predicted from exome sequencing. There was no mutation in the primary tumor which assumed that the mutation appeared during the LGX-treatment and therefore most probably has an influence on resistance mechanisms.

As *TACC1* plays a known role in Aurora Kinase regulation and therefore is supposed to have an impact on proliferation, we further focused on that gene and its function in melanoma cells.

5.1.5 Validation by Digital PCR

To screen all the tumor samples which were available from this patient, I accomplished digital PCR using Taqman probes for *BRAF*^{V600E}, *NRAS*^{Q61K} and *TACC1*^{L452V}. As we found one late metastasis that carried *NRAS*^{Q61K} we also screened the other tumor samples for that specific mutation.

For *BRAF*^{V600E} and *NRAS*^{Q61K}, I performed relative quantification to address the exact copy numbers in the same sample. As dPCR is quite sensitive, comparing two dPCR chips is not recommended because copy numbers might vary due to a known variance in chip loading. Data for relative quantification are shown in table 7.

Table 7. Digital PCR data from relative quantification (*BRAF*^{V600E} vs. *NRAS*^{Q61K}) including copies/microliter, CI (confidence interval) and precision for each mutation.

Sample	Copies/microliter BRAF^{V600E}	CI Copies/microliter BRAF^{V600E}	Precision BRAF^{V600E}	Copies/microliter NRAS^{Q61K}	CI Copies/microliter NRAS^{Q61K}	Precision NRAS^{Q61K}
neg. control	34.64	28.557 -- 42.02	21.30%	27.898	22.497 -- 34.594	24.00%
blood	15.776	11.095 -- 22.433	42.19%	13.739	9.422 -- 20.034	45.82%
nevus I	9.247	7.811 -- 10.946	18.38%	5.882	4.761 -- 7.266	23.53%
primary	356.17	339.28 -- 373.9	4.98%	12.887	10.067 -- 16.496	28.01%
early met II	775.6	754.86 -- 796.91	2.75%	5.501	4.093 -- 7.392	34.38%
late met I	174.2	165.22 -- 183.67	5.44%	8.945	7.112 -- 11.252	25.78%
late met II	273.99	260.34 -- 288.36	5.24%	18.581	15.332 -- 22.519	21.19%
late met IV	35.058	32.285 -- 38.068	8.59%	3.789	2.954 -- 4.86	28.26%
late met V	57.048	51.101 -- 63.686	11.64%	12.151	9.581 -- 15.411	26.83%
late met VI	7469.5	7328.9 -- 7612.7	1.92%	12251	12017 -- 12490	1.95%

Using digital PCR, I could demonstrate that *BRAF*^{V600E} is present in all the metastases and in the primary tumor. The patient`s blood and the nevus I were both negative for the mutation; both DNA samples showed a lower copy number than the negative control sample and additionally had a precision higher than 15%. A precision of 15% was set as a threshold meaning that every sample which has a precision higher than 15% was determined as negative for the screened mutation.

Furthermore, I could verify *NRAS*^{Q61K} in the late metastasis VI which provided the cell line M121224. None of the other samples showed a copy number per microliter higher than the negative control and the according precision was always higher than 15%. Therefore *NRAS*^{Q61K} was only detectable in one of the resistant metastases which ruled it out as a possible shared resistance mechanism in the whole patient.

Moreover, it should be taken into consideration that the copy numbers varied within a large interval because the extracted DNA also contained non-tumorigenic material which did not carry one of the mutations.

In addition to the relative quantification, I also performed absolute quantification for *TACC1*^{L452V} to demonstrate the presence and absence in the tumor samples. The results are shown in table 8.

Table 8. Digital PCR results for absolute quantification of *TACC1*^{L452V} copy numbers; positive samples are red-rimmed.

Sample	Copies/microliter TACC1^{L452V}	CI Copies/microliter TACC1^{L452V}	Precision TACC1^{L452V}
neg. control	10.058	7.916 -- 12.779	46.87%
blood	56.124	46.894 -- 67.171	19.68%
primary	6.151	4.529 -- 8.353	35.81%
early met II	9.022	7.173 -- 11.348	25.78%
late met I	426.97	411.86 -- 442.63	3.67%
late met II	100.82	95.049 -- 106.95	6.07%
late met IV	212.55	205.17 -- 220.2	3.60%
late met V	27.718	24.802 -- 30.976	11.76%
late met VI	46.038	39.033 -- 54.3	17.95%

All the samples taken from before the treatment (blood, primary and early met II) are negative for *TACC1*^{L452V}. For each of these samples, the precision is higher than 15% and the *TACC1*^{L452V} was found in all of the resistant metastases excised after the treatment; the copy numbers are all higher than the value for the negative control and the precision was below 15% for all samples except for the late met VI. Concerning the late metastasis VI, the precision was indeed higher than 15%, but from Sanger sequencing we knew that the DNA carried *TACC1*^{L452V} (figure 11).

Figure 11. DNA fragment of *TACC1* carrying the L452V mutation. For explanation of the base pair change in the sequence and the corresponding amino acid change in the protein, see figure 8.

Sanger sequencing confirmed *TACC1*^{L452V} in the late metastasis VI, hence all resistant/late metastases carried this specific mutation which had occurred during the treatment.

For relative and absolute quantification, the negative control sample was derived from normal healthy skin.

5.1.6 Detection of Melanoma Cells in the Blood

In order to isolate circulating melanoma cells, I depleted all the immune cells and accomplished all the following experiments with DNA from cells which were present in the flow through of the depletion column.

Firstly, I performed Sanger sequencing for this sample in order to detect *BRAF*^{V600E} but the sequence did not show any heterozygous peak and was therefore rated negative for the mutation (data not shown).

Secondly, I used digital PCR for mutation detection as it was much more sensitive than Sanger sequencing. The data for the *BRAF*^{V600E} detection are shown in table 9.

Table 9. Digital PCR results for absolute quantification of *BRAF*^{V600E} copies.

Sample	Copies/microliter $BRAF^{V600E}$	CI Copies/microliter $BRAF^{V600E}$	Precision $BRAF^{V600E}$
neg. control	2.214	1.574 -- 3.115	40.66%
blood	435.58	422.77 -- 448.78	3.03%

The isolated DNA was derived from the same blood sample which I had already used for relative quantification in 5.1.5. Validation by digital PCR. However, the sample was negative for *BRAF*^{V600E} in relative quantification but gave reasonable results for absolute quantification: The precision was far below the set threshold of 15% and showed a higher copy number than the negative control. These results suggest that there were *BRAF*^{V600E} melanoma cells present in the blood. Therefore it is probably positive in low levels but to confirm this result other approaches (e.g. deep sequencing) should be used.

The negative control sample was derived from a melanoma patient who had been screened negative for *BRAF*^{V600E}.

5.2 Functional Analysis of TACC1

The fact that *TACC1*^{L452V} was present in all of the resistant tumor samples from excised after the treatment contributes – together with the Kaplan-Meier survival curve (Figure 12) for *TACC1*^{WT} – that it acted as a tumor suppressor and that its function was lost during the treatment due to the mutation L452V.

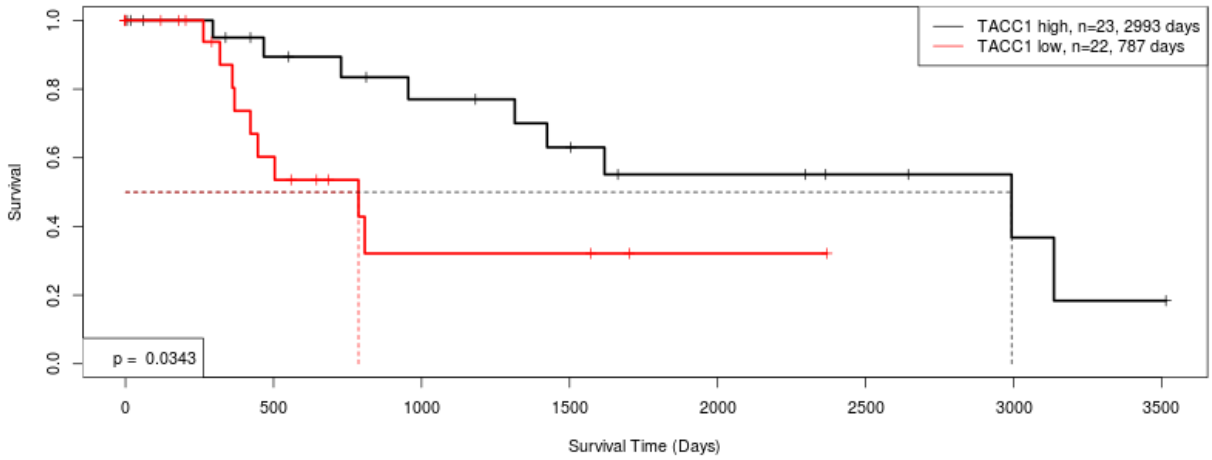

Figure 12. Kaplan-Meier survival curve for *TACC1* comparing the differences in survival depending on high and low expression.

The Kaplan-Meier survival curve suggested that *TACC1* acted as a tumor suppressor because patients expressing high levels of *TACC1* survive longer than those expressing low levels.

Moreover, we performed tissue micro arrays in order to demonstrate that *TACC1* was present in a majority of melanoma samples. Figure 13 shows a positive and a negative example for the protein staining.

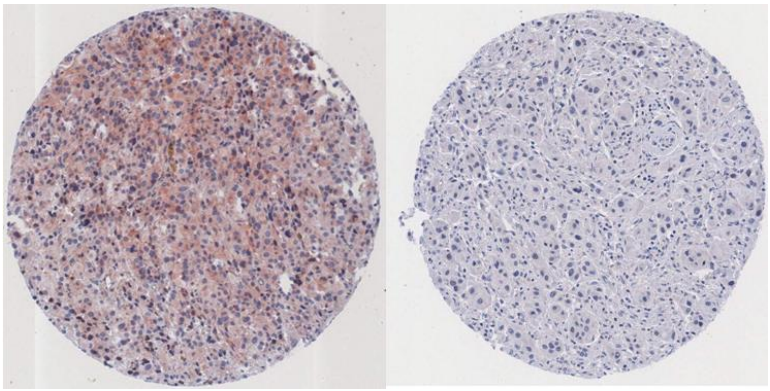

Figure 13. Tissue micro arrays from melanoma samples; examples for positive staining (left) and negative staining (right).

We performed tissue micro arrays of 269 melanoma samples and these data showed that Tacc1 was present in 88% of the screened tumor samples which suggests it plays a role not even in breast cancer and colon cancer but also in melanoma.

Hence, I performed siRNA knock down and overexpression of the gene and compared the impact on proliferation and viability between resistant and non-resistant cell lines M121224 (*BRAF*^{V600E}/*TACC1*^{L452V}) and M000921 (*BRAF*^{V600E}/*TACC1*^{L452L}). Additionally, I investigated the influence of *TACC1* expression on the MAPK pathway as this was the most affected one causing melanoma.

5.2.1 Confirmation of Knock Down and Overexpression of TACC1

In order to accomplish the following experiments, I tested the knock down and the overexpression of *TACC1* concerning their efficiency on the non-resistant cell line. Figure 14 shows the differences in expression on protein levels, the differences on RNA levels showed the same results (data not shown).

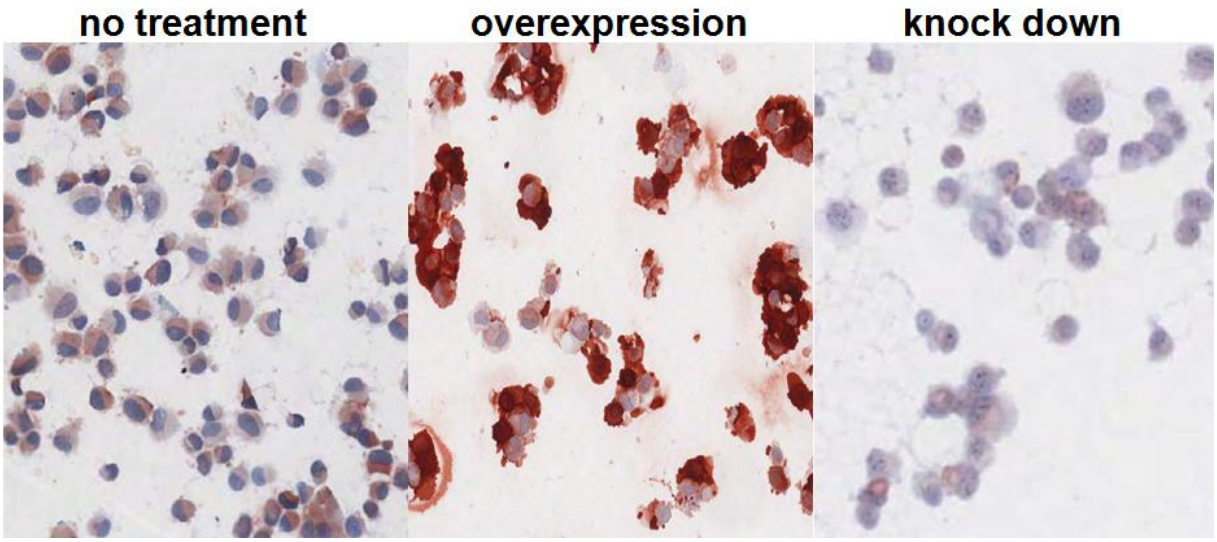

Figure 14. Cytospins of the cell line M000921(*BRAF*^{V600E}/*TACC1*^{L452L}) showing untreated cells (left), cells treated with overexpression vector (middle) and cells treated with siRNA (right).

Cytospins and qPCR showed that expression levels increased/decreased as expected; consequently the overexpression as well as the knock down were successful. Hence, the further experiments were conducted using the same concentrations and procedures.

5.2.2 Influence of TACC1 on Proliferation and Viability

To test the hypothesis that TACC1 acted as a tumor suppressor, I performed a proliferation assay (BrdU assay) on the resistant (M000921) and the non-resistant (M121224) cell lines. Figure 15 shows the results for the knock down and the overexpression.

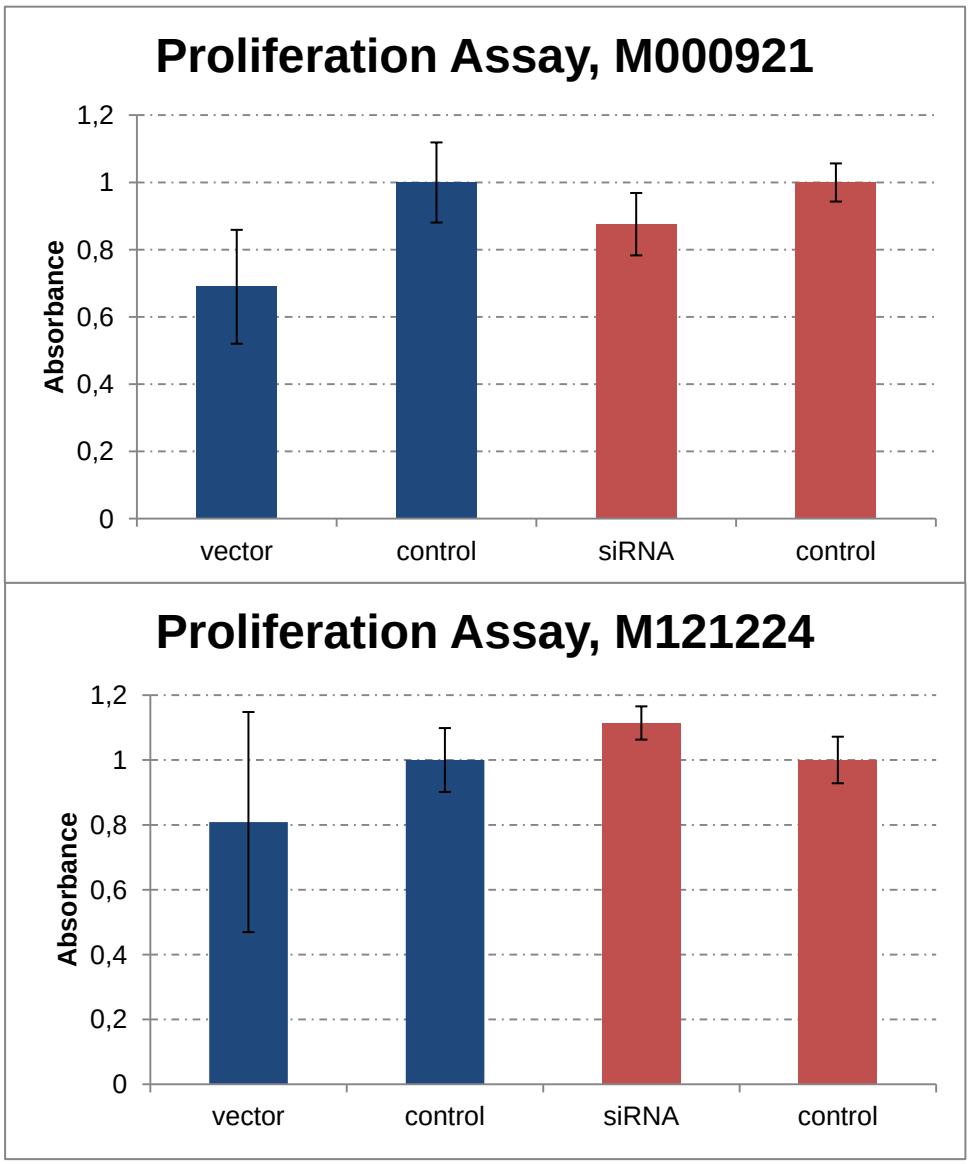

Figure 15. Absorbance of samples treated with overexpression vector and siRNA, the absorbance of samples treated with the vector and the correspnding control are shown in blue, the siRNA treated samples and the corresponding control are shown in red.

The proliferation of the cell line M000921 did not show any significant differences between the overexpression and the knock down of *TACC1*, whereas results of the M121224 (resistant) cell line supported the assumption of *TACC1* acting as a tumor suppressor because the signal for the overexpression was slightly lower than for the

control and the signal for the siRNA treated samples were higher than the corresponding scrambled control suggesting that the cells were more proliferative when *TACC1* had been knocked down and the other way round concerning the overexpression. However, none of these results was statistically significant and thus I made use of another approach to find out if the overexpression and the knock down did have an impact on cell growth. I then performed a viability assay (MTT assay) with the same cell lines under the same conditions as the proliferation assay and gained the results shown in figure 16.

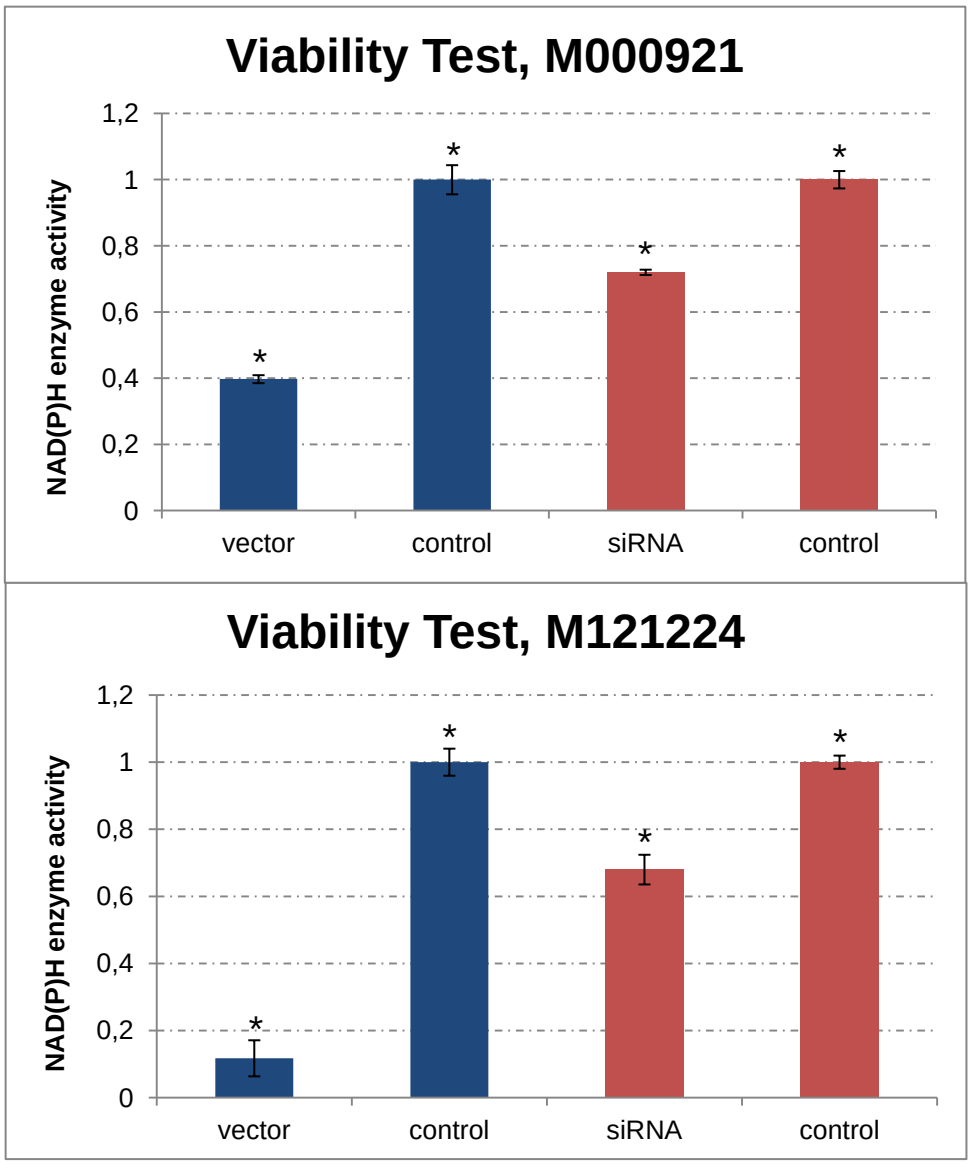

Figure 16. Measured absorbance of treated samples as a function of enzyme activity; samples treated with the overexpression vector are shown in blue, samples treated with siRNA are shown in red. All values were statistically significant.

Both cell lines treated with the vector or the siRNA showed an explicit and significant decrease of viability which suggested that the differences in *TACC1* expression made

the cells more viable. Moreover, the change in viability for the cells overexpressing *TACC1* is more significant than the cells treated with siRNA. However, the resistant (M121224) and the non-resistant (M000921) cells both showed the same signal patterns which leads to the conclusion that *TACC1* probably did not have an influence on resistance.

As our results showed, the resistant cell line (M121224) was less proliferative and less viable when transfected with the overexpression vector. Therefore, the expression of *TACC1* in high levels did not show a gain of function concerning survival of the cells.

I additionally transfected another resistant cell line and another non-resistant cell line with the overexpression vector and could also demonstrate a clear decrease in viability compared to the control (data not shown).

It should be mentioned that the M121224 cells were hardly viable after being treated with the overexpression vector (data not shown).

5.2.3 TACC1 and its Role in Resistance

To test the hypothesis that TACC1 did not have an influence on resistance further, I accomplished the following experiment: I transfected the cell lines with siRNA and afterwards treated them with the BRAF inhibitor LGX-818 which was also used to treat the patients of whom the two cell lines had been derived. I then performed an MTT viability test because we had aready made use of this test in order to confirm the resistance of M121224 (see 5.1.2. Confirmation of resistance). The results are shown in figure 17.

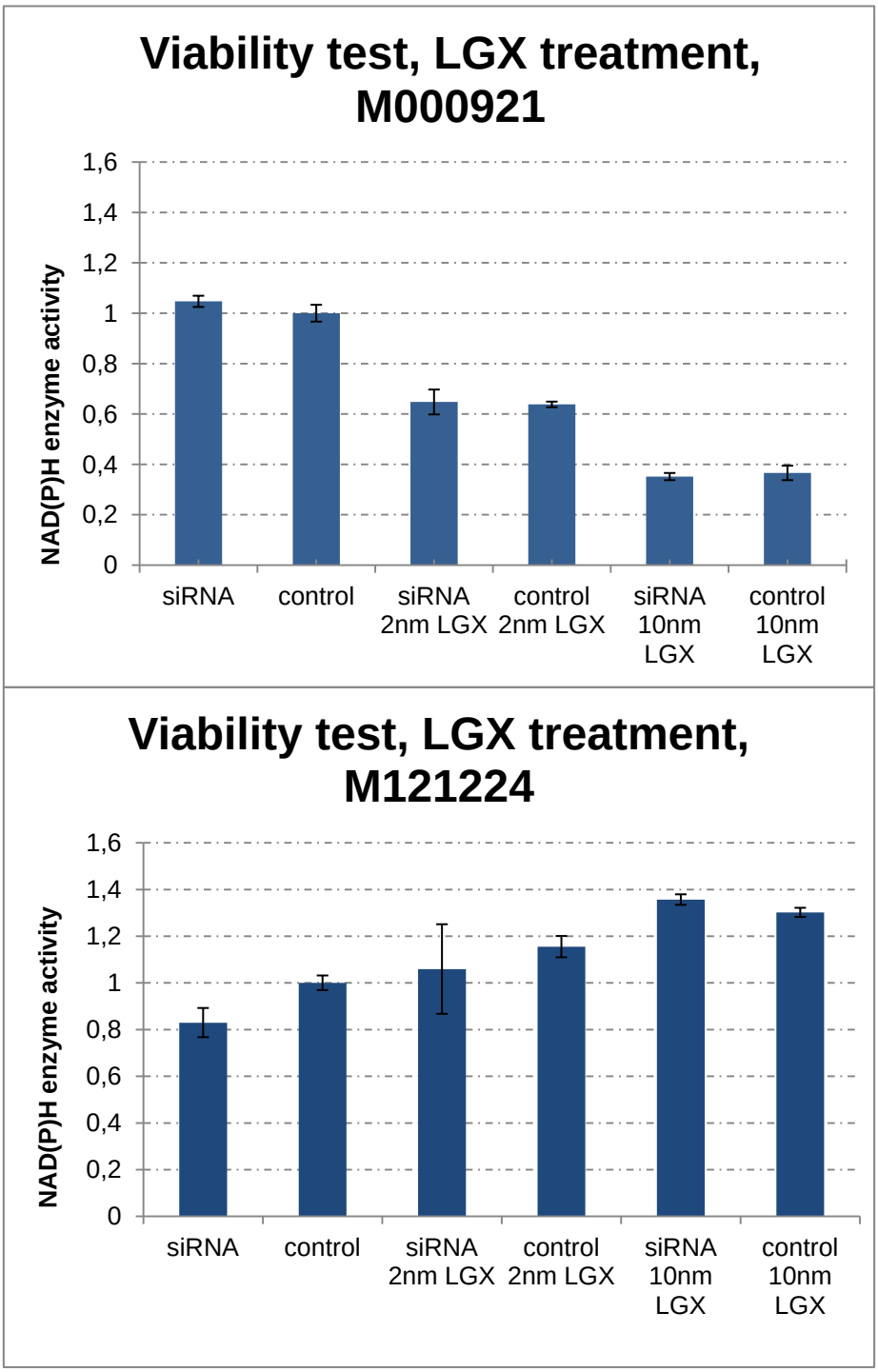

Figure 17. Viability test for the cell lines M000921 and M121224 transfected with siRNA and treated with 2nm and 10nm LGX. All samples are shown as fold-change to the untreated control.

These results showed the same characteristics as those of the viability test without siRNA transfected cells. For the M000921 (non-resistant), the signals decreased the higher the LGX concentration was, whereas the viability of the M121224 (resistant) did not decrease but even gained viability when treated with siRNA and LGX.

These results demonstrated that *TACC1* was not involved in resistance because the signal for the M121224 did not decrease at all. Moreover, I only had reasonable results for the experiment with cells transfected with siRNA; M121224 cells

transfected with the overexpression vector were not viable and therefore could not be measured.

5.2.4 TACC1 and its Impact on the MAPK Pathway

I already demonstrated that *TACC1* knock-down did not have an impact on resistance. With the following experiments I investigated the role of this gene on the MAPK pathway. To address this approach, I analyzed the expression levels of pERK and PI3K target genes. The qPCR results of the *TACC1* knock down in the cell lines M000921 (non-resistant) and M121224 (resistant) are shown in figure 18.

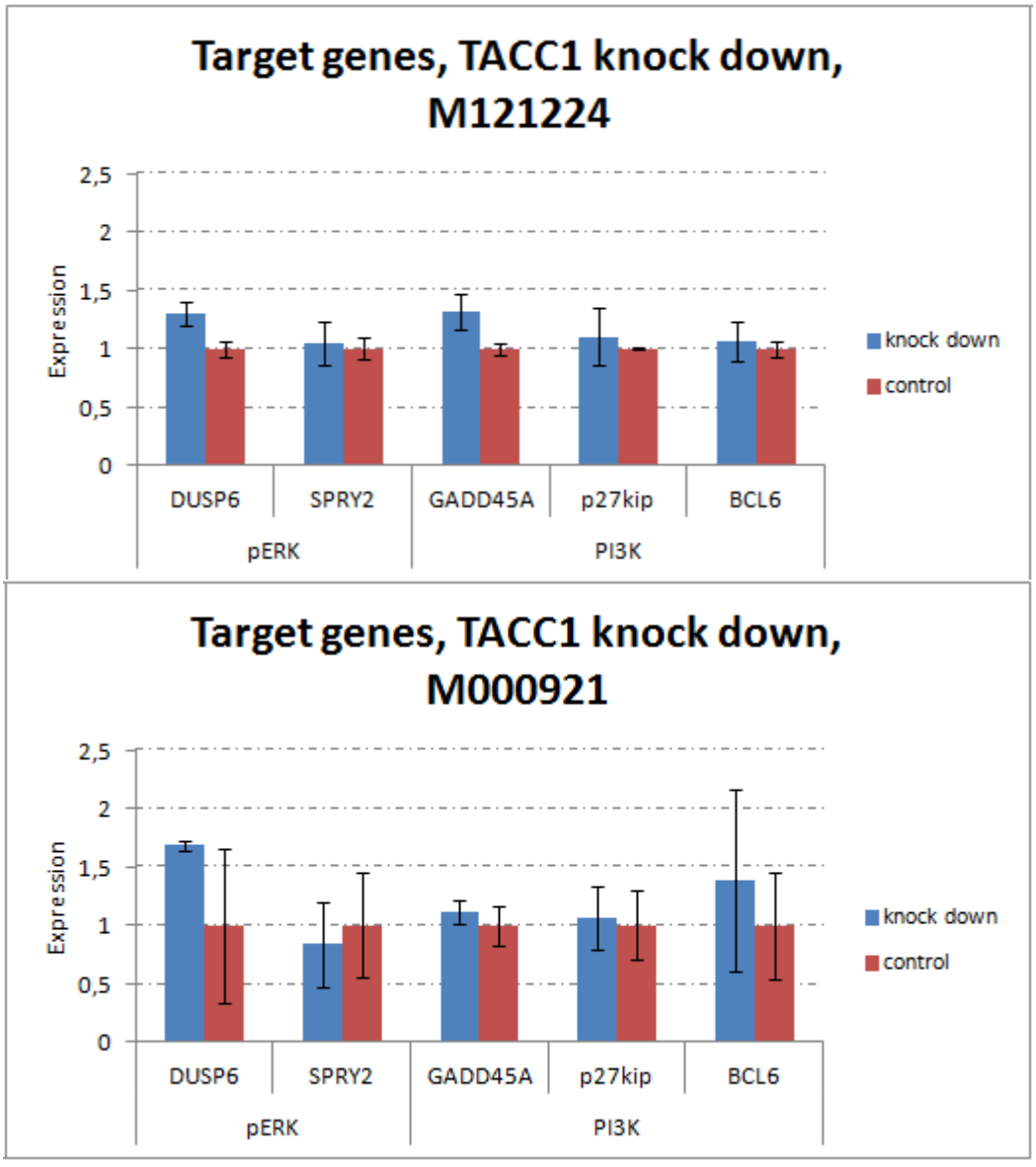

Figure 18. qPCR results for pERK and PI3K target genes. Both charts show the same target genes amplified after knock down of *TACC1*.

Concerning the non-resistant cell line (M000921), there were no reasonable differences in expression detectable because the standard deviations were quite high because of the large variance within the biological replicates. Hence, it was hard to answer the question if there were any differences in expression levels. However, the resistant cell line (M121224) showed at least some slight differences in the expression of *DUSP6* and *GADD45A* when transfected with siRNA. *DUSP6* belonged to the pERK target genes whereas *GADD45A* belonged to the PI3K target genes. If this result was reproducible, *TACC1* might play a role in both pathways.
Furthermore, I also analyzed the expression of these target genes when *TACC1* was overexpressed in the M000921 cell line (figure 19). Unfortunately, M121224 was not viable after the transfection with the vector.

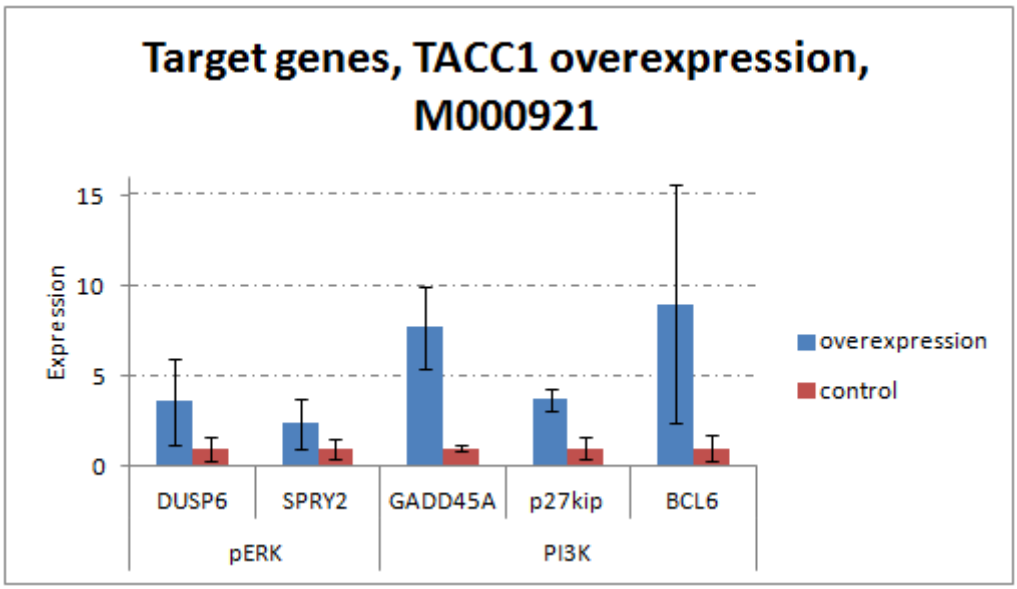

Figure 19. Expression levels of pERK and PI3K target genes after TACC1 overexpression in M000921.

GADD45A and *p27kip* showed different expression levels after transfection with the vector but none of these was statistically significant. Therefore, I performed Western blot analysis in order to detect differences of ERK and pERK on protein levels. The cell line used for this experiment was the non-resistant cell line (M000921); the data are shown in figure 20.

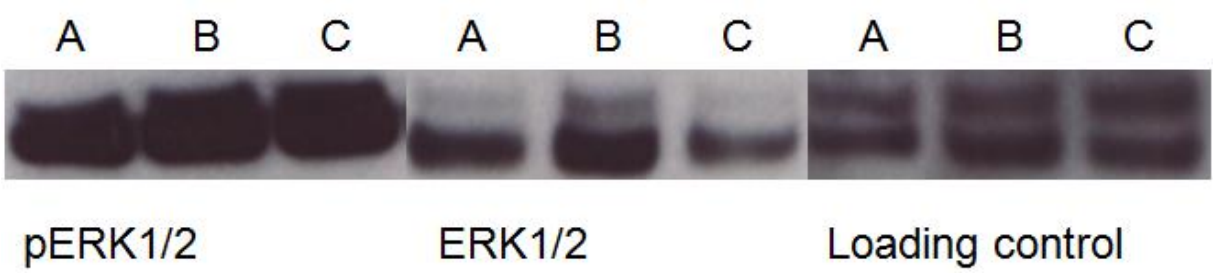

Figure 20. Protein levels of pERK (left) and ERK (middle) for **A** TACC1 overexpression **B** TACC1 knock down and **C** untreated. GAPDH served as a loading control (right).

In comparison to the untreated cells, ERK levels increased in cells after treatment with siRNA and after treatment with the vector, whereas pERK levels did not change after the transfection. pERK levels should be higher due to the increase of ERK. However, from qPCR data it was obvious that *DUSP6* (pERK target) expression decreased when knocked down in M121224 suggesting that pERK was affected in the sense that it was less active. Moreover, Western blot analysis is not a quantitative method and therefore this result is hard to interpret.

6 Discussion

6.1 Investigation of Known Resistance Mechanisms

6.1.1 Cot1activates Erk1/2

Cot1 is a protein encoded by *MAP3K8* and is known to play an important role in acquiring resistance to the BRAF inhibitor. Cot1 activates Erk1/2 through a Mek-dependent mechanism that does not need Raf signaling. Therefore Erk1/2 is activated in high levels which leads to increased cellular growth and proliferation (Johannessen et al.). I could rule out that Cot1 caused resistance to the inhibitor as I investigated the Cot1 expression levels in three resistant metastases and the resistant cell line and could show that - compared to a sensitive cell line - Cot1 was hardly expressed in these samples. The other resistant metastases were not tested for Cot1 amplification as only DNA samples were available.

6.1.2 B-Raf is replaced by C-Raf

From literature, it is known that differently spliced isoforms of *RAF* are able to cause resistance as C-Raf takes over the function of Braf in melanoma cells resistant to the BRAF inhibitor (Kaplan et al.). C-Raf signaling provokes the reactivation of the MAPK pathway which finally leads to the reactivation of Erk1/2. In order to exclude a splicing defect provoking the resistance, I amplified cDNA around the V600E mutation from the same samples - three resistant metastases, the resistant cell line and a sensitive $BRAF^{V600E}$ cell line - I had already investigated for Cot1 expression. All samples showed the same amplified product size of approximately 230bp which excluded a splicing defect within these amplified sequences. Moreover, it needs to be mentioned that there was a second band for the non-resistant and for the resistant cell line visible on the gel which was approximately 600bp in size. It was shown to be an artifact as I cut out the band from the gel and subsequent Sanger sequencing of this product revealed amplification of chromosome 3 (*RAF* is localized on chromosome 7).

6.1.3 Mutations in NRAS induce MAPK Overactivation

Melanoma carrying the activating $BRAF^{V600E}$ can overcome the inhibition by the drug by reactivating the MAPK pathway through an additional *NRAS* mutation (Nazarian et al.). Concerning our patient, I found one resistant metastasis (whereof the resistant

cell line derived as well) which was positive for *BRAF*^{V600E} and for *NRAS*^{Q61K}. These cells were sent to single cell sorting in order to figure out if there were two subpopulations present in this tumor carrying either *BRAF*^{V600E} or *NRAS*^{Q61K} or if both mutations occurred within the same cell. Therefore, I performed clonal analyses of 23 clones and all of these were positive for both mutations; hence, *BRAF*^{V600E} and *NRAS*^{Q61K} were present in the same cell. However, the *NRAS*^{Q61K} appeared only in one resistant metastasis (late metastasis VI) and not in all of the resistant metastases. As a consequence, activated *NRAS* was probably the driver for resistance in this one metastasis but not in the others.

6.2 Digital PCR for Mutation Detection

6.2.1 Detection of BRAF^{V600E} *and NRAS*^{Q61K}

Both activating mutations were detected with relative quantification using digital PCR and the corresponding Taqman Probe. The *BRAF* mutation was present in all of the tissue samples except in the nevus I and in the blood. Additionally, *NRAS*^{Q61K} was detected in one of the metastases (late metastasis VI), which was then single cell sorted (discussed in 6.1.3. Mutations in *NRAS* induce MAPK overactivation). Concerning the readout (Copies per Microliter), the copy numbers of tissue samples positive for *BRAF*^{V600E} varied. This was due to the fact that cryo-samples and punches from paraffin blocks did not contain the same ratio of malignant and benign tissues; this is why copy numbers are different for each sample although there was the same amount of DNA loaded. Generally, it is known that dPCR has a high false positive rate. For that reason, it is important to add a negative control sample to every run. Samples which have a higher copy number than the negative control and a precision below 15% were rated as positive.

Furthermore, copy numbers for *NRAS*^{Q61K} in the late metastasis VI were higher than for *BRAF*^{V600E}. *NRAS*^{Q61K} was not detectable in all of the other samples which leads one to assume that this metastasis appeared independently and was originally only *BRAF* mutated. Of course, it is still possible that *BRAF*^{V600E} could have got lost again – which is a rare event.

6.2.2 Presence of TACC1^{L452V} *in all Resistant Metastases*

TACC1^{L452V} was absent in all tissue samples which had been excised prior to treatment, whereas all the resistant metastases had *TACC1*^{L452V} in common.

Therefore, these results suggest that this event was a loss of function mutation and in consequence the protein lost its function. Possible functions of *TACC1* are discussed in 6.3 *TACC1* and its function. Concerning the readout of the digital PCR, the precision should not exceed 15%, nevertheless the late metastasis VI showed a precision of 17.95%. Hence, I performed Sanger-sequencing of this tissue sample and could prove that the mutation L452V was definitely present in this metastasis. Additionally, I also sequenced the blood sample as its precision was 19.68% with 56.124 copies/microliter but Sanger sequencing did not detect the mutation. This is the reason why it is rated negative for $TACC1^{L452V}$.

6.2.3 Detection of Melanoma Cells in the Blood

As the patient suffered from progressive disease, we assumed that there were also melanoma cells present in the blood. Hence, PBMCs were isolated from full blood and in order to concentrate the melanoma cells, I depleted all the residual immune cells from the PBMCs using magnetic beads. The flow through was used to perform absolute and relative quantification using dPCR. As far as the relative quantification is concerned, the blood sample was rated negative for $BRAF^{V600E}$ due to the high precision and the copy number which was below the copy number of the negative control. Nevertheless, I also performed absolute quantification for $BRAF^{V600E}$ for this sample and the precision and the copy number were within the positive range. Thereafter, I performed Sanger sequencing and was unable to detect the mutation. Sanger sequencing is very robust and does not detect rare mutations in a mixture of a few mutated and high wild-type alleles.

6.3 Tacc1 and its Function

6.3.1 The Expression of TACC1

In order to investigate the function of Tacc1, it was important to prove that Tacc1 is expressed in melanoma. Therefore, we performed tissue micro arrays and stained for Tacc1. 88% of all the analyzed melanoma samples (n=269) were stained positive for the expression of the protein. All of the screened samples were melanoma samples from patients who suffered from progressive disease. The fact that the staining was negative for 12% leads to the assumption that the expression of Tacc1 is not exclusively necessary for melanoma cells but the presence in the majority of the

tissues suggests that it plays a role in pathways which lead to malfunction of the cells.

6.3.2 TACC1 as a Tumor-Suppressor

The Kaplan-Meier survival curve shows that the higher *TACC1* is expressed in patients with longer survival, which means that patients die earlier when the expression is low. Between the terms “high” and “low”, there is a 3-fold difference in the expression of this gene. Moreover, there are many sites which can be mutated in *TACC1* (Hodis et al.), which is a typical characteristic of a loss-of-function tumor-suppressor. Furthermore, $TACC1^{L452V}$ showed up in the resistant late metastases only, meaning that this mutation had occurred de novo during the treatment with the BRAF inhibitor. All these facts support the assumption that *TACC1* acts as a tumor suppressor in its wild-type version and the L452V mutation is a loss of function mutation leading to a dysfunction of the protein and therefore to increased cellular proliferation. In order to test this hypothesis, I overexpressed and knocked down *TACC1* in a resistant (M121224) and in a non-resistant (M000921) cell line and subsequently performed a viability assay. The viability of both cell lines decreased when *TACC1* was overexpressed meaning that a high expression of *TACC1* leads to less viable melanoma cells. In contrast, knocking down this gene showed a decrease in viability of only one third compared to the control. In order to prove if the cellular proliferation is affected as well, I additionally performed a proliferation assay under the same conditions. Both cell lines did not show a decrease in proliferation. However, one of my colleagues repeated this experiment under the same conditions and could show a proliferative decrease for both cell lines. Therefore, I cannot exclude that the proliferation assays accomplished by myself were technically relevant.

Furthermore, it needs to be mentioned that the single cell sorted clones from the late metastasis VI ($BRAF^{V600E}$/$NRAS^{Q61K}$) were negative for $TACC1^{L452V}$. All the 23 sequenced clones carried wild-type alleles for *TACC1* which is inconsistent with the assumption that $TACC1^{WT}$ acts as a tumor-suppressor and loses its function due to the mutation L452V. However, only the 23 fast growing clones were sequenced and negative for the mutation; I additionally sequenced the original cell line M121224 which derived from the metastasis VI and could confirm the presence of $TACC1^{L452V}$ in this culture. This contributes to the fact that tumors harbor heterogeneous

subpopulations. Therefore, single cell sorted clones that grew slower would probably have carried the mutation but it could not be investigated until now if *TACC1*^{L452V} cells are also positive for *BRAF*^{V600E} and/or for *NRAS*^{Q61K}. Hence, further viability and proliferation assays should be conducted with one of the clonal cell lines in order to make sure that there are no different subpopulations present in the cell line, as siRNA, for example, knocks down the mutated and the non-mutated *TACC1* and therefore the function of the wild-type/mutated gene is hard to interpret.

6.3.3 The Role of TACC1 in Resistance

As the results from digital PCR revealed, *TACC1*^{L452V} occurred as a de novo mutation during the treatment with the BRAF inhibitor. The fact that these metastases became resistant during this period suggests that the mutation has an influence on the acquirement of resistance. To prove that, I conducted the following experiment: The resistant (*TACC1*^{L452V}) and the non-resistant (*TACC1*^{WT}) cell line were treated with siRNA in order to knock down *TACC1*. Subsequently, I treated the cells with two different concentrations (2nm and 10nm) of LGX818 and performed a viability assay. Both cell lines did not change their patterns concerning viability after the treatment with the inhibitor only. Thus, knocking down *TACC1* in a non-resistant cell line (M000921) is not sufficient to make it resistant to the BRAF inhibitor. Moreover, the resistant cell line (M121224) harbors not only *BRAF*^{V600E} but also *NRAS*^{Q61K}; this is a possible explanation why the knock down of *TACC1* did not show any effect on resistance. Therefore, a possible effect of the knock down is hard to detect but at least in these two cell lines it was not sufficient to knock down *TACC1* in order to see a significant difference in viability.

6.3.4 Pathway Activation by TACC1

The PI3K pathway and the MAPK pathway are the most affected signal transduction pathways in melanoma. This is why I investigated the role of *TACC1* concerning its impact on one of these pathways. Therefore, I knocked down *TACC1* in the cell lines and used RT-qPCR for expression detection of PI3K and pErk1/2 target genes. Both, the resistant cell line (M121224, *TACC1*^{L452V}) and the non-resistant cell line (M000921, *TACC1*^{WT}) did not show differences in expression between untreated cells and cells treated with siRNA, the standard deviations of all the tested target genes were too high to make a conclusion. This is because the biological triplicates

themselves showed differences in their expressions. This - at least for the M121224 - might be due to the fact that there were the mutated and the wild-type alleles of *TACC1* present in the cell line.

Furthermore, I overexpressed *TACC1* in the non-resistant cell line (M000921) and again investigated the expression levels of the target genes. Thereby I found out that there were differences in the expression of the PI3K target genes *GADD45A* and $p27^{kip}$. For the third target gene *BCL6* the variation between the samples was quite high which results in a high standard deviation. However, the overexpression of $TACC1^{WT}$ has an influence on the PI3K pathway and needs to be investigated further concerning its activation and signal transduction.

Concerning the pErk1/2 target genes, the results from RT-qPCR were hard to interpret due to the high variance of the triplicates. However, I investigated the protein levels of pErk1/2 and Erk1/2 and showed that Erk1/2 levels were increased when $TACC1^{WT}$ was overexpressed or *TACC1* was knocked down. However, levels of pErk1/2 did not show any differences on protein levels when cells were treated with the overexpression vector/siRNA compared to the untreated cells. Therefore, knock down or overexpression of *TACC1* increase Erk1/2, but not pErk1/2 protein levels; this suggests that the phosphorylation of pErk1/2 is the limiting factor and the influence on *TACC1* cannot be revealed as pErk1/2 is probably constantly active due to the activating mutations in *BRAF* and/or *NRAS*.

7 Conclusion and Outlook

Referring to the performed experiments, there are different mechanisms of resistance present within one single patient. In order to investigate and find new resistance mechanisms, I ruled out the known ones and thereby revealed by clonal analysis that cells in one resistant metastasis were positive for *BRAF*^{V600E} and also for *NRAS*^{Q61K}. I could confirm this with digital PCR and additionally validated the results from whole exome sequencing data using the same technique. Moreover, whole exome sequencing data showed 13 genes that were commonly mutated in the resistant metastases of this patient. I investigated the function of one gene (*TACC1*) further which was positive for the L452V mutation in all of the late metastases but not in tissues which were excised before the treatment with the Braf inhibitor. In order to reveal the role of *TACC1* in resistance, I knocked it down in a resistant and in a non-resistant cell line and found out that the knock down of *TACC1* is not sufficient for making the cells resistant to LGX818. Notably, the resistant cell line carries *BRAF*^{V600E} and also *NRAS*^{Q61K} and therefore the activating mutation in *NRAS* might cause the resistance through overactivation of the MAPK pathway. However, the expression of *TACC1* is related to longer survival due to the Kaplan-Meier survival curve and additionally it is expressed in 88% of the screened melanoma samples. Moreover, the overexpression of *TACC1*^{WT} resulted in weak viability in resistant as well as in non-resistant cell lines, but further work is needed in order to exclude that the treatment with the overexpression vector is not toxic for the cells. Hence, further investigations should be focused on the overexpression of *TACC1* in healthy cells (e.g. fibroblasts) in order to show that the melanoma cells do not have decreased viability because of the treatment itself but because of the overexpression of *TACC1*. Furthermore, one should also repeat the *TACC1*^{WT} overexpression experiments with *TACC1*^{L452V} in order to reveal the function of the mutated form of this gene and additionally to show differences in localization and function between *TACC1*^{WT} and *TACC1*^{L452V}. However, it is necessary to screen through a larger patient cohort in order to detect other mutations in *TACC1* which also occur during the treatment with the Braf inhibitor. Additionally, there might also be different splicing variants of *TACC1* present. We could show that the resistant cell line appeared to have different splicing of about 35bp shorter for the mutant allele than the wild-type allele of *TACC1*, but further work is needed to prove this. Lastly, the single cell sorted clones from the resistant cell line should all be sequenced in order to find clones that have a

different mutational status concerning *BRAF*, *NRAS* and *TACC1* for the further experiments – thereby one can gain different cell lines out of one resistant metastases which then could exclude that two activating mutations (e.g. $BRAF^{V600E}$ and $NRAS^{Q61K}$) cause the resistance and not the mutated *TACC1*.

8 References

Ascierto, P. A., et al. "The Role of Braf V600 Mutation in Melanoma." *J Transl Med* 10 (2012): 85. Print.

Avruch, J., et al. "Ras Activation of the Raf Kinase: Tyrosine Kinase Recruitment of the Map Kinase Cascade." *Recent Prog Horm Res* 56 (2001): 127-55. Print.

Balan, V., et al. "Identification of Novel in Vivo Raf-1 Phosphorylation Sites Mediating Positive Feedback Raf-1 Regulation by Extracellular Signal-Regulated Kinase." *Mol Biol Cell* 17.3 (2006): 1141-53. Print.

Bandarchi, B., et al. "From Melanocyte to Metastatic Malignant Melanoma." *Dermatol Res Pract* 2010 (2010). Print.

Bollag, G., et al. "Vemurafenib: The First Drug Approved for Braf-Mutant Cancer." *Nat Rev Drug Discov* 11.11 (2012): 873-86. Print.

Buday, L., P. H. Warne, and J. Downward. "Downregulation of the Ras Activation Pathway by Map Kinase Phosphorylation of Sos." *Oncogene* 11.7 (1995): 1327-31. Print.

Carpten, J. D., et al. "A Transforming Mutation in the Pleckstrin Homology Domain of Akt1 in Cancer." *Nature* 448.7152 (2007): 439-44. Print.

Chapman, P. B. "Mechanisms of Resistance to Raf Inhibition in Melanomas Harboring a Braf Mutation." *Am Soc Clin Oncol Educ Book* (2013). Print.

Chappell, W. H., et al. "Ras/Raf/Mek/Erk and Pi3k/Pten/Akt/Mtor Inhibitors: Rationale and Importance to Inhibiting These Pathways in Human Health." *Oncotarget* 2.3 (2011): 135-64. Print.

Chen, H. M., et al. "Azu-1: A Candidate Breast Tumor Suppressor and Biomarker for Tumor Progression." *Mol Biol Cell* 11.4 (2000): 1357-67. Print.

Conte, N., et al. "Carcinogenesis and Translational Controls: Tacc1 Is Down-Regulated in Human Cancers and Associates with Mrna Regulators." *Oncogene* 21.36 (2002): 5619-30. Print.

Curtin, J. A., et al. "Distinct Sets of Genetic Alterations in Melanoma." *N Engl J Med* 353.20 (2005): 2135-47. Print.

Cutler, R. E., et al. "Autoregulation of the Raf-1 Serine/Threonine Kinase." *Proc Natl Acad Sci U S A* 95.16 (1998): 9214-9. Print.

Daum, G., et al. "The Ins and Outs of Raf Kinases." *Trends Biochem Sci* 19.11 (1994): 474-80. Print.

Davies, H., et al. "Mutations of the Braf Gene in Human Cancer." *Nature* 417.6892 (2002): 949-54. Print.

Delaval, B., et al. "Aurora B -Tacc1 Protein Complex in Cytokinesis." *Oncogene* 23.26 (2004): 4516-22. Print.

Dougherty, M. K., et al. "Regulation of Raf-1 by Direct Feedback Phosphorylation." *Mol Cell* 17.2 (2005): 215-24. Print.

Dumaz, N., et al. "In Melanoma, Ras Mutations Are Accompanied by Switching Signaling from Braf to Craf and Disrupted Cyclic Amp Signaling." *Cancer Res* 66.19 (2006): 9483-91. Print.

Edling, C. E., and B. Hallberg. "C-Kit--a Hematopoietic Cell Essential Receptor Tyrosine Kinase." *Int J Biochem Cell Biol* 39.11 (2007): 1995-8. Print.

Ellerhorst, J. A., et al. "Clinical Correlates of Nras and Braf Mutations in Primary Human Melanoma." *Clin Cancer Res* 17.2 (2011): 229-35. Print.

Emery, C. M., et al. "Mek1 Mutations Confer Resistance to Mek and B-Raf Inhibition." *Proc Natl Acad Sci U S A* 106.48 (2009): 20411-6. Print.

Flaherty, K. T., et al. "Inhibition of Mutated, Activated Braf in Metastatic Melanoma." *N Engl J Med* 363.9 (2010): 809-19. Print.

Gabillard, J. C., et al. "Aurora-C Interacts with and Phosphorylates the Transforming Acidic Coiled-Coil 1 Protein." *Biochem Biophys Res Commun* 408.4 (2011): 647-53. Print.

Gangisetty, O., et al. "The Transforming Acidic Coiled Coil Proteins Interact with Nuclear Histone Acetyltransferases." *Oncogene* 23.14 (2004): 2559-63. Print.

Garnett, M. J., et al. "Wild-Type and Mutant B-Raf Activate C-Raf through Distinct Mechanisms Involving Heterodimerization." *Mol Cell* 20.6 (2005): 963-9. Print.
Gergely, F. "Centrosomal Tacctics." *Bioessays* 24.10 (2002): 915-25. Print.
Goodsell, D. S. "The Molecular Perspective: Ultraviolet Light and Pyrimidine Dimers." *Oncologist* 6.3 (2001): 298-9. Print.
Guyot, R., et al. "The Transforming Acidic Coiled Coil (Tacc1) Protein Modulates the Transcriptional Activity of the Nuclear Receptors Tr and Rar." *BMC Mol Biol* 11 (2010): 3. Print.
Ha, G. H., J. L. Kim, and E. K. Breuer. "Transforming Acidic Coiled-Coil Proteins (Taccs) in Human Cancer." *Cancer Lett* 336.1 (2013): 24-33. Print.
Ha, G. H., J. S. Park, and E. K. Breuer. "Tacc3 Promotes Epithelial-Mesenchymal Transition (Emt) through the Activation of Pi3k/Akt and Erk Signaling Pathways." *Cancer Lett* 332.1 (2013): 63-73. Print.
Hanks, S. K., and T. Hunter. "Protein Kinases 6. The Eukaryotic Protein Kinase Superfamily: Kinase (Catalytic) Domain Structure and Classification." *FASEB J* 9.8 (1995): 576-96. Print.
Hatzivassiliou, G., et al. "Raf Inhibitors Prime Wild-Type Raf to Activate the Mapk Pathway and Enhance Growth." *Nature* 464.7287 (2010): 431-5. Print.
Hayashi, K., et al. "Insulin Receptor Substrate-1/Shp-2 Interaction, a Phenotype-Dependent Switching Machinery of Insulin-Like Growth Factor-I Signaling in Vascular Smooth Muscle Cells." *J Biol Chem* 279.39 (2004): 40807-18. Print.
Hocker, T., and H. Tsao. "Ultraviolet Radiation and Melanoma: A Systematic Review and Analysis of Reported Sequence Variants." *Hum Mutat* 28.6 (2007): 578-88. Print.
Hodis, E., et al. "A Landscape of Driver Mutations in Melanoma." *Cell* 150.2 (2012): 251-63. Print.
Huggett, J. F., et al. "The Digital Miqe Guidelines: Minimum Information for Publication of Quantitative Digital Pcr Experiments." *Clin Chem* 59.6 (2013): 892-902. Print.
Jerant, A. F., et al. "Early Detection and Treatment of Skin Cancer." *Am Fam Physician* 62.2 (2000): 357-68, 75-6, 81-2. Print.
Johannessen, C. M., et al. "Cot Drives Resistance to Raf Inhibition through Map Kinase Pathway Reactivation." *Nature* 468.7326 (2010): 968-72. Print.
Kanavy, H. E., and M. R. Gerstenblith. "Ultraviolet Radiation and Melanoma." *Semin Cutan Med Surg* 30.4 (2011): 222-8. Print.
Kaplan, F. M., et al. "Shoc2 and Craf Mediate Erk1/2 Reactivation in Mutant Nras-Mediated Resistance to Raf Inhibitor." *J Biol Chem* 287.50 (2012): 41797-807. Print.
Kyriakis, J. M., and J. Avruch. "Mammalian Mitogen-Activated Protein Kinase Signal Transduction Pathways Activated by Stress and Inflammation." *Physiol Rev* 81.2 (2001): 807-69. Print.
Lauffart, B., et al. "Interaction of the Transforming Acidic Coiled-Coil 1 (Tacc1) Protein with Ch-Tog and Gas41/Nubi1 Suggests Multiple Tacc1-Containing Protein Complexes in Human Cells." *Biochem J* 363.Pt 1 (2002): 195-200. Print.
Li, X., et al. "Erk-Dependent Threonine Phosphorylation of Egf Receptor Modulates Receptor Downregulation and Signaling." *Cell Signal* 20.11 (2008): 2145-55. Print.
McCubrey, J. A., et al. "Mutations and Deregulation of Ras/Raf/Mek/Erk and Pi3k/Pten/Akt/Mtor Cascades Which Alter Therapy Response." *Oncotarget* 3.9 (2012): 954-87. Print.
McKay, M. M., A. K. Freeman, and D. K. Morrison. "Complexity in Ksr Function Revealed by Raf Inhibitor and Ksr Structure Studies." *Small GTPases* 2.5 (2011): 276-81. Print.
Mehnert, J. M., and H. M. Kluger. "Driver Mutations in Melanoma: Lessons Learned from Bench-to-Bedside Studies." *Curr Oncol Rep* 14.5 (2012): 449-57. Print.
Nazarian, R., et al. "Melanomas Acquire Resistance to B-Raf(V600e) Inhibition by Rtk or N-Ras Upregulation." *Nature* 468.7326 (2010): 973-7. Print.
Nikolaou, V. A., et al. "Melanoma: New Insights and New Therapies." *J Invest Dermatol* 132.3 Pt 2 (2012): 854-63. Print.
Omholt, K., et al. "Mutations of Pik3ca Are Rare in Cutaneous Melanoma." *Melanoma Res* 16.2 (2006): 197-200. Print.

Pearson, G., et al. "Mitogen-Activated Protein (Map) Kinase Pathways: Regulation and Physiological Functions." *Endocr Rev* 22.2 (2001): 153-83. Print.
Peset, I., and I. Vernos. "The Tacc Proteins: Tacc-Ling Microtubule Dynamics and Centrosome Function." *Trends Cell Biol* 18.8 (2008): 379-88. Print.
Piekorz, R. P., et al. "The Centrosomal Protein Tacc3 Is Essential for Hematopoietic Stem Cell Function and Genetically Interfaces with P53-Regulated Apoptosis." *EMBO J* 21.4 (2002): 653-64. Print.
Pihan, G. A., et al. "Centrosome Defects and Genetic Instability in Malignant Tumors." *Cancer Res* 58.17 (1998): 3974-85. Print.
Poulikakos, P. I., et al. "Raf Inhibitor Resistance Is Mediated by Dimerization of Aberrantly Spliced Braf(V600e)." *Nature* 480.7377 (2011): 387-90. Print.
Raaijmakers, M. I., et al. "Melanoma Immunotherapy: Historical Precedents, Recent Successes and Future Prospects." *Immunotherapy* 5.2 (2013): 169-82. Print.
Rünger, T. M., et al. "Comparison of Dna Damage Responses Following Equimutagenic Doses of Uva and Uvb: A Less Effective Cell Cycle Arrest with Uva May Render Uva-Induced Pyrimidine Dimers More Mutagenic Than Uvb-Induced Ones." *Photochem Photobiol Sci* 11.1 (2012): 207-15. Print.
Sage, E., P. M. Girard, and S. Francesconi. "Unravelling Uva-Induced Mutagenesis." *Photochem Photobiol Sci* 11.1 (2012): 74-80. Print.
Sala, E., et al. "Braf Silencing by Short Hairpin Rna or Chemical Blockade by Plx4032 Leads to Different Responses in Melanoma and Thyroid Carcinoma Cells." *Mol Cancer Res* 6.5 (2008): 751-9. Print.
Salzano, M., et al. "Calcium/Calmodulin-Dependent Protein Kinase Ii (Camkii) Phosphorylates Raf-1 at Serine 338 and Mediates Ras-Stimulated Raf-1 Activation." *Cell Cycle* 11.11 (2012): 2100-6. Print.
Shull, A. Y., et al. "Novel Somatic Mutations to Pi3k Pathway Genes in Metastatic Melanoma." *PLoS One* 7.8 (2012): e43369. Print.
Simmons, G. W., et al. "Neurofibromatosis-1 Heterozygosity Increases Microglia in a Spatially and Temporally Restricted Pattern Relevant to Mouse Optic Glioma Formation and Growth." *J Neuropathol Exp Neurol* 70.1 (2011): 51-62. Print.
Stahl, J. M., et al. "Loss of Pten Promotes Tumor Development in Malignant Melanoma." *Cancer Res* 63.11 (2003): 2881-90. Print.
Steelman, L. S., et al. "Roles of the Raf/Mek/Erk and Pi3k/Pten/Akt/Mtor Pathways in Controlling Growth and Sensitivity to Therapy-Implications for Cancer and Aging." *Aging (Albany NY)* 3.3 (2011): 192-222. Print.
Still, I. H., et al. "Cloning of Tacc1, an Embryonically Expressed, Potentially Transforming Coiled Coil Containing Gene, from the 8p11 Breast Cancer Amplicon." *Oncogene* 18.27 (1999): 4032-8. Print.
Straussman, R., et al. "Tumour Micro-Environment Elicits Innate Resistance to Raf Inhibitors through Hgf Secretion." *Nature* 487.7408 (2012): 500-4. Print.
Takayama, K., et al. "Tacc2 Is an Androgen-Responsive Cell Cycle Regulator Promoting Androgen-Mediated and Castration-Resistant Growth of Prostate Cancer." *Mol Endocrinol* 26.5 (2012): 748-61. Print.
Trunzer, K., et al. "Pharmacodynamic Effects and Mechanisms of Resistance to Vemurafenib in Patients with Metastatic Melanoma." *J Clin Oncol* 31.14 (2013): 1767-74. Print.
van der Vaart, B., A. Akhmanova, and A. Straube. "Regulation of Microtubule Dynamic Instability." *Biochem Soc Trans* 37.Pt 5 (2009): 1007-13. Print.
Villanueva, J., et al. "Concurrent Mek2 Mutation and Braf Amplification Confer Resistance to Braf and Mek Inhibitors in Melanoma." *Cell Rep* 4.6 (2013): 1090-9. Print.
Waris, G., and H. Ahsan. "Reactive Oxygen Species: Role in the Development of Cancer and Various Chronic Conditions." *J Carcinog* 5 (2006): 14. Print.

9 Appendix

9.1 Abbreviations

ABCA13	ATP-binding cassette sub-family A member 13
ADAMTS19	ADAM Metallopeptidase with thrombospondin Type 1 Motif, 19
ADP	Adenosindiphosphat
ARMC4	Armadillo repeat containing 4
ATP	Adenosintriphosphat
BCL6	B-cell lymphoma 6
BSA	Bovine serum albumin
C11orf30	chromosome 11 open reading frame 30
CACL2	Calcium chloride
CAMK-II	Calcium/calmodulin-dependent protein kinase II
CCDC48	Coiled-coil domain containing 48
DNA	Deoxyribonucleic acid
DMEM	Dulbecco modified Eagle's medium
DMSO	Dimethyl sulfoxide
DUSP 6	Dual specificity phosphatase 6
EDTA	Ethylenediaminetetraacetic acid
EGFR	Epidermal growth factor receptor
EIF4E	Eukaryotic translation initiation factor 4E
ERK	Extracellular-signal regulated kinases
6-FAM	6-carboxyfluorescein
FCS	Fetal calf serum
FDA	Food and drug administration
FGFR	Fibroblast growth factor receptor
GADD45A	Growth arrest and DNA-damage-inducible protein GADD45 alpha
GAP	GTPase activating protein
GAPDH	Glycerinaldehyd-3-phosphat-dehydrogenase
GDP	Guanosine diphosphate
GEF	Guanine nucleotide exchange factor
GRB2	Growth factor receptor-bound protein 2
GTP	Guanosine-5'-triphosphate
HEATR2	HEAT Repeat containing 2
HGF	Hepatocyte growth factor
HRP	Horseradish peroxidase
IR	Insulin receptors
IRS	Insulin receptor substrate
KCL	Potassium chloride
KIT	Mast/stem cell growth factor receptor
KSR	Kinase suppressor of Ras
LYPD5	LY6/PLAUR Domain containing 5
MAP	Mitogen-activated protein
MAPK	Mitogen-activated protein kinases
MBD2	mCpG-binding domain 2
MEK	MAPK/ERK kinase
MGCL2	Magnesium chloride
MRNA	Messenger RNA
MSK	Mitogen and stress-activated protein kinase
MTOR	Mechanistic target of rapamycin
MTT	3-(4,5-dimethylthiazol-2-yl)-2,5-diphenyltetrazolium bromide
NACL	Sodium chloride
NFASC	Neurofascin
NOD2	Nucleotide-binding oligomerization domain-containing protein 2
P27KIP1	Cyclin-dependent kinase inhibitor 1B
PBMC	Peripheral blood mononucleated cell
PBS	Phosphate buffered saline
CMV	Cytomegalovirus
PCR	Polymerase chain reaction
PDGFR	Platelet-derived growth factor receptors
PERK	Phosphorylated Erk
PI3K	Phosphatidylinositol-4,5-bisphosphate 3-kinase
PTEN	Phosphatase and tensin homolog
RAF	Rapidly accelerated fibrosarcoma
RAS	Rat sarcoma
RIPA	Immunoprecipitation assay
RNA	Ribonucleic acid
RPMI	Roswell Park Memorial Institute medium
RTK	Receptor tyrosine kinases
SDS	Sodium dodecyl sulfate
SHC2	Src homology 2 domain containing protein
SNAP91	Synaptosomal-associated protein, 91kDa
SOS	Son of sevenless
SPRY2	sprouty homolog 2
SPTBN1	Spectrin, beta, non-erythrocytic 1
STAT	Signal transducers and activators of transcription
TACC	Transforming acidic coiled coil
TAE	TRIS-acetate-EDTA
TBS	Tris-buffered saline
TRIS	Tris(hydroxymethyl)aminomethane
UV	Ultraviolet
VIC	4,7,2′-trichloro-7′-phenyl-6-carboxyfluorescein
WT	Wild-type
ZNF267	Zinc finger protein 267

9.2 Curriculum Vitae

Tel: +43664 / 1264023
E-Mail: judith.wenzina@gmail.com

Judith Wenzina, BSc
Marktgasse 60/18
A-1090 Vienna

Date of birth: 04/04/90
Nationality: Austria
Marital status: Unmarried

Education and Training

Since 09/2012	*University of Vienna* Molecular Biology, Focus on Medicine (Master's studies) Grade (June 14) 1.73
09/2008 – 05/2012	*University of Vienna* Biology, Microbiology and Genetics (Bachelor's studies) Grade 2.41
09/2000 – 06/2008	*Grammar school* General qualifications for university entrance Grade 1.5
09/1996 – 06/2000	*Primary school Gars/Kamp* Grade 1.0

Work Experience

10/2013 – 04/2014	*University of Zurich Hospital* Master's Thesis „Validation of biomarkers of resistance to BRAF inhibitors in melanoma" Group Dummer Rämistrasse 100 CH-8091 Zurich
Since 01/2011	*Dipl.-Ing. Reinhardt Wenzina Software&EDV-Beratung* Wilhelm-Mantlergasse 608 Part-time employee: evaluation of preliminary software models, testing collaboration tools, Wilhelm-Mantlergasse 608 A-3571 Gars am Kamp
03/2013 – 05/2013	*Medical University of Vienna – Anna Spiegel Institute* "Elucidate the protective capacities of natural antibodies in atherosclerosis" Group Binder Lazarettgasse 14 A-1090 Vienna
06/2012 – 09/2012	*AIT Austrian Institute of Technology GmbH* Health & Environment Department "Enzymatic detection of biogenic amines" - Group Preininger Konrad-Lorenz-Straße 24 A-3430 Tulln

10/2011	Max F. Perutz Laboratories Bachelor's Thesis "Influence of differently tagged Fkh2-Proteins on Transcription in Saccharomyces cerevisiae" Group Ammerer Dr. Bohr-Gasse 9 A-1030 Vienna
09/2011	*Labor Berset* Microbiological Laboratory Margaretenstraße 5 A-1040 Vienna
08/2010	*Labor Berset* Microbiological Laboratory Margaretenstraße 5 A-1040 Vienna
08/2009	*Hospital Waldviertel – Horn* Microbiological Laboratory, PCR Laboratory Spitalgasse 10 A-3580 Horn
07/2009	*Labor Berset* Microbiological Laboratory Margaretenstraße 5 A-1040 Vienna

Extra Qualifications

Languages	German (Mother tongue) English (C1) French (B2) Japanese (A2)
Methods in Mol. Biology	Isolation of DNA and RNA, cDNA Generation, Vector Cloning, DNA-Digestion and Ligation, Transformation of Bacteria, Knock Down and Overexpression Experiments, Working with Reportergenes (GFP, Lac-Z), PCR, Gelelectrophoresis, Quantitative Real Time PCR, Digital PCR, Working with Taqman Probes, Sanger Sequencing, SDS-Page, Western Blot, Chromatin Immunoprecipitation, Microarrays, Cell Culture, Working with Mouse Models, Various Types of Chromatography, Densitygradient-Centrifugation, Cultivation and Identification of Microorganisms, Basic Knowledge in Bioinformatics
Scholarships	Erasmus-Scholarship (2013/14) Research-Fellowship of Lower Austria (2013) Member of the Students for Excellence community (since 2013) University of Vienna – Scholarship (2013 and 2014) University of Vienna – Achievement Scholarship (2013) Member of the "Talente@Alpbach" Community of the Federal Ministry for Innovation Nominated for the Women's Prize of Lower Austria (2009)
Voluntary Work	Active member of the local drama club („Spektakel Gars") since 2006 Voluntary work in Nongkhai (Thailand), July 2008 Voluntary work in Pokhara (Nepal), August 2011

9.3 Paper submitted to Cancer Cell

Exome sequencing detects targeted therapy driven evolution of subclonal diversity in melanocytic nevi, primary, and metastatic melanomas including NRAS/BRAF double-mutated tumor cells

Daniel S. Widmer[1], Marieke I. G. Raaijmakers[1], Apurva Narechania[2], Judith Wenzina[1], Phil F. Cheng[1], Volker Teichgräber[3], Lars E. French[1], Rob Desalle[2], Michael Krauthammer[4], , Reinhard Dummer[1], Mitchell P. Levesque[1*]

[1]Department of Dermatology, University Hospital Zürich, ZH, 8091 Zürich, Switzerland
[2]American Museum of Natural History, NY, 10024-5192 New York, USA
[3]F. Hoffmann-La-Roche AG, 4070 Basel, Switzerland
[4]Department of Pathology, Yale University School of Medicine, CT, 06511 New Haven, USA

[*]Contact: Mitchell P. Levesque (MitchellPaul.Levesque@usz.ch)

Running Title
Exome sequencing of multiple melanocytic nevi and metastases reveals treatment-dependent monophyletic evolution and intrapatient heterogeneity of resistance.

Summary
To better understand how cancer genomes evolve in different therapeutic environments, we sequenced the exomes from multiple lesions from 3 metastatic melanoma patients treated with targeted (BRAF and MEK) and non-targeted (multi-receptor tyrosine kinase) inhibitors, generating deep sequencing data from germline DNA, dysplastic nevi, primary tumors, and metastases before and after therapy. Using phylogenetic techniques, we observed a rapid monophyletic evolution of melanoma subpopulations in response to targeted therapy that was not observed in non-targeted therapy. We also show that multiple resistance mechanisms are present within a BRAF-mutant stage IV melanoma patient, including activating NRAS mutations that co-occur with the BRAF mutations in the same cells, as shown by Digital-PCR and clonal sequencing of a patient-derived early-passage melanoma culture.

Significance
Despite the dramatic response rate to drugs targeting the MAPK pathway in melanoma, patients eventually develop resistance within months of treatment. Although several mechanisms of pathway reactivation have been identified, how genetic heterogeneity contributes to rapid resistance is still poorly understood. The results of this study allowed us to identify patient-specific resistance mechanisms, and to develop phylogenetic tools to measure treatment-specific evolution of genetic variability. In particular, the clonal evolution of melanoma subpopulations during targeted therapy, and the novel identification of subpopulations with coexisting NRAS and BRAF mutations in single melanoma cells may directly impact the selection of second-line therapies.

Highlights
- activating NRAS and BRAF mutations can be present in the same cells
- primary melanoma tumors show high subclonal diversity
- we identified inter- and intra-tumor heterogeneity of resistance mechanisms
- whole-exome phylogenetic analysis identified signatures of clonal selection
- cells resistant to BRAFi treatment are sensitive to MEKi treatment

Introduction

Melanoma therapies for advanced disease have made great progress in the last few years (Bollag et al., 2010; Chapman et al., 2011; Flaherty et al., 2010), but primary intrinsic resistance of some patients to targeted therapy, as well as the onset of delayed acquired resistance in most other patients, continue to pose a major challenge for the clinical management of metastatic melanoma (Aplin et al., 2011). However, the advent of next generation sequencing (NGS) technologies allows us to address the question of how conventional therapies influence the heterogeneous landscape of genetic variations within patients, and to identify the source of therapeutic resistance. Aside from elucidating new mechanisms of cancer progression, NGS applications also provide large datasets for the quantification and modeling of clonal diversity changes over time. In some cancers, global genetic diversity metrics have been shown to be predictive of neoplastic progression (Maley et al., 2006). Metastatic melanoma in particular has one of the highest mutation rates of any cancer (Krauthammer et al., 2012), and thus a very high degree of genetic heterogeneity is expected. Some studies have identified genomic characters such as the loss of heterozygosity that vary between primary tumors and metastases (Takata et al., 2000), and others have shown that this genetic heterogeneity is also present within individual tumors (Wilmott et al., 2012).
Within the context of therapeutic resistance, many genetic and transcriptional mechanisms of response to targeted therapy have recently been demonstrated across large patient cohorts, but the evolution of individual cancer genomes to systemic therapy remains poorly understood (Nazarian et al., 2010; Van Allen et al., 2014). Minor subclones have been shown to exhibit decreased sensitivity to therapy (Takata et al., 2000), and more recent studies have revealed that patients receiving targeted BRAF inhibitors have diverse mechanisms of resistance arising from this underlying intra-tumoral molecular heterogeneity (Shi et al., 2014).
To better characterize the evolution of intrapatient heterogeneity under different treatment regimens, we performed exome sequencing on multiple samples from three stage IV melanoma patients who each received a different therapy but progressed quickly under treatment. We used surplus biopsy material from different stages (depending on availability) including blood, dysplastic nevi, primary tumors and metastases before treatment as well as metastases after death obtained during autopsy. To better characterize intra-tumor heterogeneity, we sequenced multiple histologically distinct regions of the same primary tumor when possible, and made single-cell clones from early passage cultures for targeted re-sequencing.

Results

Tumor-type dependent, intra-patient heterogeneity

We sequenced the whole exome of multiple samples from three metastatic melanoma patients, which included diverse anatomical sites, therapies, and stages of disease progression (**Figure 1 A-F**). Patient 1 had a $BRAF^{V600E}$ mutation (Figure 1A), patient 2 had an unknown oncogenic driver (Figure 1B), and patient 3 had an activating $NRAS^{Q61R}$ mutation (Figure 1C) at initial diagnosis. Patient 1 received a targeted BRAF inhibitor (i.e. LGX818) and had a partial response according to computed tomography (CT) (Figure 1D). Patient 2 progressed under multi-kinase inhibitor treatment i.e (i.e. pazopanib), according to PET/CT (Figure 1E). Patient 3 received a targeted MEK inhibitor (i.e. MEK162), and was also progressive according to CT (Figure 1F). Analysis of the sequencing results showed expected numbers of total single nucleotide variations (SNVs) in the tumor samples (**suppl. Table 1**), as published in previous studies (Hodis et al., 2012; Krauthammer et al., 2012). Both dysplastic nevi from patient 1 had a lower protein-coding mutational burden than any tumor biopsy from the three patients, as measured by the total number of genes with nonsynonymous SNVs (**suppl. Table 1**). Nevus 1 had 133 and nevus 2 had 101 mutated genes, whereas patient 1's tumor biopsies had an average of 186 mutated genes (**suppl. Table 1**). Patient 2 and patient 3 averaged 196 and 234 mutated genes in their tumors, respectively. Interestingly, in addition to having on average fewer numbers of mutated genes, the nevi had a reduced ratio of non-synonymous to synonymous mutations (i.e. 0.79) as compared to all other sequenced primary (1.20) and metastatic melanoma (1.22) lesions, indicating a lower proportion of protein coding changes in nevi versus melanoma tumors in general (**suppl. Table 1**). It is also interesting to note that the primary tumors each had higher numbers of private SNVs than each patient's metastases, suggesting an increased exclusive genetic diversity in primary tumors than in metastases (**suppl. Table 1**) (Nekrutenko et al., 2002). For instance, patient 1 had 96 private SNVs exclusive to the primary tumor, and an average of 35 private SNVs in all metastases (suppl. Table 1). Patient 2 had an average of 48 private SNVs exclusive to each of the three punches of the primary tumor, and on average 24 private SNVs in the metastases. Likewise, except for the one clear outlier metastasis (i.e. Late 1) in patient 3, each of the two primary tumor punches had higher numbers of private SNVs (i.e. 89) than the metastases (i.e. 38). Thus, overall the primary tumors had 2-2.7 fold significantly higher numbers (t-test, $p<.00048$) of private SNVs than the same patient's metastases in our cohort, with one outlier metastasis showing extraordinary numbers of private mutations **(suppl. Table 1)**.

Exome sequencing could confirm the known *BRAF* and *NRAS* mutation status that was initially identified by Sanger sequencing at the time of diagnosis for each patient (**Figure 1, suppl. Table 2**). Additionally, we screened the data for other known oncogenes and tumor suppressors that could play a role in melanoma progression in our cohort **(suppl. Table 2)**. Although patient 2 had no known oncogenic drivers at the time of diagnosis, we identified a nonsynonymous germline mutation in the Melanocortin receptor $MC1R^{V92M}$, which has been shown to be significantly associated with an elevated risk of acquiring metastatic melanoma (data not shown) (Fernandez et al., 2007). In addition, patient 3 had the germline mutation $MITF^{E318K}$ that was recently associated with an increased risk of developing melanoma (Berwick et al., 2014) (data not shown).

In order to identify genomic losses in potential tumor suppressor loci in these three patients, we analyzed the exome data with the EXCAVATOR and CONTRA algorithms (Li et al., 2012; Magi et al., 2013), which allowed us to infer copy number variations (CNVs). We could detect a high number of CNVs in many chromosomes, with some samples exhibiting large losses throughout the genome (**Figure 1 G-I**).

We could identify chromosomal imbalances in our cohort that are known to occur frequently in melanoma **(Figure 1 G-I)**. Patient 1 gained copies in 6p, 7, 8q and 17q **(Figure 1G)** in the late metastases 3 and 4 **(Figure 1G)**. Patient 2 had gains in chromosome 1q, 7 and 22 in the late metastases **(Figure 1H)**. In patient 3, we found gains in chromosome 1q, 6p and 20q **(Figure 1I)**. All patients showed at least partial losses in chromosome 6q, 9p and 10 as well as in some samples in chromosome 11, 2 and 17 **(Figure 1 G-I)**.

In addition, CONTRA provides gene-specific information on CNVs. We could find a consistent loss of the *CDKN2A* locus on chromosome 9 **(Figure 1G-I suppl. Table 3)** in all of the tumor samples, except in the nevi from patient 1. These losses were confirmed by qPCR to be homozygous in Patients 1 and 3, and heterozygous in patient 2 (data not shown), as predicted by both the EXCAVATOR and CONTRA algorithms (Figures 1G-I, suppl. Table 3). Furthermore, *PTEN* (chromosome 10) was lost in all samples of patient 2 **(Figure 1H)** and most of the samples from patient 1, except in the early met1 and the primary tumor **(suppl. Table 3)**.

One method to group tumor samples and build relationships between biopsies is to assume that CNVs, once lost, cannot be regained. Tumor phylogenies may thus be inferred by identifying specific genomic losses in a primary tumor, which cannot be recovered in a metastasis deriving from this primary. However, the high variability in intra-patient chromosomal imbalances we identified would lead to many different possible relationships within the sampled biopsies **(Figure 1 G-I)**. For example, in patient 3 the chromosome 10 CNVs would suggest that the late metastases derived from primary punch #2; however, the chromosome 14 CNVs are more suggestive of a late lineage deriving from primary punch #1 **(Figure 1I)** Likewise, in patient 2 the primary punch #2 has fewer losses in chromosome 11 than the other two primary punches, which suggests less similarity to the late metastases, whereas the pattern of losses on chromosome 3 would suggest a closer relationship between primary punch #2 and the late metastases **(Figure 1 H)**. In general, intra-patient CNV heterogeneity was quite high, as can be observed in patients where we sequenced multiple regions of the same primary tumor **(Figure 1 H,I)**. For example, in chromosome 11 of patient 2 and chromosomes 7, 10, 12 and 14 of patient 3, we found losses in only one of the two primary tumor punches. Heterogeneity in CNVs can also be clearly seen in patient 1 chromosome 22, for example, which has a predicted copy-number gain of the telomeric region in the primary tumor, which does not appear in any of the later metastases (Figure 1J).

Whole-exome phylogenetic analysis identifies inter-tumor relationships and progression-relevant SNVs

In order to investigate the evolutionary relationship between individual patient tumors in different therapeutic environments, we applied phylogenetic algorithms to our SNV and indel calls from each patient. Whole-exome phylogenetic analysis allowed us to not only group tumor samples based on their total SNVs, insertions and deletions, but also to determine evolutionary relationships among the samples and to even find diagnostic characters supporting specific phylogenetic nodes **(Figure 2, suppl. Table 4)**. The biopsies from patient 1 and 3 (i.e. treated with BRAF and MEK targeted inhibitors, respectively) exhibited trees with post-resistance tumors forming monophyletic clades, meaning that all post resistant samples originated from only one node. Confidence is shown by bootstrap supports (arrow) which reflects the percentage of bootstrap trees also resolving the clade at the endpoints of that branch. Patient 2, who received non-targeted therapy (i.e. the multi-receptor tyrosine kinase inhibitor pazopanib) did not show this strong, monophyletic support of late tumor metastases **(Figure 2)** but the post resistant samples originated from multiple nodes (arrows).

The robust monophyletic topology of the phylogenetic trees from patient 1 and 3 upon targeted therapy suggest that the mechanism for therapeutic resistance may support the nodes that discriminate between the pre- and post-treatment clades **(Figure 2 A, C)**. However, no known and shared mechanism of resistance to BRAF-inhibitor or MEK-inhibitor treatment could be identified in these node supports or in the whole-exome data that could explain the therapeutic resistance observed in patients 1 and 3 **(suppl. Table 4)**. We further investigated the intersection of non-synonymous SNVs between all post-relapse tumor exomes in each patient to find novel potential genetic resistance mechanisms. In patient 1 we found a somatic non-synonymous

mutation in *TACC1*^{L452V} that was ubiquitous and exclusive to the inhibitor-resistant tumor samples **(suppl. Table 2 and suppl. Table 4)**. Although *TACC1* has been found to be frequently mutated in melanoma tumors, no role for *TACC1* in treatment resistance has yet been identified (Hodis et al., 2012) (Krauthammer et al., 2012). Since there may be intrapatient, inter-tumor heterogeneity of resistance mechanisms, we also sought to identify explanatory protein-coding changes in any of the post-treatment samples. In patient 1, we detected a nonsynonymous mutation in *GNAQ*^{T96S} in the primary and late metastasis 1, and *TACC1*^{C133A} in the same biopsy **(suppl. Table 2)**. Although these mutations are in genes previously shown to be affected in melanoma, their role in treatment resistance remains unknown. Likewise, no known mechanisms of resistance were identified in the exome data of the other two patients.

Intrapatient genetic heterogeneity of LGX818 resistance

Given the lack of known, shared mechanisms of resistance in the two targeted therapy patients, we further investigated the BRAF-inhibitor treated patient samples (i.e. patient 1), due to the greater knowledge of BRAF-inhibitor resistance mechanisms in the literature (Van Allen et al., 2014). We conducted Sanger sequencing on the same biopsy samples and on additional biopsies for which DNA was too limiting for exome sequencing without amplification. The *BRAF*^{V600E} mutation could be confirmed by standard Sanger sequencing of PCR amplicons from all tumor samples (data not shown). Given that activating *NRAS* mutations are the most common resistance mechanism so far identified, being present in 17.8% of BRAF-inhibitor resistant tumors (Van Allen et al., 2014), we chose to first conduct Sanger sequencing of exons 2 and 3 of the *NRAS* locus in all patient 1 samples. In doing so, we identified the activating mutation *NRAS*^{Q61K} in patient 1 late metastasis number 6 which arose after relapse. The same mutation was absent in all other metastatic samples. Furthermore we could confirm that this metastasis still had the *BRAF*^{V600E} mutation, as well as two additional mutations that were found exclusively and ubiquitously in all of patient 1's other post-treatment metastases: *TACC1*^{L452V} and *C11orf30*^{K22N} (data not shown). No other specific mutations were tested by Sanger sequencing, but subsequent exome sequencing of a primary cell culture derived from late metastasis 6 (i.e. culture number M121224), could also confirm the presence of these mutations (suppl. Table 2).

Since whole-exome sequencing provides broad genomic coverage, but limited depth at specific loci (in our case 101x average coverage across all samples), it is difficult to detect low-abundance subclones of cancer cells with alternative genotypes (Flaherty et al., 2012; Gerstung et al., 2012). For this reason, we applied digital PCR to further investigate the possibility of a small subpopulation of mutated and resistant cells in patient 1's post-treatment tumors. Our digital PCR platform is based on 20'000 simultaneous PCR reactions per run, which allows for the detection of genomic variants present in as little as 5% of the tumor cell population.

By the use of this technique we measured the number of BRAF^{V600E} or NRAS^{Q61K} mutated copies per microliter of DNA for each sample. Values with a precision of less than 15%, indicating a confidence interval of +/- 15% around the measured copy number, were considered acceptable. Digital PCR confirmed the presence of the *BRAF*^{V600E} mutation in all tumors but not in DNA obtained from the patient's blood or nevus 1 **(Figure 3A)**. However, absolute quantification of the purified blood sample could detect the BRAFV600E allele with a good precision (data not shown). Although late met 4 had a low copy number per microliter, (i.e. 35 copies) the precision was within the acceptable range (i.e. 8.59%). However, all other tumor biopsies from patient 1, including those that had not been exome-sequenced (i.e. late metastases 5 & 6) had higher *BRAF*^{V600E} copy numbers with good precision **(Figure 3A)**. Also the presence of the NRAS^{Q61K} mutation in the late metastasis 6 was validated by digital PCR, and shown to have a high copy number in that metastasis **(Figure 3A, green box)**. The digital PCR results also show the absence of detectable *NRAS*^{Q61K} subclones in any of the other resistant metastases aside from metastasis number 6 **(Figure 3A)**.

Two activating MAPK mutations are present in single, BRAF-inhibitor resistant, but MEK and ERK-inhibitor sensitive melanoma cells

Although we could show the presence of both MAPK-activation mutations *BRAF*^{V600E} and *NRAS*^{Q61K} in a single post-resistance tumor from patient 1, these results may be explained by either the presence of two separate subpopulations of cells, each with one activating MAPK mutation, or the presence of both mutations in single cells. To distinguish between these possibilities, we isolated single melanoma cells from M121224 by FACS-sorting, and grew new cultures from each of these individual cells. Sanger sequencing of 23 cultures derived from 23 different single-cell clones could confirm the continued presence of both *BRAF*^{V600E} and *NRAS*^{Q61K} mutations in all 23 independently derived colonies **(Figure 3 B, C)**. To confirm that M121224 retained the BRAF inhibitor resistance of late metastasis 6, we treated M121224 with LGX818 and two other commercially available BRAF inhibitors (i.e. PLX4032 and GSK2128436), and measured cell viability by the MTT assay **(Figure 4A)**. We included a BRAF^{V600E} mutated melanoma cell culture (M980513) as a positive control and an NRAS^{Q61R} mutated cell culture (M010817) as a negative control for BRAF inhibitor treatment. The M121224 line was still resistant to LGX818 to the same extent as the BRAF^{wt} cell culture, M010817 **(Figure 4A)**. Likewise, M121224 was also resistant to PLX4032 and GSK2118436 but to a lesser extent than the LGX818 inhibitor, to which the patient derived resistance **(Figure 4A)**. Phosphorylated ERK (pERK) levels in M121224 were significantly decreased at the IC_{50} concentration of LGX818 and PLX4032 **(Figure 4B).** Significant down-regulation of three pERK target genes in M980513 and M121224 was observed at the IC_{50} concentration of PLX4032 and LGX818 **(Figure 4C)**, but not in the control NRAS^{Q61R} cell line.

Although the M121224 double-mutated cells remained viable in the presence of high concentrations of the LGX818 drug **(Figure 4A)**, we were curious how the co-existence of two activating MAPK mutations might affect the sensitivity of these cells to other MAPK pathway inhibitors. Treatment of M121224 cells with both the standard IC_{50} concentration of LGX818 and increasing concentrations of the MEK inhibitor (MEK162), could show viability profiles similar to cells with single *NRAS*^{Q61R} mutations **(Figure 4D)**. Likewise, the MEK inhibitor alone was just as effective in reducing the viability of M121224 cells as it was with *NRAS*^{Q61R} mutated cells **(Figure 4D)**. Finally, a specific ERK inhibitor alone also abrogated M121224 viability to the same degree as in *BRAF*^{V600E} cells **(Figure 4D)**.

Primary tumors exhibit highest subclonality

It is fair to assume that the majority of somatic mutations in cancer affect one but not the other allele and are thus heterozygous. In a clonal and pure cancer population, such mutations demonstrate a mutant allele ratio (MAR) of 0.5, that is, half of all sequenced bases show the mutant allele. A deviation from this number may be indicative of the presence of cancer subclones, which give rise to MARs smaller than 0.5. Alternatively, a reduced MAR may indicate higher stroma content. However, the proportion of BRAF^{V600E} or NRAS^{Q61R} alleles may also be used to estimate tumor content (for patients 1 and 3, respectively), and was found to be at expected levels in all tumors in tumors (data not shown). To study the presence of subclones in our primary tumors, we calculated the MARs across the multiple punches in patients 2 and 3. Presumably, these punches characterize different portions of the tumor, with some mutations found exclusively in one punch, but not the other (i.e. private mutations). One must assume that these private mutations are subclonal, and are therefore present in a smaller set of cells. The results in **Figure 5B** clearly show that the mean MAR of the private SNVs of each primary tumor punch were considerably less than the overall MAR of all SNVs. The mean MAR of private vs the mean MAR of total SNVs of each punch from patient two was

between 6% and 16% less in each case **(Figure 5B)**, and the mean MAR was between 9% and 15% less in the private SNVs of patient 3 than the total SNVs **(Figure 5C)**. These results suggest that the primary tumors contain subclonal diversity that can be characterized by a large number of private SNVs with low mutant allele frequencies. In addition, In patient 1, we observed a bimodal distribution of the MARs in the primary tumor, with a peak at 0.35 and a secondary peak at 0.15. The first peak likely corresponds to clonal heterozygous mutations and indicates a tumor purity of 70%.

Discussion

The confluence of increasingly more specific targeted pathway inhibitor pipelines and the application of powerful next-generation sequencing technologies have allowed for an improved characterization and treatment approach tailored to the key driver pathways most relevant to metastatic melanoma progression (Ascierto et al., 2013; Chapman et al., 2011; Guo et al., 2011). However, the frequent intrinsic and acquired resistance of many melanoma patients to targeted therapy suggests that more work is necessary to understand how intra-patient genetic heterogeneity contributes to progressive disease. Generally two different treatment resistance mechanisms can be distinguished: intrinsic (primary) and acquired (secondary). Intrinsically resistant tumors either do not initially respond or include a resistant subclone, which is rapidly selected during treatment, resulting in a failure to reduce tumor burden and rapid relapse. Acquired resistance mechanisms arise during treatment and may include selection or occurrence of additional activating mutations in genes of the MAPK pathway (Emery et al., 2009; Nazarian et al., 2010; Wagle et al., 2011) or inactivating mutations in MAPK inhibitors (Nissan et al., 2014). Also, alternative splicing of the BRAF transcript and other non-genetic mechanisms have been reported to play a role in therapeutic resistance (Poulikakos et al., 2011). Despite a high number of studies dealing with this problem, the list of known resistance mechanisms is far from complete and in many individual cases, the mechanism of resistance remains unknown.

In order to better characterize how individual cancer patients respond to standard therapies, we identified three patients with similar treatment time courses, but different oncogenic mutations and therapeutic regimens. The first patient had a $BRAF^{V600E}$ mutation and had an initial response to targeted BRAF-inhibitor therapy. Patient 2 was homozygous wild-type for both BRAF and NRAS, and received pazopanib, which is a multi-receptor tyrosine kinase inhibitor. Lastly, patient 3 had an $NRAS^{Q61R}$ mutation, and was administered a MEK-inhibitor. Whole exome sequencing data were generated from punches of FFPE material obtained from multiple biopsies, and were referenced to germline DNA isolated from each patient's blood. This approach provided a more comprehensive view of intra-patient genomic heterogeneity than earlier studies that investigated larger patient cohorts, but with fewer samples from each patient.

By analyzing high-quality single nucleotide variations (SNVs) present in the patient tumors, we could show that each patient's primary tumors contained the largest genetic diversity compared to all of their metastases. This is consistent with the expectation that the site of cancer origin would contain more genetic variants than the descendants that arose later and presumably had less time for the acquisition of de novo mutations. Interestingly, both dysplastic nevi from patient 1 had a lower protein-coding mutational burden than any of the tumor samples sequenced from the three patients. Although the reason for this is unclear, the reduced genetic diversity of the nevi may be the result of less genomic instability or possibly a shorter time period to accumulate mutations, amongst other possible causes.

Whole-exome phylogenetic analysis of these data was further used to infer the evolutionary relationships between the tumors within each patient, and to determine how each therapeutic regimen affected the evolution of genetic heterogeneity. Unlike in previous studies that showed a branching evolution of clones subsequent to targeted therapy, we could see a strong, well-supported monophyletic evolution of metastases following both BRAF and MEK inhibitor treatment and relapse. In contrast, patient 2, who received a multi-kinase inhibitor (i.e. pazopanib), did not have a monophyletic topology of late tumor metastases, which is suggestive of genetic drift between the late metastases.

Interestingly, despite the monophyletic segregation of late metastases in the patient who received the BRAF inhibitor, no known mechanism of resistance was shared between all sequenced biopsies. In fact, the activating mutation $NRAS^{Q61K}$ was identified by both Sanger sequencing and digital PCR to be present in a single metastasis of patient 1, but absent in all other resistant tumor samples from that patient. This is consistent with previously published data showing heterogeneity in resistance mechanisms within individual patients (Shi et al., 2014), and exacerbates the efforts to both catalog the causes and treat patients who have developed therapeutic resistance. Thus, the different metastases likely contain divergent mechanisms of resistance, although we observed a monophyletic selection of subclones subsequent to treatment.

By isolating and sequencing colonies derived from 23 single cell clones of this resistant tumor, we could show for the first time that both activating MAPK mutations were present in a single tumor cell. These double-mutated cells grew in normal culturing conditions, were resistant to the BRAF-inhibitor with which the patient had been treated, but were only partially resistant to two other BRAF-inhibitors. A reduction in pERK levels could still be observed in the presence of LGX818 and PLX4032, although the cells remained resistant to BRAF inhibition. Importantly, the double-mutated cells remained sensitive to combined MEK and BRAF inhibition, as well as mono-agent MEK and ERK inhibition. This observation suggests that simultaneous or second-line treatment with other MAPK-pathway inhibitors may still be effective in controlling progression, despite the presence of resistance-conferring mutations. However, as the double-mutated genotype was only present in late metastasis #6 out of the other 5 metastases of patient 1 and the underlying mechanisms that conferred therapeutic resistance on the other tumors remain unclear, the efficacy of these second-line or combination treatments in controlling overall tumor burden is questionable. This would be especially true if the other tumors in patient 1 activated different pathways, such as PI3K, PTEN, and AKT, thereby rendering them insensitive to MAPK inhibition. By digital PCR, we demonstrate that the frequency of double-mutated cells is variable even within a single resistant tumor, suggesting that these cells may also contribute to resistance in a paracrine manner or may have intra-tumor heterogeneity in resistance mechanisms.

Our demonstration of monophyletic evolution of cancer cells in patients who received targeted inhibition suggests a selection of heterogeneous subclones that could better survive that therapeutic environment. However, the apparent lack of a common mechanism of resistance between these tumors indicates that the subsequent emergence of resistance may have occurred through a shared genetic mechanism not identifiable by our approaches, through non-genetic means, or in a divergent way in each individual metastasis. All of those possibilities pose serious therapeutic challenges. But the remaining sensitivity to MAPK-inhibition of the double-mutated melanoma cells we isolated suggest that combination and second-line therapies in the context of precision medicine may still be effective if they consider the spatial and temporal genetic heterogeneity present in metastatic melanoma patients.

Experimental Procedures

Sample preparation

Patient material was only used after written consent of the patient was given through the university biobank program according to ethical approval numbers 647 and 800. DNA was either isolated from paraffin embedded tissue stored in the biobank of the institute of Dermatology of the University Hospital of Zürich, fresh frozen tissue, or PBMCs. DNA from paraffin blocks was isolated using the FFPE DNA isolation kit from Qiagen (QIAamp DNA FFPE Tissue Kit #56404) and optimized protocols

developed by Ultan McDermott at the Sanger institute. For DNA isolation from non-paraffin embedded samples we followed standard DNA isolation protocols published earlier. Given patient consent we collected samples during autopsy shortly after death. Samples were processed immediately after collection to ensure best possible DNA and RNA quality. Where possible, primary cell cultures were established as in previous studies (Widmer et al., 2012).
To reduce contamination with stromal tissue we punched the paraffin blocks and isolated the DNA out of the punches rather than from cuts of the whole block. Prior to DNA isolation, each tumor sample was evaluated by a trained dermato-histopathologist. Quality of the tissue as well as tumor content was checked and regions suitable for DNA isolation were marked. When available, we sequenced DNA from dysplastic nevi, primary melanoma tumors and metastases taken before therapy, as well as metastases obtained during necropsy. Germline DNA from PBMCs was sequenced for all patients if available as a reference (Böyum, 1968).

Library preparation and sequencing
DNA quality was measured by an Agilent 2100 Bioanalyzer or Agilent 2200 Tapestation. One to three µg of high quality DNA was used to prepare the whole exome library using the Agilent SureSelect V4 or V5 kit. Sequencing was performed on an Illumina Hiseq 2000 machine in the Functional Genomics Center at University of Zürich. For the whole exome sequencing we sequenced 0.25 lanes per sample, paired-end, with 100bp reads.

Whole exome sequencing analysis
Bioinformatics analysis was conducted with a modified GATK pipeline (DePristo et al., 2011; McKenna et al., 2010; Van der Auwera, 2013): Quality control was done with „FASTQC" (Andrews). Alignment of the FASTQ file to the reference genome "hg19" (Lander et al., 2001) was done with "BWA" (Li and Durbin, 2009). Transformation from SAM to BAM file format was done with "BWA". PCR duplicates were marked by MarkDuplicates from "Picard" , Local realignment around indels with RealignerTargetCreator (GATK), realigning with IndelRealigner (GATK), fix mate information with FixMateInformation (Picard), base quality score recalibration with Baserecalibrator (GATK) and PrintReads (GATK). Variant calling was done with UnifiedGenotyper (GATK). For annotation of the VCF files we used Annovar (Wang et al., 2010). Furthermore we used Samtools (Li et al., 2009) and Bedtools (Quinlan and Hall, 2010). For data interpretation we used Microsoft Access, Microsoft Excel, Venny (Oliveros, 2007), ConSet (Kim et al., 2007) and IGV (Robinson et al., 2011; Thorvaldsdóttir et al., 2013).
We calculated the mutant allele frequency for all the samples to get an impression of the degree of contamination with non-tumor tissue. Most of the samples showed a mutant allele frequency of 0.4 to 0.5 which corresponds to close to 100% tumor material being (Data not shown).
For copy number analysis we used Excavator (Magi et al., 2013) and Contra (Li et al., 2012), results of the analysis with Excavator were visualized with Circos (Krzywinski et al., 2009).
SNVs were filtered according to the following read count criteria: A base must have at least four mutant reads and at least 10 total reads, if less than 10 total reads, at least half of them must be mutated. Also all SNVs with a phred-scaled quality score of <50 were excluded from further analysis. A SNV was called somatic if the unfiltered blood sample from the same patient did not show any mutant read for this position.
Mutant allele ratios (MAR) were calculated by dividing mutant read counts by total read counts for each called SNV. Frequencies for these ratios were calculated and trendlines were plotted in Excel with the Moving Average method (period: 3). To reduce the number of false positive SNVs we applied more strict filtering on the private SNVs. Quality threshold was raised to a phred score of 100, and the SNV needed to have at least 10 total reads. Genes that had more than 8 SNVs were excluded.

dPCR
Digital PCR was carried out using the AB Gene Amp PCR System 9700 (Applied Biosystems Carlsbad, CA, USA), and with 15µl of the supplied mastermix (AB Quant Studio 3D) and equal amounts (0.6µM) of primers from Microsynth (Balgach, Switzerland).
BRAF forward: 5`CTACTGTTTTCCTTTACTTACTACACCTCAGA
reverse: 5`ATCCAGACAACTGTTCAAACTGAT
NRAS forward: 5`GGTGAAACCTGTTTGTTGGACAT
reverse: 5`TGTATTGGTCTCTCATGGCACTGT
Additionally we used probes from Life Technologies (Carlsbad, CA, USA):
BRAF V600E: 6-VIC-TAGCTACAGAGAAATC-MGB
NRAS Q61K: 6-FAM-CAGCTGGAAAAGAA-MGB
The DNA was diluted to a final concentration of 4 µM; DNA concentration varied from 0.3ng/µl to 6.6ng/µl depending on the expected frequency of the target sequence. Chip loading and thermocycling conditions were according to the Life Technologies instructions. Fluorescence measurement was performed using the Quant Studio 3D and output was processed by QuantStudio 3D AnalysisSuite Software. Fluorescence values were Poisson corrected and copies per µl were calculated. Every sample showing a precision higher than 15% was classified as negative for the specific mutation.

Sanger sequencing
After DNA amplification, 12ng of each PCR product, 5x Terminator Sequencing Buffer (Applied Biosystems), 1.5µM primers (Microsynth)
BRAF forward: 5`CTAAGAGGAAAGATGAAGTACTATG
reverse: 5`CTAGTAACTCAGCAGCATCTCAG
NRAS forward: 5`GATAGGCAGAAATGGGCTTGA
reverse: 5`ATCATCCTTTCAGAGAAAATAATGC
and 2µl of BigDye Ready reaction Mix (Applied Biosystems) were added up to a 10µl reaction mix. Cycling conditions were performed as follows: 60s at 96°C were followed by 16 cycles for 10s at 96°C, 5s at 50°C and 240s at 60°C in a Lab Cycler (Sensoquest, Göttingen, Germany). Samples were purified using the Big Dye XTerminator purification Kit (Applied Biosystems) according to the manufacturer`s manual. Subsequent Sanger Sequencing was carried out using the 3500 Genetic Analyzer (Applied Biosystems). Analysis was performed with the Variant Reporter Software (Life Technologies) where every mutation in the sequence which surpassed the threshold of 25% was classified as positive.

Cell sorting
In order to perform single cell sorting of melanoma cells, the cells from a confluent T75 cell culture flask were pelleted and resuspended in 100µl FACS buffer (1% FBS, 5mM EDTA pH8, 0.01% NaN_3/ddH_2O in PBS). Cells were incubated for 20 minutes at 4°C with the following photosensitive antibodies: Anti-human MCSP-FITC (Miltenyi Biotec 130-098-794, Bergisch Gladbach Germany), diluted 1:20 in FACS buffer. Anti-human Fibroblasts/Epithelial-PE (ABIN319868, Aachen Germany),

diluted 1:200 in FACS buffer. After washing, cells were resuspended in 200µl FACS buffer and sorted using the Aria IIb (BD Biosciences, Franklin Lakes, New Jersey, USA).

Isolation of Melanoma cells from PBMCs
$1x10^7$ PBMCs were used for isolating melanoma cells with the CD56+CD16+NK cell isolation kit from Miltenyi Biotec (Bergisch Gladbach, Germany), according to the manufacturer`s instructions. One deviation from the manual was in the last step, which is a positive selection for NK cells, whereas the flow-through contained the melanoma cells; other immune non-NK cells were depleted in the first step. After collecting the flow-through containing all non-immune cells, cells were pelleted for 5 minutes at 1500rpm and DNA isolation followed as with the non-paraffin samples reported here.

Phylogenetic analysis:
We constructed Maximum Parsimony, Bayesian and Maximum likelihood (ML) phylogenies with the POSIX-threads version of RAxML v8.0.19 (7). We used an ascertainment bias correction and a general time-reversible (GTR) substitution model accounting for among-site rate heterogeneity using the Γ distribution and four rate categories (ASC_GTRGAMMA model) for calculation of the optimal tree. Node support was evaluated with 100 nonparametric bootstrap pseudoreplicates filtering the optimal ML tree through the bootstrap trees. Node support values therefore indicate the percent proportion of bootstrap trees that contained a given internode branch.
Variants diagnostic for a given clade are defined as existing solely in that clade and nowhere else for that position. All leaves emanating from the node in question must share a variant and all other leaves must contain a different character for a variant to be diagnostic. Diagnostic variants can therefore also be termed an apomorphy.

Cell culture
Cell cultures were obtained from patient biopsies of cutaneous melanoma and melanoma metastasis after informed consent through the university biobank program according to ethical approval numbers 647 and 800. Tumor material was cut in small pieces and digested with 2.4U/ml Dispase (Roche, Basel, Switzerland) in RPMI1640 (Invitrogen (Carlsbad, CA, USA))for 3 hours at 37°C. Subsequently, the material was centrifuged (1500rpm/ 5min) and the supernatant was removed. Thereafter the pellet was dissolved in 0.005M Calcium Chloride dihydrate and 62.5U/ml Collagenase (Sigma, St. Louis, MO, USA) in Tris-buffered saline (pH 7.4) and incubated for 2 hours at 37°C. Subsequently, the material was centrifuged (1500rpm/ 5min) and the supernatant was removed. Stop solution (0.05M Tris Base, 0.15M NaCl and 0.01M EDTA in H_2O, final pH 7.4) was added for 10 minutes. Thereafter, the pellet was washed two times with RPMI1640 and finally the cells were cultured in RPMI1640supplemented with 5mM L-glutamine (Biochrom, Berlin, Germany), 1mM sodium pyruvate (Gibco, Carlsbad, CA, USA) and 10% FCS (Gibco (Carlsbad, CA, USA)) in 37°C and 5% CO_2 atmosphere. After several passages melanoma culture was confirmed by immunohistochemistry and mutation status of the cells was assessed.

Cell viability assay
Cell sensitivity for different small molecule inhibitors was evaluated for the cell cultures M980513 ($BRAF^{V600E}$, $NRAS^{WT}$), M000921 ($BRAF^{V600E}$, $NRAS^{WT}$), M010817 ($BRAF^{WT}$, $NRAS^{Q61R}$) and M121224 ($BRAF^{V600E}$, $NRAS^{Q61K}$). 1x10^4 cells were seeded and treated for 72 hours with different concentrations of either a BRAF inhibitor (PLX4032, LGX818 or GSK2118436), a MEK inhibitor (MEK162), an ERK inhibitor (SCH772984), or a combination of a BRAF and MEK inhibitor (LGX818+MEK162). DMSO treatment was used as a control. After 72 hours, the medium was removed and fresh RPMI1640 supplemented with 10% FCS and 8% MTT reagent (Sigma, 5mg/ml in PBS) was added, and the cells were incubated at 37°C. After 1 hour, the RPMI1640 with MTT reagent was removed and 10% SDS (Sigma) and 95% isopropanol/ 5% Formic Acid (Sigma) (ratio 1:1) were added. After 5 min of incubation at 37°C, absorbance was measured at 595nm (reference 620nm) using a microplate reader.

Western blot
Total protein was collected by washing cells twice with ice cold PBS and subsequent lysis in RIPA buffer (20mM Tris-HCl (pH 7.5), 1% Triton X-100 (Sigma), 137mM NaCl, 10% glycerol and protease inhibitors (Roche). Concentration of the protein was measured with the Bio-Rad Dc Protein Assay (Bio-Rad, Hercules, CA, USA) according to the manufacturer's protocol. SDS-Page was used to separate the proteins, after which they were transferred onto a nitrocellulose membrane. Membranes were probed with a rabbit anti-pERK antibody (Cell Signaling, product nr #4376S) and a rabbit anti-GAPDH antibody (Abcam, Cambridge, UK, product nr ab9385), followed by horseradish peroxidase-conjugated goat anti-rabbit IgG (Santa Cruz, product nr sc-2030)Bound antibodies were detected using chemiluminescence (ECL, GE Healthcare, Chalfont St. Giles, UK). Afterwards, band intensity was measured using ImageJ software (imagej.nih.gov/ij/) and pERK band intensity was corrected for corresponding GAPDH band intensity.

qPCR analysis
Total RNA was extracted from cell cultures using TRIzol (Life Technologies), and afterwards 1µg of RNA was transcribed into cDNA with the Reverse Transcription System (A3500, Promega, Madison, WI, USA). For q-PCR, the ViiA7 (Life Technologies) was used, and the reaction mix consisted of 5µl SYBR Green (Roche), 3.5µl H_2O, 0.5µl forward + reverse primer (10 µM) (Microsynth) and 1µl of cDNA (50 ng)
Cycling conditions were: 10min of 95°C, followed by 40 cycles of 95°C for 10 seconds and 58°C for 30 seconds, ending with 15 seconds of 95°C, 1 minute 60°C and 15 seconds 95°C.
Gene expression differences of the pERK target genes DUSP6, SPRY2 and EGR1 (PMID19251651) were calculated using the ΔΔCT method. GAPDH was used as housekeeping gene.

Author's contributions
DSW participated in sample acquisition, carried out DNA isolation, library preparation, whole exome sequencing analysis, interpretation and drafted the manuscript.
MIGR participated in sample acquisition, performed in vitro experiments.
AN performed phylogenetic analyses
JW conducted dPCR experiments
PFC contributed to sequencing analysis and the statistical analyses
VT participated in the design and coordination of the study
LF participated in the design and coordination of the study
MK helped to draft the manuscript and helped in copy number analysis and sequencing analysis
RD: participated in the design and coordination of the study

MPL participated in the design of the study, supervised and planned experiments and the drafting of the manuscript
All authors read and approved the final manuscript

Acknowledgements:
Functional Genomics Center, Nikita Kobert, Ines Kleiber-Schaaf, Mirka Schmid, Melanie Maudrich, Daniela Mihic-Probst, Markus Rechsteiner, The Roche-Zurich Hub Network, URPP in Translational Cancer Research biobank , The Society for Skin Cancer Research, the Schwyzer Stiftung, Empiris Stiftung.

References

Picard. In.
Andrews, S. FastQC A Quality Control tool for High Throughput Sequence Data. In.
Aplin, A. E., Kaplan, F. M., and Shao, Y. (2011). Mechanisms of resistance to RAF inhibitors in melanoma. J Invest Dermatol *131*, 1817-1820.
Ascierto, P. A., Schadendorf, D., Berking, C., Agarwala, S. S., van Herpen, C. M., Queirolo, P., Blank, C. U., Hauschild, A., Beck, J. T., St-Pierre, A.*, et al.* (2013). MEK162 for patients with advanced melanoma harbouring NRAS or Val600 BRAF mutations: a non-randomised, open-label phase 2 study. Lancet Oncol *14*, 249-256.
Berwick, M., Macarthur, J., Orlow, I., Kanetsky, P., Begg, C. B., Luo, L., Reiner, A., Sharma, A., Armstrong, B. K., Kricker, A.*, et al.* (2014). MITF E318K's effect on melanoma risk independent of, but modified by, other risk factors. Pigment Cell Melanoma Res *27*, 485-488.
Bollag, G., Hirth, P., Tsai, J., Zhang, J., Ibrahim, P. N., Cho, H., Spevak, W., Zhang, C., Zhang, Y., Habets, G.*, et al.* (2010). Clinical efficacy of a RAF inhibitor needs broad target blockade in BRAF-mutant melanoma. Nature *467*, 596-599.
Böyum, A. (1968). Isolation of mononuclear cells and granulocytes from human blood. Isolation of monuclear cells by one centrifugation, and of granulocytes by combining centrifugation and sedimentation at 1 g. Scand J Clin Lab Invest Suppl *97*, 77-89.
Chapman, P. B., Hauschild, A., Robert, C., Haanen, J. B., Ascierto, P., Larkin, J., Dummer, R., Garbe, C., Testori, A., Maio, M.*, et al.* (2011). Improved survival with vemurafenib in melanoma with BRAF V600E mutation. N Engl J Med *364*, 2507-2516.
DePristo, M. A., Banks, E., Poplin, R., Garimella, K. V., Maguire, J. R., Hartl, C., Philippakis, A. A., del Angel, G., Rivas, M. A., Hanna, M.*, et al.* (2011). A framework for variation discovery and genotyping using next-generation DNA sequencing data. Nat Genet *43*, 491-498.
Emery, C. M., Vijayendran, K. G., Zipser, M. C., Sawyer, A. M., Niu, L., Kim, J. J., Hatton, C., Chopra, R., Oberholzer, P. A., Karpova, M. B.*, et al.* (2009). MEK1 mutations confer resistance to MEK and B-RAF inhibition. Proc Natl Acad Sci U S A *106*, 20411-20416.
Fernandez, L., Milne, R., Bravo, J., Lopez, J., Avilés, J., Longo, M., Benítez, J., Lázaro, P., and Ribas, G. (2007). MC1R: three novel variants identified in a malignant melanoma association study in the Spanish population. Carcinogenesis *28*, 1659-1664.
Flaherty, K. T., Puzanov, I., Kim, K. B., Ribas, A., McArthur, G. A., Sosman, J. A., O'Dwyer, P. J., Lee, R. J., Grippo, J. F., Nolop, K., and Chapman, P. B. (2010). Inhibition of mutated, activated BRAF in metastatic melanoma. N Engl J Med *363*, 809-819.
Flaherty, P., Natsoulis, G., Muralidharan, O., Winters, M., Buenrostro, J., Bell, J., Brown, S., Holodniy, M., Zhang, N., and Ji, H. P. (2012). Ultrasensitive detection of rare mutations using next-generation targeted resequencing. Nucleic Acids Res *40*, e2.
Gerstung, M., Beisel, C., Rechsteiner, M., Wild, P., Schraml, P., Moch, H., and Beerenwinkel, N. (2012). Reliable detection of subclonal single-nucleotide variants in tumour cell populations. Nat Commun *3*, 811.
Guo, J., Si, L., Kong, Y., Flaherty, K. T., Xu, X., Zhu, Y., Corless, C. L., Li, L., Li, H., Sheng, X.*, et al.* (2011). Phase II, open-label, single-arm trial of imatinib mesylate in patients with metastatic melanoma harboring c-Kit mutation or amplification. J Clin Oncol *29*, 2904-2909.
Hodis, E., Watson, I. R., Kryukov, G. V., Arold, S. T., Imielinski, M., Theurillat, J. P., Nickerson, E., Auclair, D., Li, L., Place, C.*, et al.* (2012). A landscape of driver mutations in melanoma. Cell *150*, 251-263.
Kim, B., Lee, B., and Seo, J. (2007). Visualizing Set Concordance with Permutation Matrices and Fan Diagrams. Interact Comput *19*, 630-643.
Krauthammer, M., Kong, Y., Ha, B. H., Evans, P., Bacchiocchi, A., McCusker, J. P., Cheng, E., Davis, M. J., Goh, G., Choi, M.*, et al.* (2012). Exome sequencing identifies recurrent somatic RAC1 mutations in melanoma. Nat Genet *44*, 1006-1014.
Krzywinski, M., Schein, J., Birol, I., Connors, J., Gascoyne, R., Horsman, D., Jones, S. J., and Marra, M. A. (2009). Circos: an information aesthetic for comparative genomics. Genome Res *19*, 1639-1645.
Lander, E. S., Linton, L. M., Birren, B., Nusbaum, C., Zody, M. C., Baldwin, J., Devon, K., Dewar, K., Doyle, M., FitzHugh, W.*, et al.* (2001). Initial sequencing and analysis of the human genome. Nature *409*, 860-921.
Li, H., and Durbin, R. (2009). Fast and accurate short read alignment with Burrows-Wheeler transform. Bioinformatics *25*, 1754-1760.
Li, H., Handsaker, B., Wysoker, A., Fennell, T., Ruan, J., Homer, N., Marth, G., Abecasis, G., Durbin, R., and Subgroup, G. P. D. P. (2009). The Sequence Alignment/Map format and SAMtools. Bioinformatics *25*, 2078-2079.
Li, J., Lupat, R., Amarasinghe, K. C., Thompson, E. R., Doyle, M. A., Ryland, G. L., Tothill, R. W., Halgamuge, S. K., Campbell, I. G., and Gorringe, K. L. (2012). CONTRA: copy number analysis for targeted resequencing. Bioinformatics *28*, 1307-1313.
Magi, A., Tattini, L., Cifola, I., D'Aurizio, R., Benelli, M., Mangano, E., Battaglia, C., Bonora, E., Kurg, A., Seri, M.*, et al.* (2013). EXCAVATOR: detecting copy number variants from whole-exome sequencing data. Genome Biol *14*, R120.
Maley, C. C., Galipeau, P. C., Finley, J. C., Wongsurawat, V. J., Li, X., Sanchez, C. A., Paulson, T. G., Blount, P. L., Risques, R. A., Rabinovitch, P. S., and Reid, B. J. (2006). Genetic clonal diversity predicts progression to esophageal adenocarcinoma. Nat Genet *38*, 468-473.
McKenna, A., Hanna, M., Banks, E., Sivachenko, A., Cibulskis, K., Kernytsky, A., Garimella, K., Altshuler, D., Gabriel, S., Daly, M., and DePristo, M. A. (2010). The Genome Analysis Toolkit: a MapReduce framework for analyzing next-generation DNA sequencing data. Genome Res *20*, 1297-1303.
Nazarian, R., Shi, H., Wang, Q., Kong, X., Koya, R. C., Lee, H., Chen, Z., Lee, M. K., Attar, N., Sazegar, H.*, et al.* (2010). Melanomas acquire resistance to B-RAF(V600E) inhibition by RTK or N-RAS upregulation. Nature *468*, 973-977.
Nekrutenko, A., Makova, K. D., and Li, W. H. (2002). The K(A)/K(S) ratio test for assessing the protein-coding potential of genomic regions: an empirical and simulation study. Genome Res *12*, 198-202.
Nissan, M. H., Pratilas, C. A., Jones, A. M., Ramirez, R., Won, H., Liu, C., Tiwari, S., Kong, L., Hanrahan, A. J., Yao, Z.*, et al.* (2014). Loss of NF1 in Cutaneous Melanoma Is Associated with RAS Activation and MEK Dependence. Cancer Res *74*, 2340-2350.
Oliveros, J. C. (2007). VENNY. An interactive tool for comparing lists with Venn diagrams. In.

Poulikakos, P. I., Persaud, Y., Janakiraman, M., Kong, X., Ng, C., Moriceau, G., Shi, H., Atefi, M., Titz, B., Gabay, M. T.*, et al.* (2011). RAF inhibitor resistance is mediated by dimerization of aberrantly spliced BRAF(V600E). Nature *480*, 387-390.
Quinlan, A. R., and Hall, I. M. (2010). BEDTools: a flexible suite of utilities for comparing genomic features. Bioinformatics *26*, 841-842.
Robinson, J. T., Thorvaldsdóttir, H., Winckler, W., Guttman, M., Lander, E. S., Getz, G., and Mesirov, J. P. (2011). Integrative genomics viewer. Nat Biotechnol *29*, 24-26.
Shi, H., Hugo, W., Kong, X., Hong, A., Koya, R. C., Moriceau, G., Chodon, T., Guo, R., Johnson, D. B., Dahlman, K. B.*, et al.* (2014). Acquired resistance and clonal evolution in melanoma during BRAF inhibitor therapy. Cancer Discov *4*, 80-93.
Takata, M., Morita, R., and Takehara, K. (2000). Clonal heterogeneity in sporadic melanomas as revealed by loss-of-heterozygosity analysis. Int J Cancer *85*, 492-497.
Thorvaldsdóttir, H., Robinson, J. T., and Mesirov, J. P. (2013). Integrative Genomics Viewer (IGV): high-performance genomics data visualization and exploration. Brief Bioinform *14*, 178-192.
Van Allen, E. M., Wagle, N., Sucker, A., Treacy, D. J., Johannessen, C. M., Goetz, E. M., Place, C. S., Taylor-Weiner, A., Whittaker, S., Kryukov, G. V.*, et al.* (2014). The genetic landscape of clinical resistance to RAF inhibition in metastatic melanoma. Cancer Discov *4*, 94-109.
Van der Auwera, G. A. (2013). From FastQ Data to High-Confidence Variant Calls: The Genome Analysis Toolkit Best Practices Pipeline. In, C. G. A., ed. (Current Protocols in Bioinformatics: Wiley Online Library).
Wagle, N., Emery, C., Berger, M. F., Davis, M. J., Sawyer, A., Pochanard, P., Kehoe, S. M., Johannessen, C. M., Macconaill, L. E., Hahn, W. C.*, et al.* (2011). Dissecting therapeutic resistance to RAF inhibition in melanoma by tumor genomic profiling. J Clin Oncol *29*, 3085-3096.
Wang, K., Li, M., and Hakonarson, H. (2010). ANNOVAR: functional annotation of genetic variants from high-throughput sequencing data. Nucleic Acids Res *38*, e164.
Widmer, D. S., Cheng, P. F., Eichhoff, O. M., Belloni, B. C., Zipser, M. C., Schlegel, N. C., Javelaud, D., Mauviel, A., Dummer, R., and Hoek, K. S. (2012). Systematic classification of melanoma cells by phenotype-specific gene expression mapping. Pigment Cell Melanoma Res.
Wilmott, J. S., Tembe, V., Howle, J. R., Sharma, R., Thompson, J. F., Rizos, H., Lo, R. S., Kefford, R. F., Scolyer, R. A., and Long, G. V. (2012). Intratumoral molecular heterogeneity in a BRAF-mutant, BRAF inhibitor-resistant melanoma: a case illustrating the challenges for personalized medicine. Mol Cancer Ther *11*, 2704-2708.

Figures

Figure 1

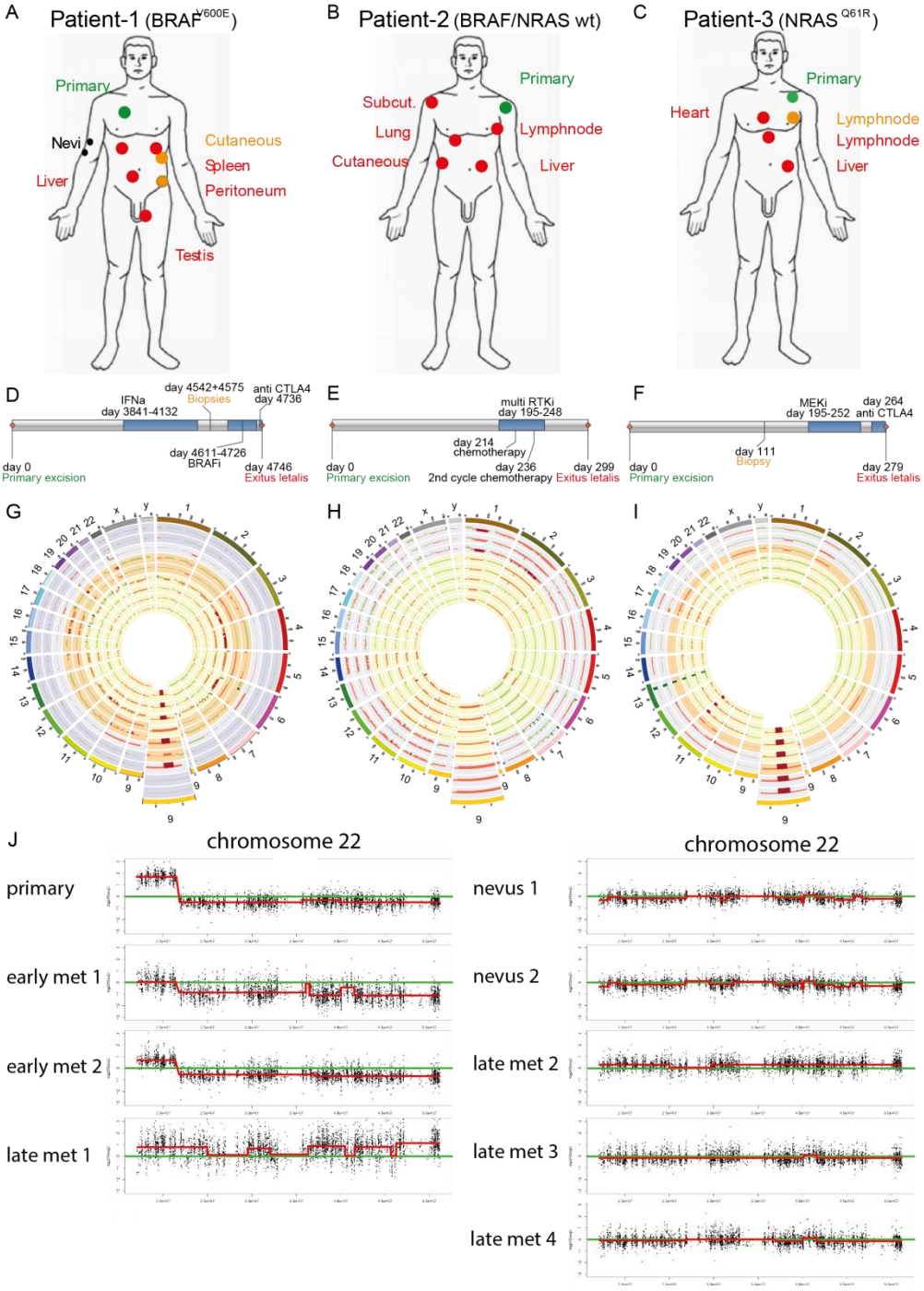

Fig.1: **Patient cohort and copy number variations. A**, Samples from patient 1 included the primary tumor (green), two dysplastic nevi (black), two early metastases (orange) and 4 late metastases after tumor relapse (red). **B,** Patient 1 had a $BRAF^{V600E}$ mutated melanoma and received first IFNa treatment followed by a specific BRAF inhibitor treatment to which he responded but then became resistant. **C**, Patient 2 was diagnosed with a melanoma that was wildtype for both BRAF and NRAS. The primary tumor was punched and sequenced three times. Additionally five late metastases were sequenced. **D,** He received the multi receptor tyrosine kinase inhibitor (Pazopanib), to which he responded but then became resistant. **E,** Patient 3 had an $NRAS^{Q61R}$ mutation. We punched the primary tumor two times and took biopsies from one early and three late metastases. **F,** He received the MEK inhibitor GSK1120212, to which he responded but then became resistant followed by a short period of anti-CTLA4 treatment. **G,** The copy number variations (CNVs) are plotted using Circos. Every ring shows the CNVs detected by Excavator of one biopsy, starting with two nevi in the two outermost circles followed by the primary tumor, the two early metastases and finally the late metastases 1 to 4. **H,** displays the CNVs of patient 2 in from outside to the center: primary tumor samples 1 to 3 and the late metastases 1 to 5. **I,** shows the same for patient 3, from outside towards the center: the primary tumor samples 1 and 2, one early metastases and the late metastases 1 to 3. The enlarged regions show a commonly lost region in chromosome 9 which is coding for the tumor suppressor CDKN2A. **K,** copy number variations in chromosome 22 of patient 1 show high degree of heterogeneity. The primary tumor has a gain in a region of 22p and a loss in a

large area of 22p and 22q. The gain, but not the loss can be seen in the early met 1 but in no other metastasis. The loss, but not the gain, can be found in the early met 2 and late metastasis 1 but no other metastasis.

Figure 2

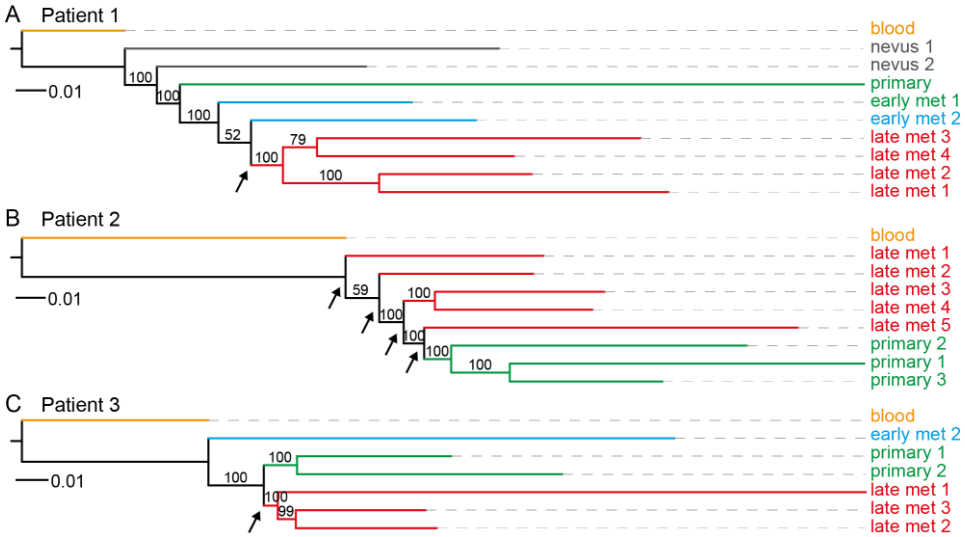

Fig.2: **Whole-exome phylogenetic trees of patient biopsies.** Branch-lengths represent relative distances based on SNVs and indels, and the branches are colored according to biopsy type. Maximum likelihood phylogenetic trees are rooted by the blood sample for patient 1 (**A**), patient 2 (**B**), and patient 3 (**C**). Node supports are given as bootstrap values, with greater than 50% considered to be strong support.

Figure 3

A

Sample	Copies/microliter ($BRAF^{V600E}$)	CI Copies/microliter ($BRAF^{V600E}$)	Precision ($BRAF^{V600E}$)	Copies/microliter ($NRAS^{Q61K}$)	CI Copies/microliter ($NRAS^{Q61K}$)	Precision ($NRAS^{Q61K}$)
neg. control	34.64	28.557 -- 42.02	21.30%	27.898	22.497 -- 34.594	24.00%
nevus 1	9.247	7.811 -- 10.946	18.38%	5.882	4.761 -- 7.266	23.53%
primary	356.17	339.28 -- 373.9	4.98%	12.887	10.067 -- 16.496	28.01%
early met 2	775.6	754.86 -- 796.91	2.75%	5.501	4.093 -- 7.392	34.38%
late met 1	174.2	165.22 -- 183.67	5.44%	8.945	7.112 -- 11.252	25.78%
late met 2	273.99	260.34 -- 288.36	5.24%	18.581	15.332 -- 22.519	21.19%
late met 4	35.058	32.285 -- 38.068	8.59%	3.789	2.954 -- 4.86	28.26%
late met 5	57.048	51.101 -- 63.686	11.64%	12.151	9.581 -- 15.411	26.83%
late met 6	7469.5	7328.9 -- 7612.7	1.92%	12251	12017 -- 12490	1.95%

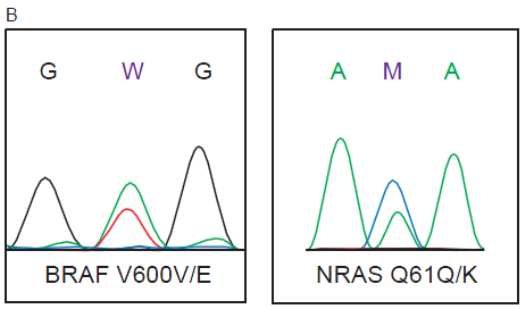

Fig.3: **Digital PCR and Sanger sequencing of patient 1 samples. A,** dPCR using a probe against $BRAF^{V600E}$ and $NRAS^{Q61K}$ showed $BRAF^{V600E}$ mutated DNA in all tumor samples (red box). dPCR reactions positive for $NRAS^{Q61K}$ could be detected only in the late metastasis 6 of this patient (green box). Precision values of less than 15% are considered to be highly reproducible, positive reactions. **B,** representative spectrogram and **C,** sequences from Sanger sequencing of 23 cell cultures grown from single melanoma cells isolated from late metastasis 6. All 23 clonal cultures had both the $BRAF^{V600E}$ and $NRAS^{Q61K}$ mutations.

Figure 4

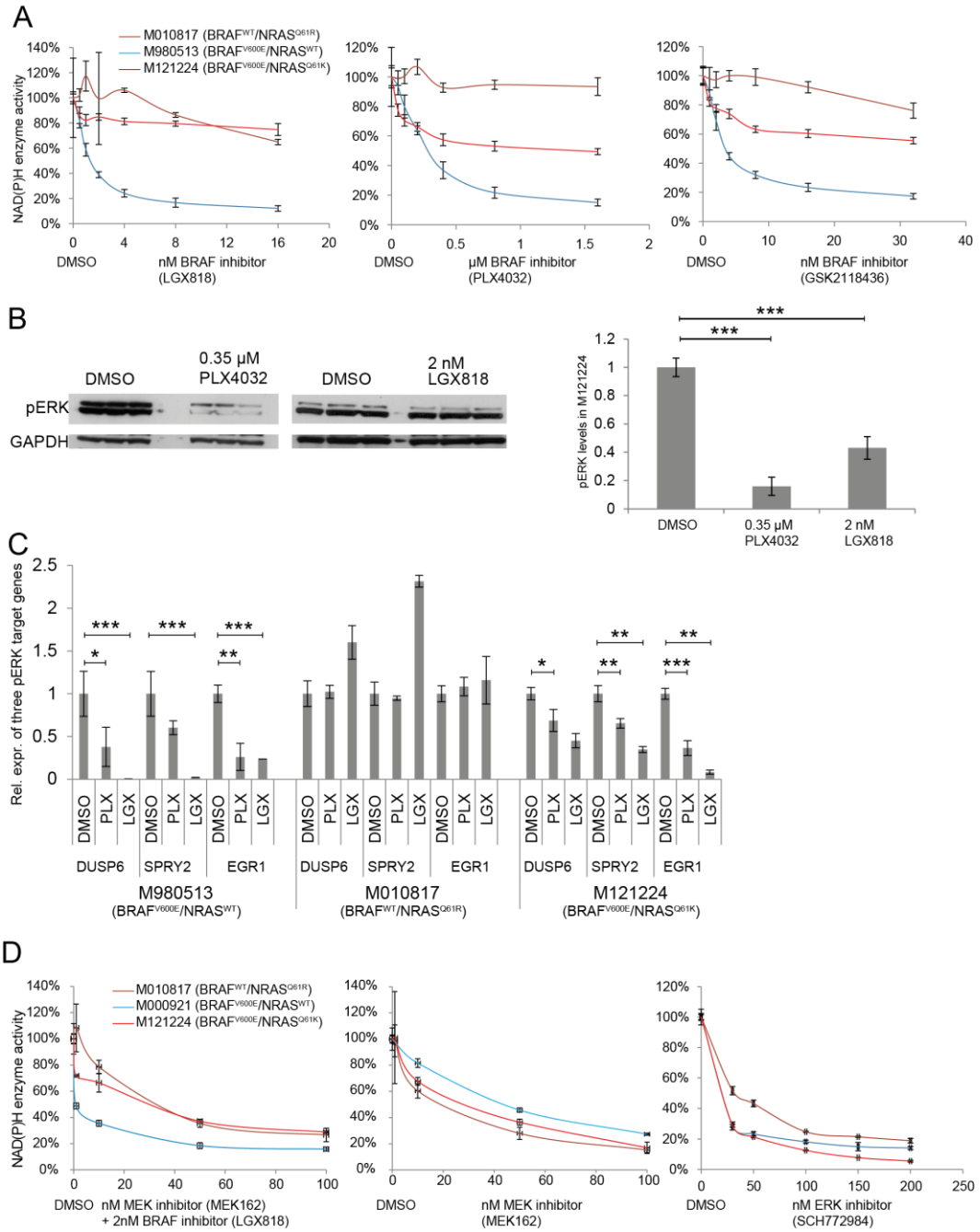

Fig.4: **Viability assays and pERK signaling in double-mutated melanoma cells.** A resistant cell culture established from late metastasis 6 of patient 1 showed variable response to different BRAF inhibitors. **A,** Triplicate MTT assays measuring NAD(P)H enzyme activity after treatment with different BRAF inhibitors normalized to DMSO treated cells. The resistant cell-line M121224, derived from a patient progressing while on LGX818 treatment, is fully resistant for LGX818, but only partially resistant to PLX4032 and GSK2118436. **B,** Western blot and its Quantification of pERK levels in M121224 cells after BRAF-inhibitor treatment. Optical density of the bands was measured with ImageJ to obtain a bar-graph. Drug concentrations were chosen based on the IC_{50} of the sensitive cell-line M000921, as well as other $BRAF^{V600E}$ mutated early passage cultures. **C,** qPCR showing the relative expression of pERK target genes after treatment with 0.35 μM PLX4032. **D,** MTT assay measuring NAD(P)H enzyme activity after treatment with a MEK inhibitor (MEK162), a combination of MEK and BRAF inhibitor (LGX818) and ERK inhibitor (SCH772984) alone.

Figure 5

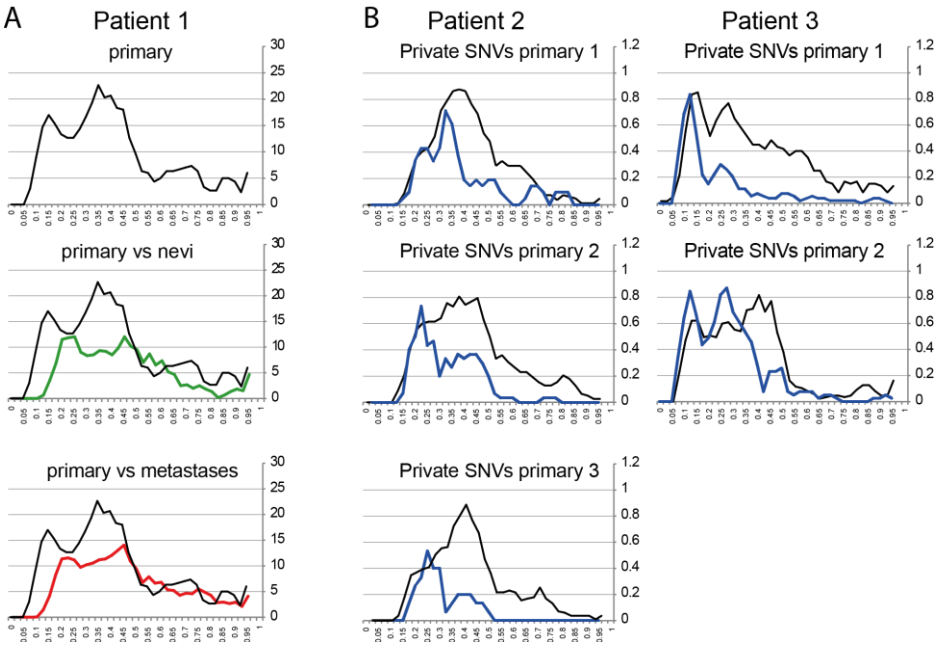

Fig.5: **Subclonal diversity measured by mutant allele ratios (MAR). A,** Frequencies of mutant allele ratios of the primary tumor of patient 1 show homozygous, heterozygous and possibly subclonal SNVs. A comparison to the nevi and metastases of patient 1 shows an increased subclonal frequency in the primary tumor (black line) versus nevi (green line) or metastases (red line). **B,** Total SNVs of primary tumor of patient 2 (black line) compared to SNVs exclusively present in the first punch of the primary tumor of patient 2 (blue line). The SNVs private to the single punches generally have a low MAR. Values below the graphs represent mean MAR.